NASA Technical Memorandum 89433

# A Comprehensive Estimate of the Static Aerodynamic Forces and Moments of the 8- by 8- by 20-Foot Cargo Container

Luigi Cicolani,
Gerd Kanning, Ames Research Center, Moffett Field, California

May 1987

**NASA**

National Aeronautics and
Space Administration

**Ames Research Center**
Moffett Field, California 94035

# TABLE OF CONTENTS

## SYMBOLS

$A_P$      projected frontal area of container (eq. 4.6)

$b_Y, b_L, b_{YM}$      corrections of $YC$, $LC$ and $YMC$ to theoretical zero values on boundaries of $\mathcal{R}_o$

$D, Y, L,$  $RM, PM, YM$      these denote the wind axes components of the aerodynamic force and moment vectors, which are $(-D, Y, -L)^T$ and $(RM, PM, YM)^T$, respectively: termed drag, sideforce, lift, and roll, pitch, yaw moments, respectively. Moments are measured about the geometric center of the box.

$DC, YC, LC,$  $RMC, PMC, YMC$      the NASA Ames Research Center's wind tunnel measurements of $D, Y, ..., YM$ (ref. 3) corrected for interference

$\widetilde{DC}, \widetilde{YC}, \widetilde{LC},$  $\widetilde{RMC}, \widetilde{PMC}, \widetilde{YMC}$      measurement errors, $DC - D, YC - Y$, etc.

$\widehat{D}, \widehat{Y}, \widehat{L},$  $\widehat{RM}, \widehat{PM}, \widehat{YM}$      estimated values of the force and moment components obtained in this paper

$DU, YU, LU,$  $RU, PU, YU$      wind tunnel measurements from University of Maryland (ref. 6)

$\mathcal{D}, \mathcal{D}_0, \mathcal{D}_1, \mathcal{D}_2, \mathcal{D}_3,$  $\mathcal{D}_4, \mathcal{D}_5, \mathcal{D}_6, \mathcal{D}_7$      attitude domain of interest in simulation: $-180° \leq \psi < 180°$, $-90° \leq \alpha \leq 90°$, and its quadrants (fig 3.1). $\mathcal{D}_0$ is the quadrant $0 \leq \psi, \alpha \leq 90°$ containing the measurements.

$E_1(\sigma), E_2(\sigma), E_3(\sigma)$      elementary rotation matrices for rotation through angle $\sigma$ about $\underline{i}, \underline{j}$ and $\underline{k}$ axes, respectively.

$$\{E_1(\sigma), E_2(\sigma), E_3(\sigma)\} =$$

$$\left\{ \begin{pmatrix} 1 & 0 & 0 \\ 0 & \cos\sigma & \sin\sigma \\ 0 & -\sin\sigma & \cos\sigma \end{pmatrix}, \begin{pmatrix} \cos\sigma & 0 & -\sin\sigma \\ 0 & 1 & 0 \\ \sin\sigma & 0 & \cos\sigma \end{pmatrix}, \begin{pmatrix} \cos\sigma & \sin\sigma & 0 \\ -\sin\sigma & \cos\sigma & 0 \\ 0 & 0 & 1 \end{pmatrix} \right\}$$

$fc, \widehat{f}$      two-dimensional vectors, $(YC, LC)^T$ and $(\widehat{Y}, \widehat{L})^T$

$\underline{i}_b, \underline{j}_b, \underline{k}_b$      container body axes; orthogonal right-handed frame with $\underline{i}_b$ parallel to a long edge and $\underline{k}_b$ perpendicular to the bottom face

| | |
|---|---|
| $\underline{i}_{b_o}, \underline{j}_{b_o}, \underline{k}_{b_o}$ | tunnel mount axes defined from the angle measurements $(\psi, \alpha)$, where $T_{b_o, w_o} = E_2(\alpha) E_3(\psi)$ |
| $\underline{i}_w, \underline{j}_w, \underline{k}_w$ | wind axes; orthogonal right-handed frame with $\underline{i}_w$ along $\underline{Va}$ and $\underline{k}_w$ in the body vertical plane. |
| $\underline{i}_{w_o}, \underline{j}_{w_o}, \underline{k}_{w_o}$ | tunnel axes in which forces and moments are measured; orthogonal right-handed frame with $\underline{i}_{w_o}$ and $\underline{k}_{w_o}$ along the tunnel longitudinal axis and the local vertical, respectively. |
| $Q$ | dynamic pressure, $\rho V a^2 / 2$ |
| $RMCS, RMCA$ | half of the sum and the difference, respectively, of the roll moment measurements at pairs of equivalent points (eq. 4.14) |
| $\mathcal{R}_0, \mathcal{R}_1, \mathcal{R}_2,$ $\overline{\mathcal{R}}_o, \overline{\mathcal{R}}_1, \overline{\mathcal{R}}_2$ | regions in $\mathcal{D}_o$ bounded by the lines $\alpha = 45°$, $\{\psi^*(\alpha), \psi^{(45)}(\alpha), \ 0 \le \alpha \le 90°\}$, respectively (figures 3.5 and 3.6); $\mathcal{R}_o$ is the region spanned by the measurements. |
| $S_1, S_2, S_3,$ $S_4, S_5, S_6$ | the subdivision of $\mathcal{D}_o$ defined by the lines $\alpha = 45°$, $\{\psi^*(\alpha)\}$, $\{\psi^{(45)}(\alpha)\}$ (fig. 3.6). |
| $S_1, S_2, S_3, S_4,$ $S_5, S_6, S_7$ | diagonal matrices which define symmetry properties and correspond to rotations of 180° about various axes (fig. 5.1). |
| $T_{a,b}$ | transformation of a vector from reference frame "b" to frame "a", where the subscripts a and b can be any of $b, b_o, w,$ or $w_o$ to indicate the reference frames used in this work (eqs. 3.1 - 3.3 ) |
| $\underline{Va}, Va$ | air-velocity vector, airspeed |
| $\alpha$ | angle of attack; $\tan \alpha = \underline{Va} \cdot \underline{k}_b / \underline{Va} \cdot \underline{i}_b, \quad -90° \le \alpha \le 90°$ |
| $\beta$ | sideslip angle; $\sin \beta = \underline{Va} \cdot \underline{j}_b / Va, \ sign(\cos \beta) = sign(\underline{Va} \cdot \underline{i}_b);$ $-180° \le \beta \le 180°$ |
| $\delta D, \delta Y, \delta L$ | differences between values of $D, Y$, and $L$ given from the Ames Research Center's data at equivalent points |
| $\Delta D, \Delta Y, \Delta L,$ $\Delta RM, \Delta PM, \Delta YM$ | interference tares (appendix A) or the differences between data from references 3 and 6 (appendix B) |
| $\xi$ | angle between air velocity vector and longitudinal body axis (eq. 4.7) |

| | |
|---|---|
| $\phi_w$ | roll angle locating wind axes relative to tunnel axes. $T_{w,w_o} = E_1(\phi_w)$ |
| $\psi$ | model heading angle relative to tunnel or wind axes: $\psi = -\beta$ |
| $\psi^*(\alpha)$ | heading angle along the line of self-equivalent points (fig. 3.6) |
| $\psi^{(45)}(\alpha)$ | heading angle along the line equivalent to the boundary of $\mathcal{R}_o$, $\alpha = 45°$ (fig. 3.6) |
| $\overline{\psi}(\psi,\alpha)$ | heading angle such that $\xi(\overline{\psi},45°) = \xi(\psi,\alpha)$  (eq. 4.8) |
| $\underline{(\ )}$ | vectors are indicated by an underbar |
| $\widetilde{(\ )}$ | error in the estimate or measurement of ( ) |
| $\widehat{(\ )}$ | estimate of ( ) |
| $(\ )^T$ | transpose of ( ) |

## UNITS

English units (lb, ft, and sec) and degrees are used throughout and are generally omitted in the figures and tables. Aerodynamic forces and moments are measured as force or moment divided by dynamic pressure, which have units of ft$^2$ and ft$^3$, respectively.

# SUMMARY

A comprehensive model of the static aerodynamics of the 8- by 8- by 20-ft container known as the MILVAN is determined by combining the available wind tunnel data from a 1972 NASA Ames Research Center study taken over the restricted attitude domain, $\{0 \leq \psi \leq 90°$; $0 \leq \alpha \leq 45°\}$, with an extrapolation to the complete domain of interest in simulations, $\{-180° \leq \psi \leq 180°$; $-90° \leq \alpha \leq 90°\}$, based on an appropriate theory derived from the geometric symmetry of rectangular boxes. The theory predicts the symmetry properties of all force and moment components about various boundaries, including all zero lines, their behavior along certain boundaries, and their interrelationships at equivalent points. It was found that the aerodynamics at any attitude can be defined from the aerodynamics at an equivalent attitude in the restricted domain $\{0 \leq \psi \leq 45°$; $0 \leq \alpha \leq 90°\}$. However, a similar comprehensive equivalence with the domain spanned by the measurements is not available; in particular, about two-thirds of the domain with $|\alpha| > 45°$ is unrelated to the domain of measurements. Nevertheless, an estimate can be given for this region consistent with the measured and theoretical values and the theoretical equivalence relations. Discrepancies between the data and the predicted symmetry properties ranged from small to gross, depending on the component, and were removed to apply the extrapolation theory. Small discrepancies were treated by imposing the required zero lines and averaging data at equivalent points. The roll- and pitching-moment data showed gross discrepancies and were discarded. Roll moment could be estimated using the available data from an independent study or assumed negligible, while pitching moment was estimated using the yaw moment data and the theory. The tunnel errors or unrealistic theoretical assumptions which account for these discrepancies cannot be formally identified because records of the original wind tunnel sensor readings and data processing had been discarded prior to the present study, nor were new tests within the scope of this study. However, limited data from independent wind tunnel studies are reviewed and show good to fair agreement with both the theory and the estimate given here.

# 1. INTRODUCTION

In rotorcraft slung load operations, a large variety of objects are carried which have a correspondingly large range of aerodynamic characteristics, and equilibrium and dynamic behavior in flight. The 8- by 8- by 20-ft container, also known as the MILVAN, is a standard cargo carrier and is a common load in these operations. It develops significant aerodynamic specific force and moment at low speeds, including static, quasi-static, and unsteady flow terms (refs. 1 - 8), and can become unstable at speeds well below the power-limited speed of the helicopter-load system. In addition, its simple shape results in static aerodynamics which are more easily documented in the wind tunnel and represented in simulations than those of arbitrarily shaped loads. Thus, it has served as the typical difficult load in much of the slung-load stabilization research of the past, and is the usual load in slung-load simulations (e.g., refs. 1 and 2).

Various slung-load configurations are illustrated in figure 1.1, including the single point suspension, the two-point suspension for tandem-rotor helicopters, and the dual-lift system. The
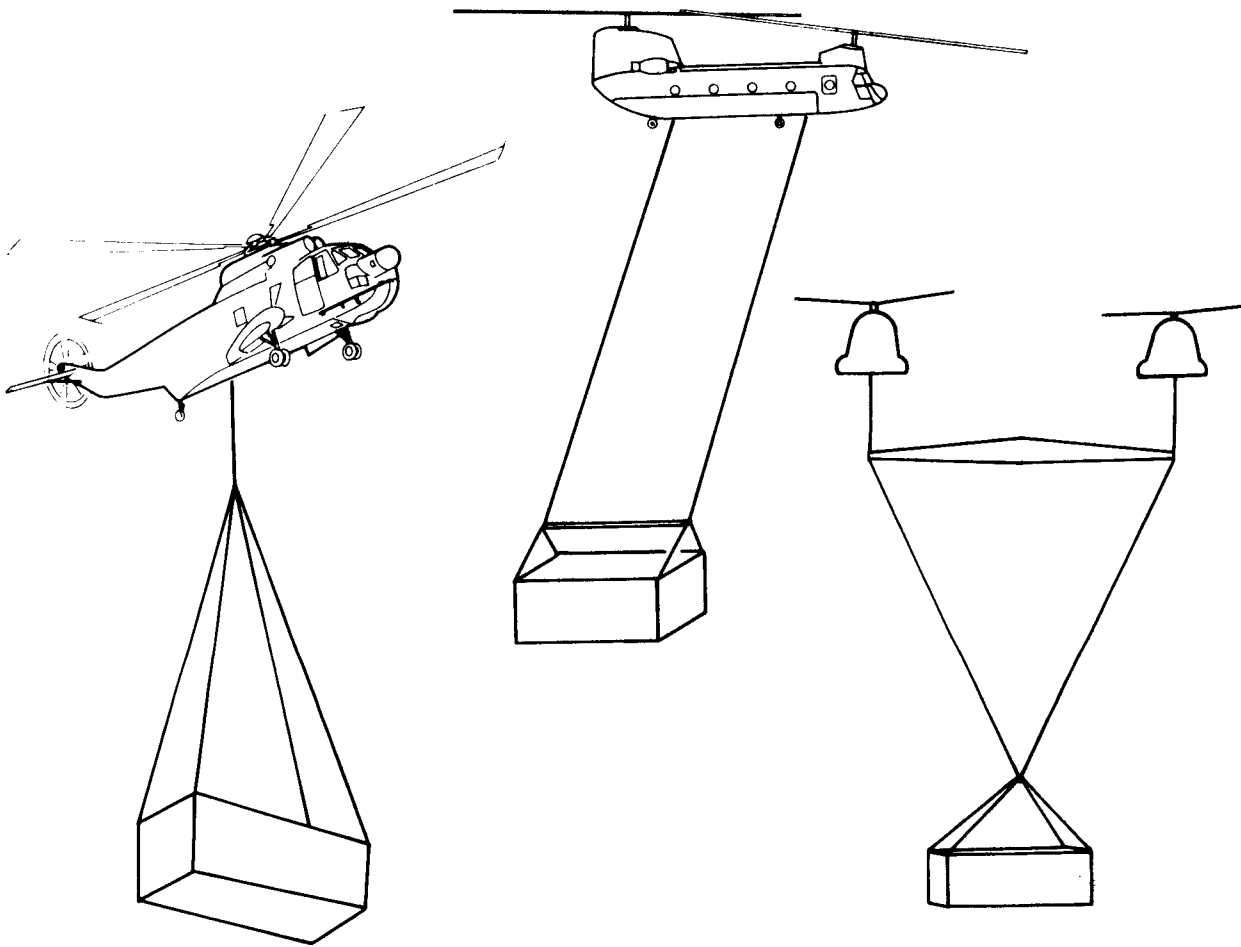
Figure 1.1.- Configuration of slung load systems.

MILVAN angle of attack in steady flight can range from $-90°$ at very low speeds to small positive values. For the single point suspension, the MILVAN trims broadside to the flow at low speeds, and becomes unstable at 40 - 60 knots. In the two-point suspension the MILVAN trims lengthwise to the flow in its minimum drag orientation and is stable to much higher speeds.

Future slung-load research may focus on the development of automatic stabilization and flightpath control systems, and the control of exotic suspensions such as the dual-lift system. These efforts can benefit from a comprehensive simulation model which captures realistic load motion for both static and dynamic condition. Towards this end, reference 8 provides a recent derivation of the system equations of motion for single-point suspensions, and the load kinematics in a two-point suspension are derived in reference 9. The present work adds a comprehensive model of the MILVAN's static aerodynamics derived from the available wind tunnel data. This suffices for realistic calculation of the MILVAN's attitude and the suspension forces in equilibrium. However,as demonstrated in references 4 and 7 , the MILVAN's dynamic behavior depends on significant unsteady aerodynamic effects, and a linear perturbation model of its unsteady

2

aerodynamics is given in reference 8 from the available wind tunnel.

Wind tunnel measurements of the MILVAN's static aerodynamics are available from several sources. The most comprehensive measurements were made at NASA Ames Research Center (ARC) and are documented in reference 3. These data (termed the Ames data hereafter) are the basis of the present work, but are almost entirely restricted to angle of attack between 0 and 45° and heading angle between 0 and 90°. Additional independent data are available from an Army/Northrop study (refs. 4 and 5), and a VERTOL/ University of Maryland study (ref. 6) (UOM data). The data in references 4 and 5 survive only in graphical form, are restricted to a few angles of attack $(0, 10°, 28°)$, and not all components are given. The data in reference 6 spans the same domain as that in reference 3, but no data were taken at heading angles between 50° and 90° where the side force and yaw moment exhibit peak magnitudes and strong nonlinearities. The reference 6 data were the source of the abbreviated MILVAN aerodynamic model in the ARC simulation of reference 2. Both of these studies provided important supplementary information in the present work. In addition, an Army/University of Bristol study, (ref. 7) provides results from surface pressure distribution measurements and flow visualization tests for a limited set of attitudes.

The static aerodynamic model of the MILVAN in the Langley Research Center's simulation (ref. 1) was also derived from the data used here. In that model, drag, lift, sideforce and yaw moment were given by trigonometric functions fitted to the data. This treatment is succinct, but of modest accuracy relative to the data in some regions because of the limited number of fitting function parameters, and erroneous in its extrapolation to angles of attack above 45° for lack of an extrapolation theory. The present work attempts to improve the static aerodynamic simulation model by; 1) providing tabulated function models, 2) deriving and applying a theory for extrapolating the model beyond the region of the measurements, and 3) adding the missing roll and pitching-moment components. Tabulated models can be used routinely and efficiently in digital simulations to represent arbitrary nonlinear functions to the accuracy of the available measurements.

A theory for extrapolating the model beyond the region of measurements is derived from the geometric symmetry of the box. The box is indistiguishable to the flow and yields identical wind tunnel measurements when rotated 90° or 180° about its longitudinal axis or turned end for end, and also possesses the usual force and moment symmetries of bodies with horizontal and vertical planes of symmetry. These factors permit the aerodynamics at any attitude to be defined from the aerodynamics at a corresponding point in a small region. The smallest such region identified in the analysis is contained in the half-quadrant $\{0 \leq \psi \leq 45°; \quad 0 \leq \alpha \leq 90°\}$. It is found that the half-quadrant spanned by the measurements of reference 3 does not suffice to define the aerodynamics at all attitudes. In particular, the aerodynamics in most of the region with angle of attack above 45° cannot be obtained from the measurements, but an estimate can be given consistent with the measurements along one boundary of this region, theoretical values along the remaining boundaries, and a theoretical relation between the aerodynamic components at equivalent points within the region.

When the measurements of reference 3 are compared with the theory, discrepancies are

3

found which range from small for some components to gross disagreement in the case of roll and pitching moments. These discrepancies must be removed to apply the extrapolation theory. Small discrepancies are treated by imposing the theoretical zero lines and averaging the data at equivalent points. The roll and pitching moment data cannot be treated in this way because the discrepancies dominate the measured values and a corrected table would be completely uncertain. These data are discarded and roll moment can then be estimated from the available independent wind tunnel data or neglected, while pitching moment is estimated from the yaw moment data and the theory. The independent wind tunnel data from references 4 - 6 are also reviewed and show good to fair agreement with both the theory and the estimate derived from the Ames data for all components. The final model consists of data tables for all six force and moment components in wind axes and extrapolation formulas for both wind axes and body axes.

We acknowledge the helpfulness of the authors and organizations of the wind tunnel studies (refs. 3 - 6) in locating and discussing the original data, and we regard with mixed feelings the penetrating questions of one reviewer which exposed an error in the fundamental symmetry equation in the first draft of this report that required all text and computations after Section 2 to be redone. Last, we note that all numerical analyses discussed here were carried out with a digital computer and that the tables of values in the text were printed directly from the computer.

## 2. A REFERENCE TABLE OF WIND TUNNEL DATA

The Ames data, reference 3, consists of two tables of force and moment measurements uncorrected for model support interference and two tables of interference tare measurements. The pairs of tables were generated by varying only angle of attack or only yaw angle in the sequences of measurements. The basic measurements were uncorrected for interference in reference 3 because of the erratic nature of the tare measurements which left their use open to individual interpretation. These four tables are combined here into a single reference table of corrected measurements covering the region

$$\mathcal{R}_o = \{(\psi, \alpha) : \quad \psi \in [0°, 90°], \quad \alpha \in [0°, 45°]\} \tag{2.1}$$

The method and results are summarized next and details are documented in appendix A.

First, the two tables of force and moment measurements are combined as follows. These tables cover the two regions shown in figure 2.1(a); these regions are not coincident but collectively they cover $\mathcal{R}_o$ and can be averaged in the common region to reduce the standard deviation of random measurement errors there. The present treatment uses all available data in $\mathcal{R}_o$. An examination of the differences between the two tables shows; 1) small differences for the force and yaw moment components (below 10Q lb, 30Q ft-lb), which indicates good repeatability and small random measurement errors for these components, and 2) large differences for the roll and pitching moment data (25Q to 100Q ft-lb over most of $\mathcal{R}_o$), which indicates large random errors for these components.

Strong vibrations of the model and corresponding variations in scale readings were observed in the ARC tunnel tests, and the static aerodynamic data were obtained by averaging numerous readings. This average is expected to converge to a unique value if the number of readings is increased indefinitely, and to show only small differences among averages obtained from sufficiently large sets of readings. This is the case for the force and yaw moment data. The source of the much larger differences in the $RM$ and $PM$ data is unknown and cannot be determined without a more careful analysis of the test conditions and data processing than is now possible. In any case, the limiting average values of $RM$ and $PM$ have not been approached in the Ames data, and this is confirmed by the large differences between these data and the data from independent studies reviewed in appendices B and C, as well as from the values predicted by the theory of the next section, and by the general agreement among these other sources.

Second, the support interference is estimated from the two tables of tare measurements as follows. The regions covered by the two tables are shown in figure 2.1(b); these are insufficient to cover $\mathcal{R}_o$. Further, the pitch sweep data measured the interference of only part of the support and are not used here except to indicate interference trends at angles of attack above 20° where there are no yaw sweep data. The yaw sweep data were reviewed with the object of estimating the interference function from the discernible systematic trends in these data and attributing the random variation around these trends to measurement errors.

For the force- and yaw-moment components, the tare data showed consistent variations with $\psi$ and random variation with $\alpha$; therefore, the interference was estimated by averaging the tare data over $\alpha$. The averaged tares are small in magnitude, and the differences between the estimated tare and the original data are also small and statistically similar to the differences between the two

5

sets of measurements just discussed, as is expected if the same random error processes account for both sets of differences. The roll-moment tare data appeared to consist almost entirely of samples of a random process; the systematic interference was estimated as the table mean, which was nearly zero, while the data measured large interference moments which were statistically similar to the differences between the two sets of roll moment measurements just discussed. Evidently, the systematic roll moment interference was much smaller than the random-roll-moment measurement errors and not detectable in the Ames data. Finally, the pitching moment data showed discernible trends in both $\psi$ and $\alpha$ and the interference was estimated by ad hoc smoothing of the table of measurements. Results showed large estimated interference moments and smaller, moderate-sized differences between the estimate and the data.

The resulting reference table is given in figure 2.2 and plotted in figures 2.3 and 2.4. These corrected data are indicated by appending "C" to the notation ($DC$, $YC$, etc.) in the remainder of this paper. A cursory examination of the plots shows that drag increases with both $\psi$ and $\alpha$, (with projected frontal area) as expected, and that side force and yaw moment approximately pass through zero at $\psi = 0$ and 90° consistent with their expected antisymmetry in $\psi$ about these points. However, lift shows significant nonzero values at $\alpha = 0$ where antisymmetry in $\alpha$ is expected, and pitching moment shows a gross departure from the same expected antisymmetry. These discrepancies suggest the presence of systematic errors remaining in the data, which are small to gross depending on the component, and they are examined in greater detail in the application section of this paper.

The remainder of the problem is to define the static aerodynamics at all possible attitudes from these data given on $\mathcal{R}_o$. The extent to which this can be done based on the geometric symmetry of the box is examined in the next section, and the resulting extrapolation theory and the data are combined in the following section to obtain a comprehensive estimate of the MILVAN'S static aerodynamics.
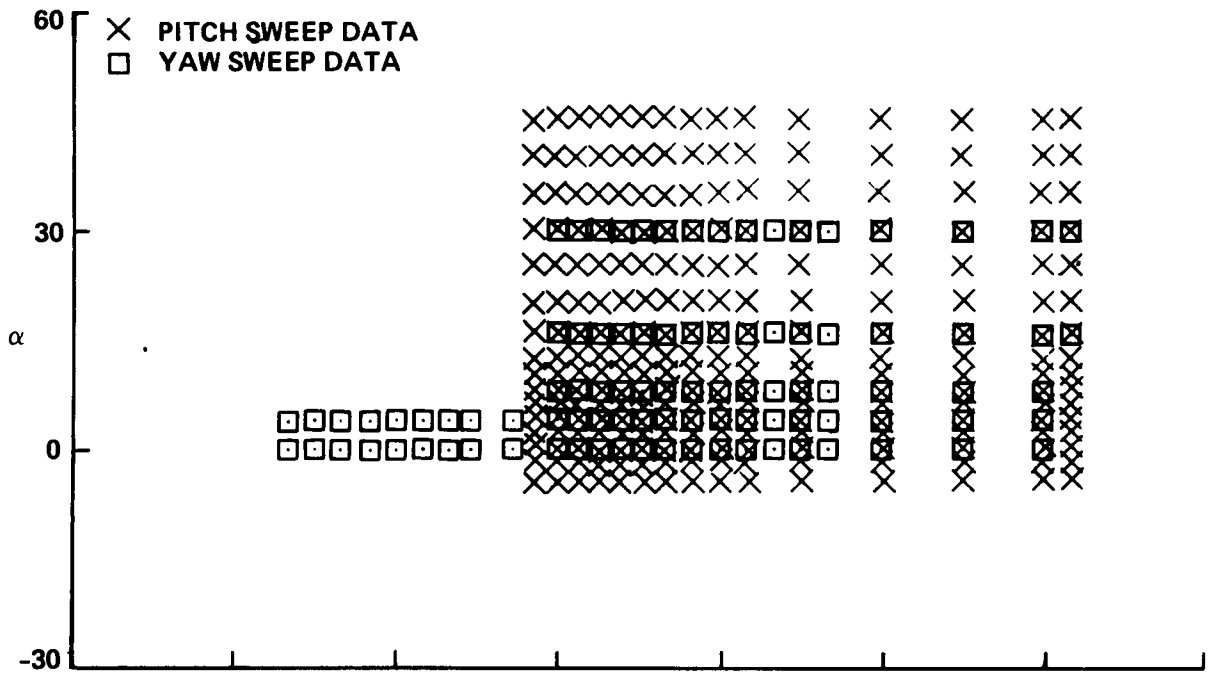
(a) FORCE AND MOMENT MEASUREMENTS
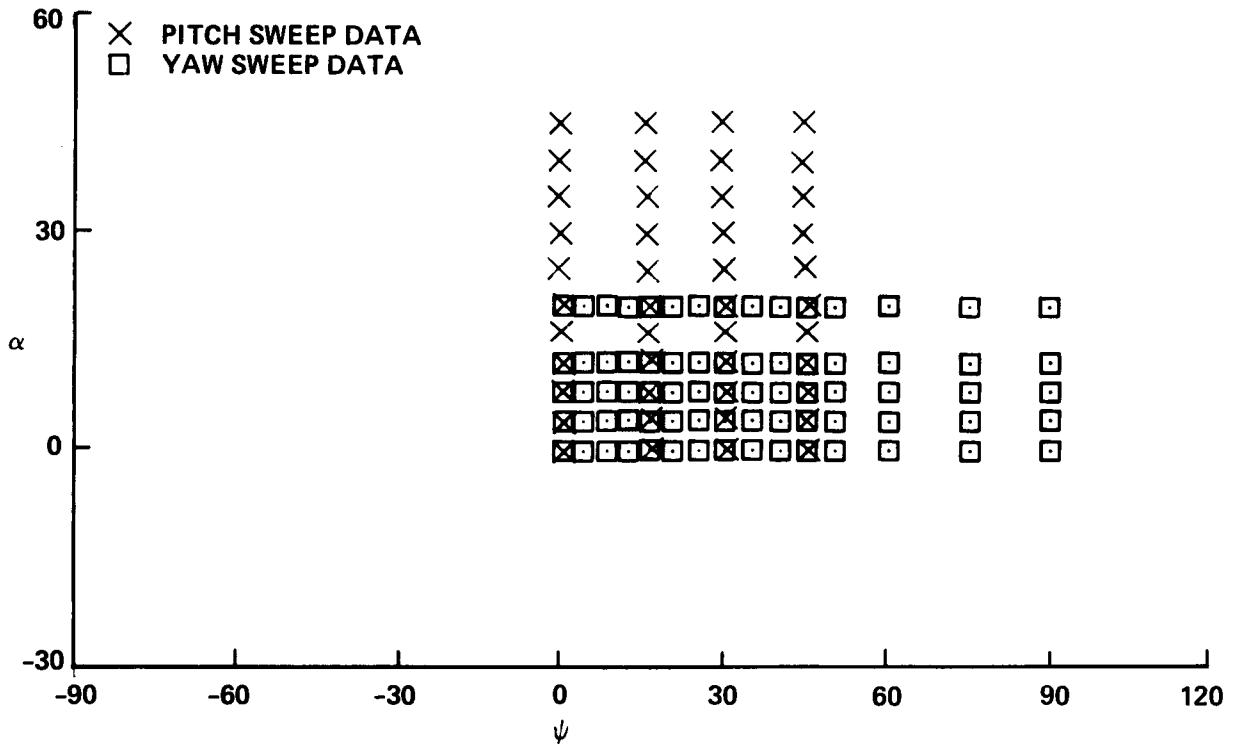


(b) INTERFERENCE TARE MEASUREMENTS

Figure 2.1.- Measurement grids of the Ames data.

$\alpha$ — DC/Q

| $\alpha$ | 0.0 | 4.0 | 8.0 | 12.0 | 16.0 | 20.0 | 25.0 | 30.0 | 35.0 | 40.0 | 45.0 | 50.0 | 60.0 | 75.0 | 90.0 |
|---|---|---|---|---|---|---|---|---|---|---|---|---|---|---|---|
| 0. | 57.9 | 60.3 | 68.2 | 77.5 | 88.3 | 96.8 | 109.6 | 121.6 | 132.4 | 140.9 | 150.8 | 165.5 | 195.1 | 213.4 | 216.4 |
| 2. | 60.9 | 62.6 | 70.3 | 78.7 | 89.4 | 98.3 | 111.4 | 123.4 | 134.8 | 143.0 | 152.1 | 167.7 | 195.9 | 212.8 | 216.4 |
| 4. | 63.8 | 66.1 | 73.5 | 80.0 | 91.0 | 101.1 | 112.9 | 125.3 | 136.6 | 144.8 | 153.6 | 170.3 | 197.5 | 213.1 | 217.9 |
| 6. | 66.8 | 69.8 | 77.2 | 83.3 | 93.2 | 103.3 | 116.3 | 127.5 | 139.0 | 146.8 | 156.3 | 173.4 | 198.0 | 212.3 | 217.6 |
| 8. | 70.5 | 73.1 | 80.3 | 87.1 | 96.1 | 106.0 | 119.3 | 130.2 | 141.8 | 149.9 | 161.0 | 177.6 | 198.4 | 212.1 | 216.6 |
| 10. | 74.2 | 76.4 | 83.8 | 90.7 | 100.4 | 110.6 | 124.2 | 133.8 | 145.1 | 153.7 | 165.0 | 180.2 | 199.1 | 212.5 | 216.9 |
| 12. | 78.1 | 80.0 | 87.1 | 94.4 | 104.7 | 115.9 | 129.1 | 138.0 | 149.4 | 157.6 | 168.1 | 182.1 | 199.8 | 211.5 | 216.8 |
| 16. | 85.7 | 87.0 | 94.2 | 102.2 | 112.2 | 124.8 | 139.1 | 147.3 | 156.1 | 163.8 | 172.9 | 184.8 | 200.8 | 210.0 | 216.5 |
| 20. | 94.6 | 97.1 | 103.8 | 111.3 | 122.3 | 133.6 | 146.3 | 152.4 | 162.4 | 169.1 | 176.8 | 187.3 | 200.9 | 208.5 | 216.9 |
| 25. | 107.0 | 109.1 | 116.4 | 123.9 | 133.3 | 144.4 | 155.3 | 161.5 | 171.0 | 177.1 | 184.2 | 192.4 | 202.1 | 206.5 | 216.2 |
| 30. | 118.9 | 120.4 | 127.1 | 136.1 | 142.1 | 152.6 | 162.4 | 170.5 | 179.6 | 185.2 | 191.3 | 197.2 | 202.9 | 206.0 | 216.9 |
| 35. | 126.6 | 131.4 | 139.1 | 144.8 | 149.7 | 160.9 | 170.5 | 182.4 | 189.6 | 193.4 | 198.7 | 201.6 | 204.6 | 204.1 | 216.1 |
| 40. | 141.8 | 143.3 | 149.8 | 154.6 | 159.9 | 166.7 | 179.4 | 190.2 | 197.8 | 202.4 | 208.5 | 208.6 | 206.1 | 204.2 | 214.4 |
| 45. | 157.2 | 159.8 | 163.8 | 164.0 | 166.5 | 176.6 | 188.9 | 197.6 | 205.9 | 210.2 | 215.9 | 214.7 | 209.6 | 201.1 | 215.2 |

$\alpha$ — YC/Q

| $\alpha$ | 0.0 | 4.0 | 8.0 | 12.0 | 16.0 | 20.0 | 25.0 | 30.0 | 35.0 | 40.0 | 45.0 | 50.0 | 60.0 | 75.0 | 90.0 |
|---|---|---|---|---|---|---|---|---|---|---|---|---|---|---|---|
| 0. | -2.5 | 10.1 | 18.5 | 24.3 | 29.1 | 38.4 | 53.5 | 63.2 | 68.5 | 73.7 | 76.6 | 80.0 | 87.0 | 70.6 | 6.0 |
| 2. | -1.5 | 11.2 | 19.3 | 23.9 | 28.1 | 37.5 | 52.5 | 60.8 | 66.5 | 70.5 | 73.3 | 78.0 | 87.9 | 70.7 | 6.4 |
| 4. | -1.0 | 11.6 | 19.9 | 27.8 | 28.1 | 37.9 | 51.7 | 60.3 | 65.4 | 68.1 | 70.5 | 76.2 | 88.4 | 71.6 | 8.0 |
| 6. | -1.5 | 12.4 | 22.5 | 28.0 | 30.1 | 40.0 | 50.7 | 58.7 | 63.4 | 66.8 | 70.8 | 77.8 | 89.5 | 72.4 | 7.3 |
| 8. | -2.3 | 12.8 | 24.4 | 28.8 | 31.5 | 41.5 | 50.8 | 57.3 | 63.2 | 66.3 | 70.6 | 78.7 | 89.5 | 73.4 | 7.5 |
| 10. | -2.9 | 12.8 | 27.2 | 31.3 | 35.8 | 44.5 | 51.6 | 57.3 | 61.7 | 65.8 | 70.9 | 78.6 | 89.7 | 74.2 | 7.8 |
| 12. | -4.3 | 13.2 | 28.8 | 33.2 | 38.9 | 46.2 | 51.9 | 56.3 | 61.9 | 66.0 | 70.8 | 78.6 | 90.8 | 75.1 | 7.5 |
| 16. | -5.8 | 12.9 | 32.3 | 42.1 | 49.7 | 51.4 | 49.2 | 53.5 | 58.4 | 64.2 | 70.0 | 77.1 | 89.8 | 76.9 | 8.3 |
| 20. | -9.9 | 14.4 | 32.0 | 42.4 | 52.2 | 52.2 | 47.9 | 49.6 | 55.1 | 60.6 | 66.9 | 73.7 | 86.4 | 77.6 | 7.4 |
| 25. | -10.9 | 12.9 | 28.8 | 41.2 | 51.1 | 55.3 | 52.8 | 47.9 | 54.2 | 57.3 | 62.3 | 69.3 | 82.9 | 75.8 | 8.0 |
| 30. | -11.0 | 10.9 | 23.5 | 35.0 | 44.8 | 50.9 | 52.9 | 47.4 | 52.3 | 53.3 | 57.4 | 64.2 | 78.1 | 75.8 | 6.4 |
| 35. | -3.9 | 9.0 | 15.2 | 22.9 | 31.7 | 42.5 | 44.8 | 45.7 | 46.8 | 48.9 | 52.7 | 59.0 | 71.0 | 75.4 | 2.3 |
| 40. | -1.7 | 3.6 | 13.0 | 14.9 | 22.2 | 31.2 | 37.1 | 40.0 | 42.2 | 43.0 | 45.4 | 52.3 | 65.3 | 73.6 | 1.7 |
| 45. | 1.0 | -1.3 | 4.3 | 3.5 | 10.7 | 18.6 | 28.7 | 32.7 | 33.8 | 34.5 | 36.9 | 44.0 | 57.4 | 70.4 | -3.7 |

$\alpha$ — LC/Q

| $\alpha$ | 0.0 | 4.0 | 8.0 | 12.0 | 16.0 | 20.0 | 25.0 | 30.0 | 35.0 | 40.0 | 45.0 | 50.0 | 60.0 | 75.0 | 90.0 |
|---|---|---|---|---|---|---|---|---|---|---|---|---|---|---|---|
| 0. | 5.4 | 4.7 | 6.5 | 7.8 | 9.3 | 15.1 | 20.3 | 27.4 | 31.4 | 32.0 | 28.7 | 18.9 | 8.6 | 3.5 | 4.3 |
| 2. | 10.0 | 9.6 | 11.3 | 14.6 | 17.6 | 23.5 | 29.7 | 37.2 | 41.5 | 40.3 | 34.5 | 20.9 | 5.3 | 3.6 | 4.9 |
| 4. | 13.6 | 13.3 | 17.9 | 21.2 | 26.3 | 32.2 | 38.6 | 46.6 | 51.8 | 47.9 | 39.0 | 22.4 | 3.2 | 3.0 | 4.0 |
| 6. | 16.8 | 16.2 | 20.6 | 25.6 | 32.1 | 38.7 | 47.8 | 55.0 | 58.4 | 51.8 | 39.7 | 23.9 | 3.8 | 2.8 | 5.3 |
| 8. | 19.7 | 18.9 | 21.6 | 28.7 | 36.1 | 43.5 | 54.1 | 62.8 | 64.4 | 54.6 | 38.9 | 24.4 | 4.5 | 2.6 | 5.6 |
| 10. | 20.9 | 21.1 | 24.7 | 30.8 | 38.6 | 48.1 | 57.8 | 64.8 | 65.7 | 55.0 | 39.9 | 26.3 | 6.2 | 2.0 | 5.9 |
| 12. | 24.2 | 23.4 | 27.2 | 32.9 | 41.8 | 53.1 | 61.3 | 66.6 | 61.9 | 53.3 | 41.9 | 28.8 | 8.0 | 1.2 | 6.2 |
| 16. | 27.9 | 29.0 | 33.9 | 40.7 | 48.5 | 61.4 | 73.0 | 67.8 | 60.4 | 51.3 | 42.8 | 31.8 | 11.6 | 1.1 | 6.6 |
| 20. | 35.5 | 35.4 | 39.8 | 46.7 | 54.0 | 65.8 | 73.3 | 69.3 | 62.1 | 53.6 | 45.4 | 34.4 | 15.2 | 3.3 | 7.1 |
| 25. | 44.6 | 43.2 | 46.4 | 52.8 | 57.3 | 63.6 | 68.9 | 71.1 | 66.5 | 58.7 | 50.9 | 39.5 | 20.6 | 7.6 | 7.6 |
| 30. | 53.4 | 50.3 | 51.8 | 58.6 | 61.5 | 65.0 | 65.1 | 71.5 | 68.8 | 62.2 | 55.4 | 43.7 | 25.7 | 10.9 | 8.2 |
| 35. | 55.2 | 56.9 | 58.2 | 59.5 | 66.1 | 68.0 | 69.1 | 70.9 | 69.8 | 63.3 | 58.3 | 45.7 | 29.6 | 14.4 | 6.8 |
| 40. | 61.4 | 59.9 | 62.8 | 66.2 | 67.5 | 68.2 | 69.9 | 70.7 | 67.3 | 62.4 | 59.1 | 47.8 | 34.2 | 19.5 | 9.0 |
| 45. | 63.2 | 64.0 | 65.7 | 66.7 | 65.9 | 68.0 | 68.8 | 67.9 | 65.2 | 60.5 | 57.4 | 47.7 | 37.4 | 23.1 | 8.2 |
| $\psi$ | 0.0 | 4.0 | 8.0 | 12.0 | 16.0 | 20.0 | 25.0 | 30.0 | 35.0 | 40.0 | 45.0 | 50.0 | 60.0 | 75.0 | 90.0 |

(a) Force components.

Figure 2.2.- Wind tunnel data corrected for estimated support interference.

$RMC/Q$

| $\alpha$ | 0.0 | 4.0 | 8.0 | 12.0 | 16.0 | 20.0 | 25.0 | 30.0 | 35.0 | 40.0 | 45.0 | 50.0 | 60.0 | 75.0 | 90.0 |
|---|---|---|---|---|---|---|---|---|---|---|---|---|---|---|---|
| 0. | 13.3 | -3.0 | 13.3 | -5.8 | 26.2 | -2.4 | -16.7 | -11.5 | -26.8 | -82.6 | -122.4 | -155.6 | -183.2 | -107.3 | -79.6 |
| 2. | -11.9 | -6.0 | 38.8 | 3.2 | 21.9 | 19.7 | -16.5 | 23.0 | -22.4 | -84.5 | -141.7 | -152.9 | -197.5 | -109.0 | -90.4 |
| 4. | -4.2 | 11.9 | -8.9 | -40.3 | 8.5 | -1.3 | -0.3 | -8.6 | -49.5 | -103.2 | -162.9 | -150.8 | -209.6 | -105.0 | -104.3 |
| 6. | 10.4 | 3.3 | -43.0 | -26.9 | 13.8 | 5.2 | -5.0 | -6.1 | -35.2 | -135.7 | -212.5 | -200.8 | -238.7 | -118.8 | -114.3 |
| 8. | 22.6 | -4.9 | -42.0 | -23.2 | 26.7 | 23.4 | 34.2 | -20.8 | -79.1 | -160.9 | -189.0 | -193.8 | -242.8 | -138.9 | -106.1 |
| 10. | 31.0 | 2.2 | -55.9 | -13.8 | -2.9 | 15.7 | 26.1 | -26.5 | -66.1 | -145.8 | -180.4 | -188.1 | -238.1 | -133.6 | -117.1 |
| 12. | 40.3 | 6.0 | -42.1 | 2.6 | 22.3 | -2.9 | 12.0 | -19.2 | -87.8 | -145.1 | -166.0 | -192.7 | -275.5 | -135.2 | -101.6 |
| 16. | 48.2 | 18.6 | -31.8 | -20.8 | -23.5 | -12.5 | -6.9 | -5.8 | -34.6 | -96.6 | -139.3 | -176.7 | -270.3 | -131.1 | -112.7 |
| 20. | 79.2 | 8.6 | -23.7 | 3.8 | -31.1 | -34.8 | -17.7 | -16.0 | -14.2 | -68.3 | -122.1 | -156.8 | -246.7 | -140.0 | -97.0 |
| 25. | 67.7 | 37.6 | 10.3 | 0.1 | -25.7 | -23.8 | -17.7 | -11.0 | -18.5 | -68.7 | -142.1 | -171.8 | -253.9 | -110.4 | -138.1 |
| 30. | 77.0 | 57.5 | 14.4 | 39.8 | -50.7 | -40.0 | -36.5 | -36.8 | -47.6 | -74.4 | -147.9 | -168.6 | -234.7 | -104.8 | -103.5 |
| 35. | 81.2 | 25.2 | 54.7 | 83.5 | 15.4 | -65.8 | -4.8 | -52.4 | -58.5 | -120.9 | -183.4 | -186.6 | -193.1 | -67.2 | -60.8 |
| 40. | 80.6 | 45.4 | 46.3 | -16.7 | -6.8 | -16.5 | -62.1 | -112.6 | -72.2 | -132.3 | -192.3 | -200.8 | -217.8 | -61.9 | -58.6 |
| 45. | 84.3 | 70.9 | 63.0 | 29.4 | -9.4 | -20.9 | -29.0 | -20.7 | -64.7 | -108.5 | -152.4 | -169.0 | -202.2 | -66.0 | -29.4 |

$PMC/Q$

| $\alpha$ | 0.0 | 4.0 | 8.0 | 12.0 | 16.0 | 20.0 | 25.0 | 30.0 | 35.0 | 40.0 | 45.0 | 50.0 | 60.0 | 75.0 | 90.0 |
|---|---|---|---|---|---|---|---|---|---|---|---|---|---|---|---|
| 0. | -22.0 | -21.9 | -46.8 | -56.4 | -42.7 | -66.3 | -91.6 | -92.0 | -65.3 | -50.3 | -48.7 | -86.3 | -243.8 | -233.3 | -183.8 |
| 2. | -84.1 | -82.3 | -85.7 | -78.1 | -58.4 | -69.2 | -77.3 | -64.3 | -52.3 | -46.2 | -43.5 | -71.5 | -232.2 | -243.1 | -184.5 |
| 4. | -111.1 | -129.6 | -127.0 | -111.7 | -80.3 | -65.1 | -62.1 | -35.0 | -32.6 | -33.4 | -27.4 | -49.7 | -221.8 | -222.1 | -207.9 |
| 6. | -126.8 | -146.6 | -132.1 | -100.6 | -86.3 | -69.0 | -53.2 | -22.6 | -15.6 | -17.1 | -6.4 | -87.6 | -215.4 | -231.6 | -223.5 |
| 8. | -144.7 | -161.9 | -132.8 | -110.8 | -85.6 | -83.8 | -62.7 | -35.4 | -14.3 | -16.1 | 0.0 | -135.4 | -209.8 | -217.9 | -223.6 |
| 10. | -133.2 | -154.0 | -135.2 | -126.8 | -95.1 | -100.2 | -73.4 | -41.6 | -31.8 | -48.1 | -58.6 | -162.9 | -204.7 | -229.3 | -241.6 |
| 12. | -110.1 | -130.4 | -131.4 | -139.1 | -112.2 | -100.1 | -64.7 | -71.8 | -51.4 | -70.0 | -95.0 | -180.7 | -214.9 | -226.2 | -249.9 |
| 16. | -82.3 | -98.4 | -91.4 | -112.1 | -85.5 | -84.0 | -75.1 | -120.8 | -126.1 | -148.4 | -138.6 | -186.3 | -241.4 | -207.1 | -290.4 |
| 20. | -51.8 | -70.6 | -57.5 | -83.0 | -65.5 | -72.4 | -77.6 | -116.2 | -137.4 | -152.7 | -117.0 | -176.2 | -261.9 | -193.6 | -324.2 |
| 25. | 19.2 | -21.1 | -33.0 | -44.8 | -13.4 | -53.7 | -64.4 | -98.2 | -118.7 | -124.9 | -89.3 | -146.1 | -239.4 | -199.9 | -329.4 |
| 30. | 65.3 | 27.3 | 25.5 | -19.7 | 6.1 | -23.5 | -37.8 | -75.2 | -121.6 | -116.7 | -79.5 | -128.2 | -217.3 | -199.4 | -335.0 |
| 35. | 102.1 | 81.3 | 71.3 | 38.4 | 51.2 | -2.9 | 7.0 | -57.5 | -104.7 | -100.9 | -55.1 | -98.3 | -181.6 | -164.0 | -357.1 |
| 40. | 112.9 | 117.5 | 54.4 | 55.9 | 39.7 | 32.9 | 15.2 | -55.8 | -51.5 | -79.4 | -65.3 | -87.5 | -128.9 | -218.0 | -344.5 |
| 45. | 116.5 | 87.3 | 93.1 | 77.5 | 67.2 | 36.1 | -14.0 | -43.8 | -58.2 | -76.0 | -51.8 | -76.6 | -123.3 | -118.3 | -270.0 |

$YMC/Q$

| $\alpha$ | 0.0 | 4.0 | 8.0 | 12.0 | 16.0 | 20.0 | 25.0 | 30.0 | 35.0 | 40.0 | 45.0 | 50.0 | 60.0 | 75.0 | 90.0 |
|---|---|---|---|---|---|---|---|---|---|---|---|---|---|---|---|
| 0. | 31.9 | -71.5 | -119.3 | -93.7 | -45.5 | 8.6 | 86.7 | 145.2 | 189.4 | 223.5 | 262.9 | 279.4 | 282.0 | 237.1 | 47.1 |
| 2. | 29.5 | -63.6 | -119.0 | -95.4 | -49.4 | 4.8 | 78.6 | 135.5 | 178.5 | 212.9 | 252.6 | 272.5 | 283.2 | 236.2 | 47.2 |
| 4. | 25.8 | -48.9 | -109.9 | -93.0 | -52.4 | 1.3 | 71.3 | 127.2 | 167.2 | 202.1 | 242.5 | 266.1 | 285.8 | 236.5 | 50.3 |
| 6. | 21.1 | -26.3 | -70.2 | -70.3 | -47.5 | -1.8 | 68.4 | 120.1 | 161.7 | 194.0 | 235.6 | 265.2 | 287.0 | 236.0 | 49.1 |
| 8. | 17.3 | -5.2 | -25.3 | -32.9 | -37.7 | 0.0 | 60.4 | 109.8 | 157.9 | 189.8 | 234.6 | 268.0 | 287.4 | 236.3 | 49.3 |
| 10. | 15.2 | 4.0 | -2.9 | -2.4 | -4.3 | 17.1 | 71.0 | 113.5 | 162.5 | 195.5 | 238.9 | 269.7 | 288.9 | 235.9 | 48.5 |
| 12. | 13.2 | 12.7 | 13.1 | 20.6 | 28.2 | 26.0 | 81.2 | 122.1 | 171.4 | 204.1 | 244.7 | 271.9 | 288.6 | 234.2 | 47.8 |
| 16. | 8.6 | 29.0 | 38.6 | 52.8 | 65.9 | 51.0 | 97.8 | 147.4 | 191.1 | 218.7 | 249.4 | 271.1 | 286.7 | 232.6 | 49.3 |
| 20. | 5.0 | 42.0 | 50.3 | 51.1 | 58.7 | 49.3 | 103.0 | 145.3 | 184.9 | 211.6 | 243.1 | 264.4 | 279.7 | 228.6 | 50.5 |
| 25. | 2.8 | 48.4 | 62.9 | 44.7 | 31.1 | 48.0 | 103.4 | 140.4 | 172.9 | 201.3 | 236.7 | 257.8 | 273.1 | 223.4 | 52.4 |
| 30. | 1.7 | 54.1 | 64.9 | 31.1 | -6.1 | 28.5 | 90.1 | 138.7 | 163.6 | 190.8 | 227.0 | 249.7 | 268.8 | 219.1 | 54.0 |
| 35. | 0.6 | 56.3 | 57.5 | 17.8 | -9.2 | 26.7 | 82.0 | 125.8 | 150.4 | 177.7 | 213.0 | 230.6 | 259.9 | 208.7 | 56.1 |
| 40. | 10.0 | 57.2 | 47.2 | -19.5 | -10.8 | 26.9 | 75.4 | 114.5 | 140.1 | 167.3 | 202.6 | 221.9 | 254.6 | 194.1 | 62.3 |
| 45. | 17.8 | 37.1 | 10.4 | -22.8 | -15.2 | 14.0 | 68.2 | 105.1 | 133.1 | 157.0 | 189.0 | 210.0 | 246.2 | 184.8 | 62.4 |
| $\psi$ | 0.0 | 4.0 | 8.0 | 12.0 | 16.0 | 20.0 | 25.0 | 30.0 | 35.0 | 40.0 | 45.0 | 50.0 | 60.0 | 75.0 | 90.0 |

(b) Moment components.

Figure 2.2.- Concluded.

9
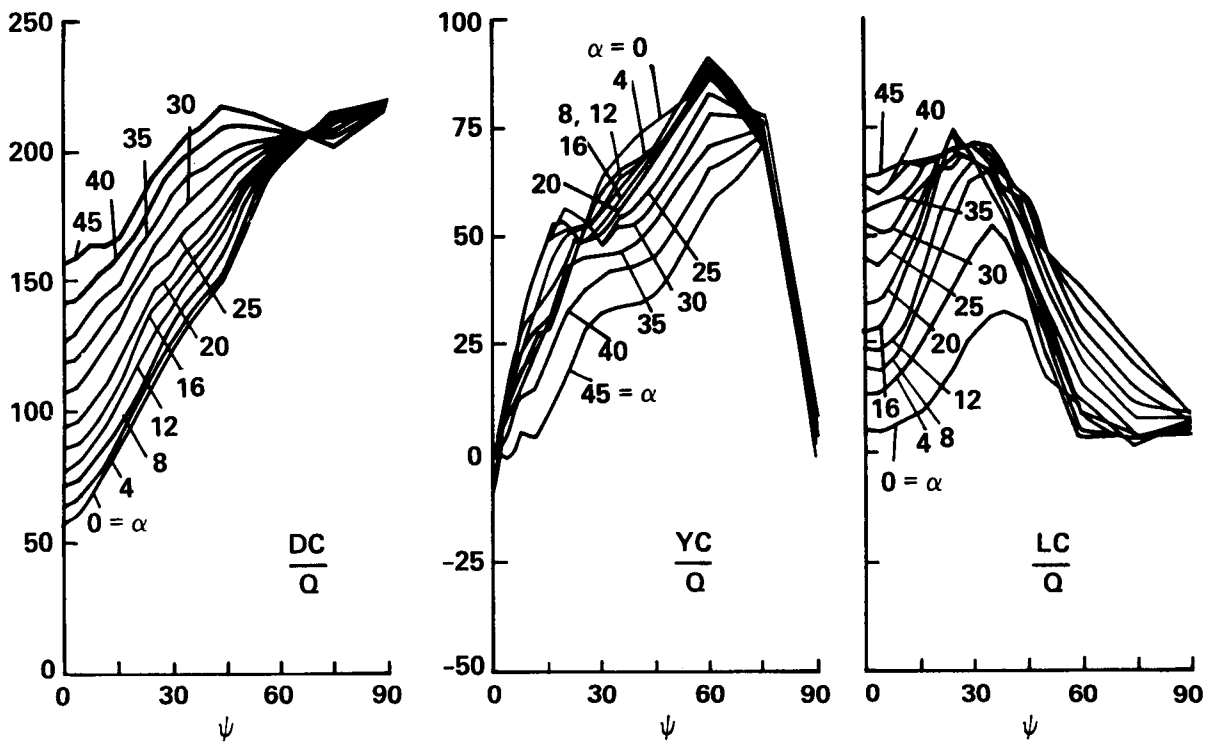
(a) FORCE-COMPONENTS, ft$^2$
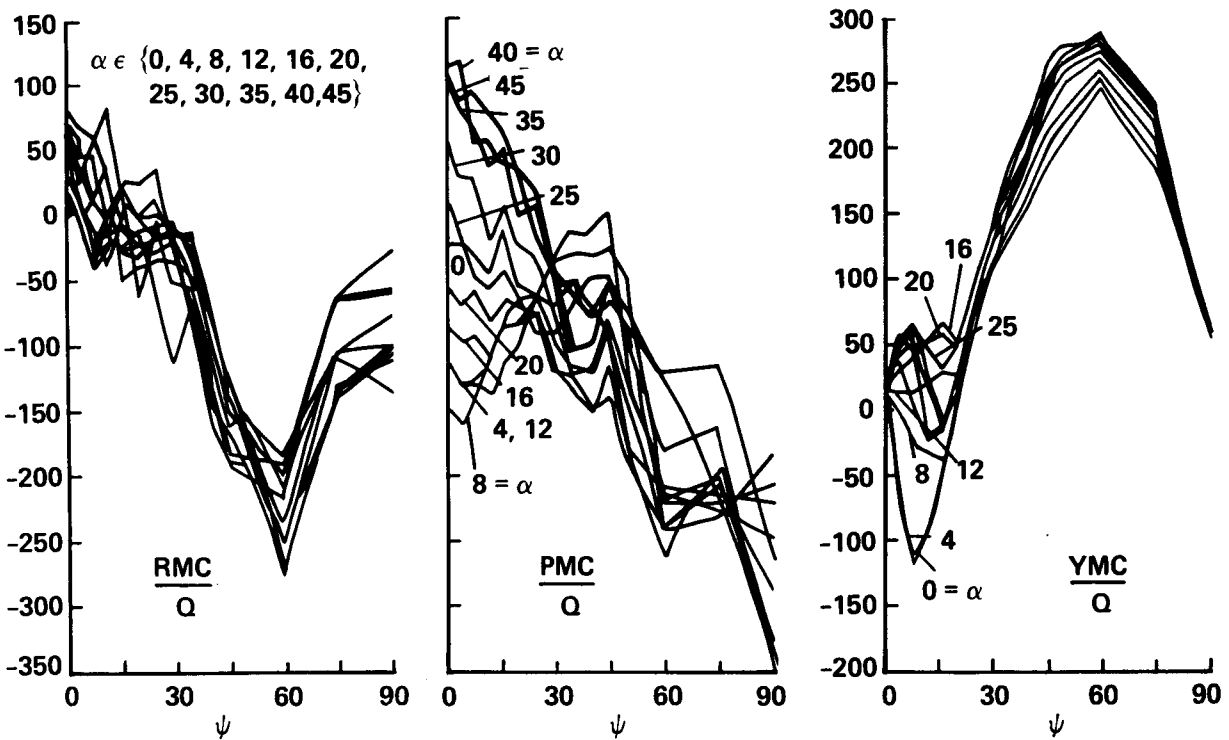
(b) MOMENT COMPONENTS, ft$^3$

Figure 2.3.- Corrected wind tunnel data.
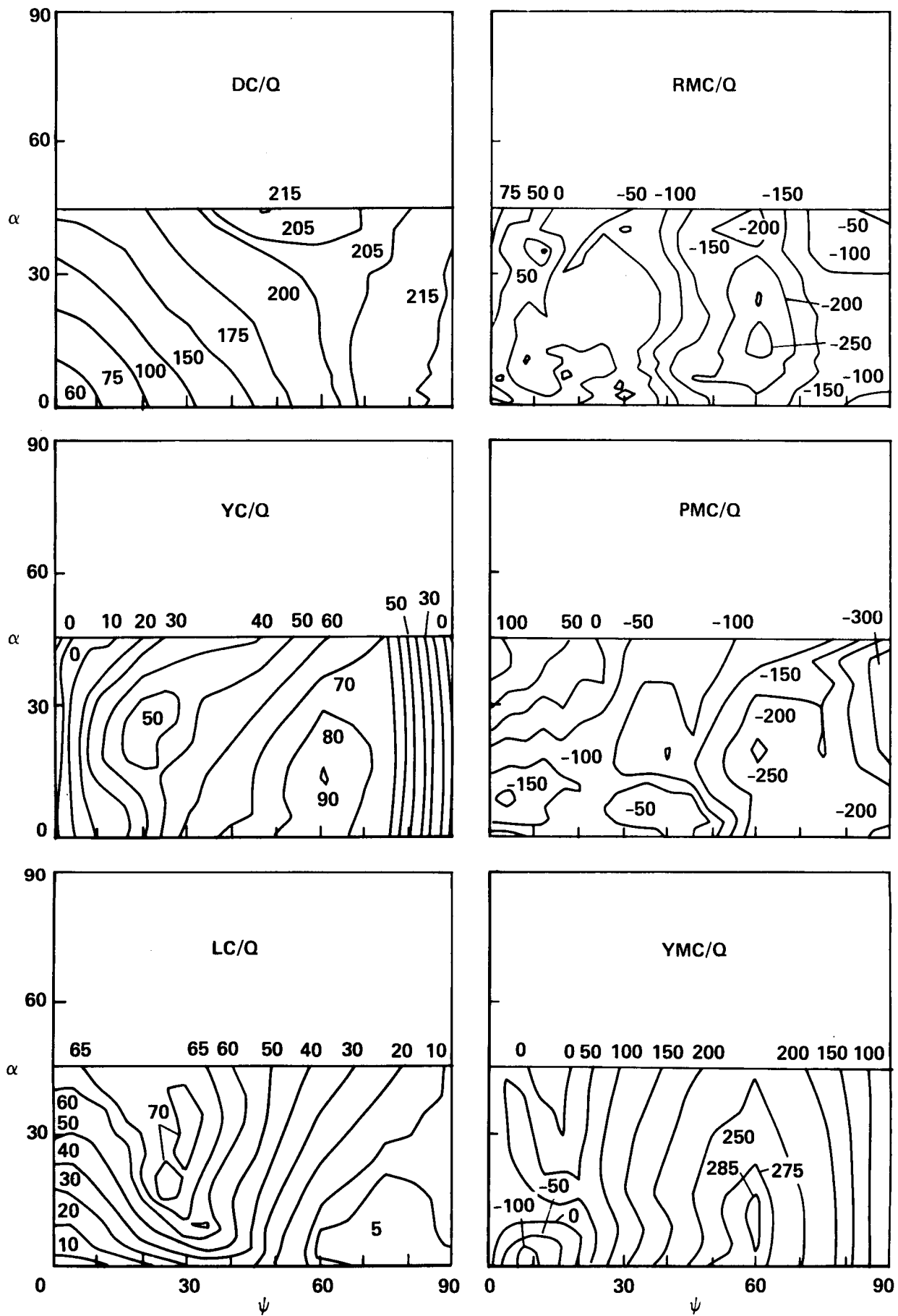
Figure 2.4.- Corrected wind tunnel data: contour plots.

11

# 3. ANALYTICAL EXTRAPOLATION

The symmetry of the MILVAN is analyzed in this section for equations to extrapolate the data in $\mathcal{R}_o$ to the complete domain of interest for simulation:

$$D = \{(\psi, \alpha): \quad \psi_w \in [-180°, 180°], \quad \alpha \in [-90°, 90°]\}$$

It is useful to divide this domain into eight quadrants as shown and labeled in figure 3.1:
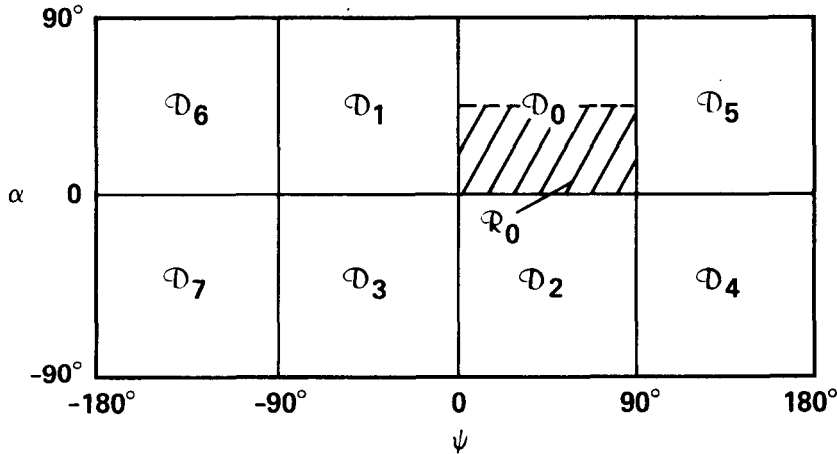


Figure 3.1.- Attitude domain for simulation models.

An arbitrarily shaped load model can be turned on its side, upside down, and reversed in the wind tunnel to obtain data for all of $D$ while only moving the model mount through angles in $D_o$. For each orientation, the wind-axes force and moment components and the angles between wind and body axes are related to the components measured along the wind tunnel's measuring axes and to the mount's attitude angles. However, if the load is not arbitrarily shaped, but is a rectangular box with identical sides, then these various mountings are indistinguishable to the flow, and the force and moment components measured on the wind tunnel scales are necessarily identical in each orientation. In this case, the aerodynamics at any point in $D$ can be defined from measurements at a corresponding point in $D_o$. Finally, if a sufficient number of symmetry properties of the components are also assumed, then the aerodynamics at points within $D_o$ are related, and then the aerodynamics everywhere in $D$ can be determined from those in a subregion of $D_o$. It is found that the subregion with $0 \leq \psi \leq 45°$ is such a region, but $\mathcal{R}_o$ is not. Nevertheless, the theory indicates relations which must be satisfied over $D_o$ by any simulation model derived from the measurements and approximation formulas, including the zero-lines of all components, and the values or behavior of each component along all boundaries of $D_o$.

We note that the ARC wind tunnel model did not have identical surfaces; the sides, bottom, and front were ribbed to represent strengthening ribs on the MILVAN while the top and rear were smooth. However, a limited amount of comparative data for an entirely smooth-surfaced box is given in reference 3 and indicates only small differences caused by the ribbing, and the same comparison is made in reference 6 with the same result.

### 3.1 Box Attitudes with Identical Wind Tunnel Measurements

These attitudes can be obtained from the relations among four reference frames. First, the tunnel axes in which measurements are made are aligned with the tunnel longitudinal axis or free-stream direction, and the local vertical. Second, the mounting angles measured in the tunnel $(\psi_o, \alpha_o)$ define the mounting body axes, where the transformation from tunnel axes to the mounting axes is;

$$T_{b_o, w_o} = E_2(\alpha_o) E_3(\psi_o) \tag{3.1}$$

The elementary rotation matrices, $(E_i(\sigma), i = 1, 2, 3)$ are defined in the nomenclature. The subcripts $w_o$ and $b_o$ indicate the tunnel and mounting axes, respectively, in the notation for vectors and transformations.

Suppose the box is mounted with its body axes aligned with the mounting axes and oriented at some attitude $(\psi_o, \alpha_o)$ in $D_o$, and the aerodynamic force and moment measured. If the box is now rotated about its longitudinal axis by any multiple of $90°$, or about its vertical axis by any multiple of $180°$ , the box appears identical to the flow and the resulting measurements are all identical to those at $(\psi_o, \alpha_o)$. For all these orientations the corresponding transformation to body axes (indicated by the subscript $b$) from mounting axes is

$$T_{b, b_o} = E_3(m\pi) E_1(n\pi/2) \qquad m, n = 0, \pm 1, \pm 2, \ldots \tag{3.2}$$

The wind axes associated with the rotated box (indicated by the subscript, $w_1$) are, by definition, oriented with the longitudinal axis in the free-stream direction and the vertical axis in the body vertical plane; consequently, the transformations from tunnel and body axes can be written, respectively, as

$$T_{w, w_o} = E_1(\phi_w) \tag{3.3a}$$

$$T_{b, w} = E_2(\alpha_1) E_3(\psi_1) \tag{3.3b}$$

The angles $\phi_w, \alpha_1$ and $\psi_1$ are shown in the figure 3.2. Since $\underline{i}_w$ and $\underline{i}_{w_o}$ are parallel to $\underline{V}_a$, then tunnel and wind axes are related by a roll rotation about $\underline{V}_a$, which is denoted $\phi_w$ here. Since $\underline{k}_w$ is in the body vertical plane then only two angles are required to locate wind axes relative to body axes, and these are taken as the usual angle of attack and (negative) sideslip angle as shown in the sketch. If the body axes are aligned with the mounting axes $((m,n)=(0,0))$ then wind axes coincide with tunnel axes, $\phi_w = 0$, and $(\psi_1, \alpha_1) = (\psi_o, \alpha_o)$, but this does not occur otherwise.

Equations 3.1 to 3.3 can be combined to equate transformations between wind and body axes:

$$T_{b, w} = T_{b, b_o} T_{b_o, w_o} T_{w_o, w}$$

from which the general equation for the attitudes $(\phi_w, \psi_1, \alpha_1)$ which have measurements identical to those at $(\psi_o, \alpha_o)$ is;

$$E_2(\alpha_1) E_3(\psi_1) E_1(\phi_w) = E_3(m\pi) E_1(n\pi/2) E_2(\alpha_o) E_3(\psi_o) \qquad m, n = 0, \pm 1, \pm 2, \ldots \tag{3.4}$$

Equation 3.4 yields nine scalar equations of which only five are independent. A convenient set of five equations used in this work is given in figure 3.3. For each case (m,n) two solutions for

WIND AND BODY AXES          WIND AND TUNNEL AXES
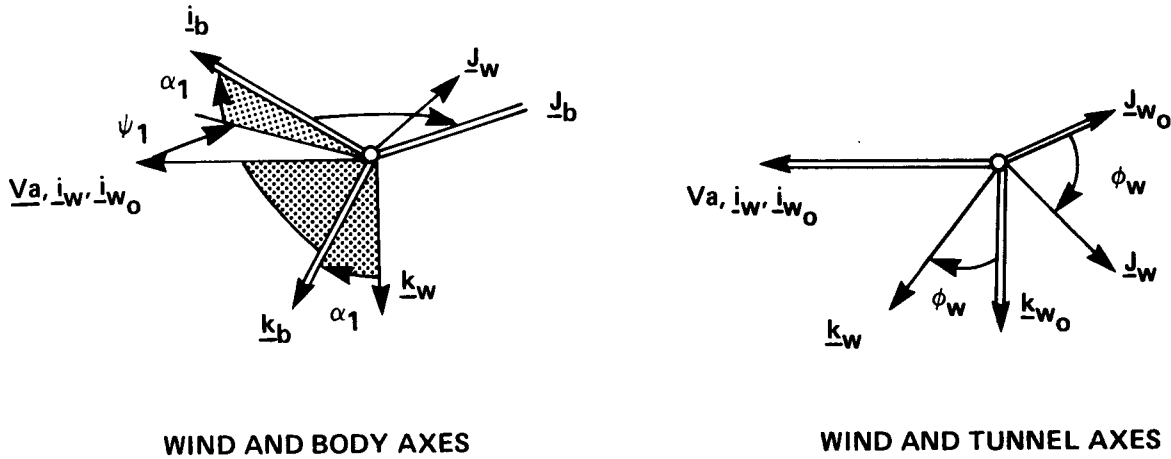
Figure 3.2.- Angles relating reference frames.

$(\phi_w, \psi_1, \alpha_1)$ are obtained. Taking all cases together, only three yield distinct solutions and these are included in figure 3.3. For each point $(\psi_o, \alpha_o)$ in $\mathcal{D}_o$ a single corresponding point in each quadrant is obtained, and, conversely, every point $(\psi_1, \alpha_1)$ in $\mathcal{D}$ is related to a single point in $\mathcal{D}_o$ by equation 3.4.

The force and moment components in wind axes are obtained from the tunnel measurements by the transformation $T_{w,w_o}$. Using the notation $D, Y, L, RM, PM$ and $YM$ to denote the customary wind axes force and moment components, and recalling that drag and lift are positive along the negative longitudinal and vertical wind axes, then

$$\begin{pmatrix} D \\ Y \\ L \end{pmatrix}_{(\psi_1,\alpha_1)} = E_1(-\phi_w) \begin{pmatrix} D \\ Y \\ L \end{pmatrix}_{(\psi_o,\alpha_o)} = \begin{pmatrix} D \\ Y\cos\phi_w - L\sin\phi_w \\ Y\sin\phi_w + L\cos\phi_w \end{pmatrix}_{(\psi_o,\alpha_o)} \qquad (3.5a)$$

$$\begin{pmatrix} RM \\ PM \\ YM \end{pmatrix}_{(\psi_1,\alpha_1)} = E_1(\phi_w) \begin{pmatrix} RM \\ PM \\ YM \end{pmatrix}_{(\psi_o,\alpha_o)} = \begin{pmatrix} RM \\ PM\cos\phi_w + YM\sin\phi_w \\ -PM\sin\phi_w + YM\cos\phi_w \end{pmatrix}_{(\psi_o,\alpha_o)} \qquad (3.5b)$$

## 3.2 Extrapolation from $\mathcal{D}_o$ to $\mathcal{D}$

The various cases $\{(m,n)\}$ in equations 3.4 and 3.5 suffice to relate the aerodynamics at any point in $\mathcal{D}$ to those at a corresponding point in $\mathcal{D}_o$. First, results for the case with 180° roll of the body axes relative to mounting angles $((m,n) = (0,2))$ relate the aerodynamics in $\mathcal{D}_2$ and $\mathcal{D}_3$

## EQUATIONS

$$\cos\alpha_1\cos\psi_1 = \cos m\pi \cos\alpha_o \cos\psi_o$$

$$\sin\psi_1 = -\cos m\pi\left(\sin n\tfrac{\pi}{2}\sin\alpha_o\cos\psi_o - \cos n\tfrac{\pi}{2}\sin\psi_o\right)$$

$$\sin\alpha_1\cos\psi_1 = \sin n\tfrac{\pi}{2}\sin\psi_o + \cos n\tfrac{\pi}{2}\sin\alpha_o\cos\psi_o$$

$$\cos\phi_w\cos\psi_1 = \cos m\pi\left(\sin n\tfrac{\pi}{2}\sin\alpha_o\sin\psi_o + \cos n\tfrac{\pi}{2}\cos\psi_o\right)$$

$$\sin\phi_w\cos\psi_1 = \cos m\pi \sin n\tfrac{\pi}{2}\cos\alpha_o$$

$$m, n = 0, \pm 1, \pm 2, \ldots$$

## SOLUTIONS

| Case: | m | 0 | 0 | 1 |
|---|---|---|---|---|
|  | n | 2 | 1 | 0 |
| First Sol'n: | $\phi_w$ | $0$ | $\cot^{-1}(\tan\alpha_o\sin\psi_o)$ | $0$ |
|  | $\psi_1$ | $-180° + \psi_o$ | $-\sin^{-1}(\sin\alpha_o\cos\psi_o)$ | $-180° + \psi_o$ |
|  | $\alpha_1$ | $180° - \alpha_o$ | $\tan^{-1}(\tan\psi_o/\cos\alpha_o)$ | $-\alpha_o$ |
| Second Sol'n: | $\phi_w$ | $180°$ | $-180° + \cot^{-1}(\tan\alpha_o\sin\psi_o)$ | $180°$ |
|  | $\psi_1$ | $-\psi_o$ | $-180° + \sin^{-1}(\sin\alpha_o\cos\psi_o)$ | $-\psi_o$ |
|  | $\alpha_1$ | $-\alpha_o$ | $-180° + \tan^{-1}(\tan\psi_o/\cos\alpha_o)$ | $180° - \alpha_o$ |

Figure 3.3.- Box attitudes with identical measured aerodynamics.

with those in $\mathcal{D}_1$ and $\mathcal{D}_o$, respectively:

$$
\begin{pmatrix} D \\ Y \\ L \\ RM \\ PM \\ YM \end{pmatrix}_{(-\psi,-\alpha)} = \begin{pmatrix} D \\ -Y \\ -L \\ RM \\ -PM \\ -YM \end{pmatrix}_{(\psi,\alpha)} \qquad (\psi,\alpha) \in \mathcal{D}_o, \mathcal{D}_1 \tag{3.6}
$$

That is, each component is either symmetric or antisymmetric about the origin of $\mathcal{D}$ along any radial line through the origin.

Second, results for the case with 90° roll of the body axes ($(m,n) = (0,1)$) define the aerodynamics in $\mathcal{D}_1$ from those in $\mathcal{D}_o$;

$$
\begin{pmatrix} D \\ Y \\ L \\ RM \\ PM \\ YM \end{pmatrix}_{(\psi_1,\alpha_1)} = \begin{pmatrix} D \\ \cos\phi_w Y - \sin\phi_w L \\ \sin\phi_w Y + \cos\phi_w L \\ RM \\ \cos\phi_w PM + \sin\phi_w YM \\ -\sin\phi_w PM + \cos\phi_w YM \end{pmatrix}_{(\psi,\alpha)} \qquad (\psi,\alpha) \in \mathcal{D}_o \tag{3.7}
$$

where

$$
\cot\phi_w = \tan\alpha \sin\psi = \tan\alpha_1 \sin\psi_1 \qquad \phi_w \in [0,90°]
$$

$$
\sin\psi_1 = -\sin\alpha \cos\psi \qquad \psi_1 \in [-90°,0]
$$

$$
\tan\alpha_1 = \tan\psi/\cos\alpha \qquad \alpha_1 \in [0,90°]
$$

Maps of $(\phi_w, \psi_1, \alpha_1)$ over $\mathcal{D}_o$ are given in figure 3.4. The wind axes roll angle varies from 90° on the boundaries $\alpha = 0$ and $\psi = 0$ to 0 on the boundary $\alpha = 90°$. Referring to the figure 3.5, the points $p_o$ and $p_1$ are equivalent; the region $\mathcal{R}_o$ in $\mathcal{D}_o$ is equivalent to the region $\mathcal{R}_1$ in $\mathcal{D}_1$ (the left boundary of $\mathcal{R}_1$ is equivalent to the line $\alpha = 45°$ and is given by $\tan\psi_1 = -\cos\alpha_1$); and their complement regions $\overline{\mathcal{R}}_o$, $\overline{\mathcal{R}}_1$, are equivalent. Further, the lines $\alpha = 0$ and $\psi = 0$ are equivalent (this particular equivalence has been recognized frequently in the literature), and the line $\psi = 90°$ is equivalent to the single point $(\psi_1, \alpha_1) = (0, 90°)$ so that the aerodynamic components are necessarily fixed on this line independent of $\alpha$.

Third, the case with a reversal of box heading ($(m,n) = (1,0)$) relates points in $\mathcal{D}_4, \mathcal{D}_5, \mathcal{D}_6$ and $\mathcal{D}_7$ to points in $\mathcal{D}_1, \mathcal{D}_3, \mathcal{D}_2$ and $\mathcal{D}_o$, respectively:

$$
\begin{pmatrix} D \\ Y \\ L \\ RM \\ PM \\ YM \end{pmatrix}_{(-180+\psi,-\alpha)} = \begin{pmatrix} D \\ Y \\ L \\ RM \\ PM \\ YM \end{pmatrix}_{(\psi,\alpha)} \qquad |\psi| < 90° \tag{3.8}
$$

16

(a) $\phi_w(\psi, \alpha)$: ROLL ANGLE FROM TUNNEL TO WIND AXES

(b) $(\psi_1, \alpha_1)$: EQUIVALENT POINTS IN $\mathcal{D}_0, \mathcal{D}_1$
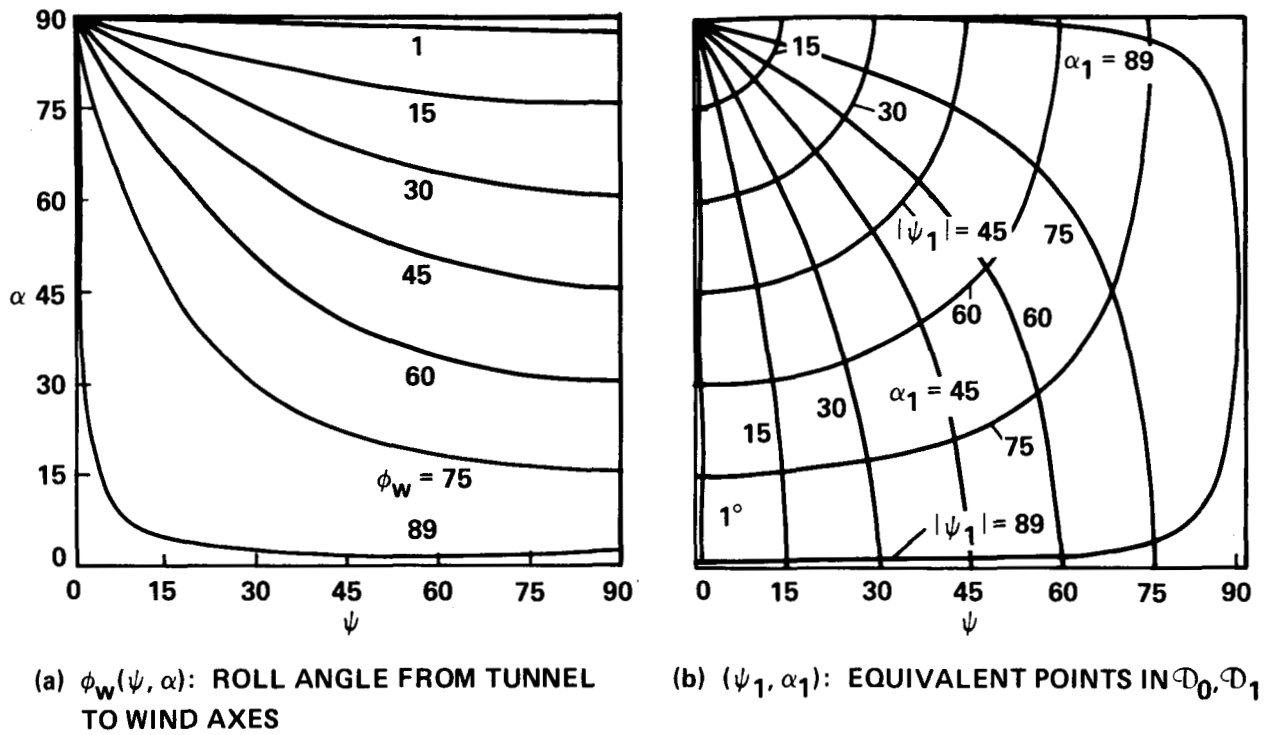
Figure 3.4.- Equivalent points in $\mathcal{D}_0$ and $\mathcal{D}_1$.
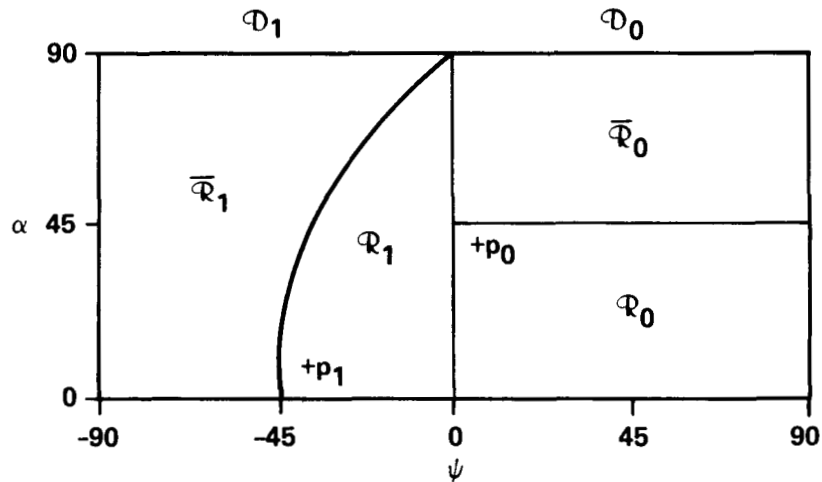


Figure 3.5.- Equivalent regions of $\mathcal{D}_0$ and $\mathcal{D}_1$.

Equations 3.6 to 3.8 define the aerodynamics at any point in $\mathcal{D}$ from measurements at a corresponding point in $\mathcal{D}_o$. However, the available measurements are confined to the lower half of $\mathcal{D}_o$, and equation 3.4 does not relate pairs of points within $\mathcal{D}_o$ nor provide a relation between every point in $\mathcal{D}$ and a point in $\mathcal{R}_o$. Additional symmetry properties of the box are considered next to obtain a relation between points in $\mathcal{D}_o$.

17

## 3.3 Symmetry Assumptions, Boundary Values, and the Equivalence of Measurements at Points within $\mathcal{D}_o$

Next, the following symmetry properties at the boundary between $\mathcal{D}_o$ and $\mathcal{D}_1$ (at $\psi = 0$) are assumed:

$$
\left.
\begin{array}{ll}
A1. & \mathcal{D} \text{ is symmetric in } \psi \text{ about } \psi = 0 \\
A2. & Y, YM \text{ are antisymmetric in } \psi \text{ about } \psi = 0 \\
A3. & RM \text{ is antisymmetric in } \psi \text{ about } \psi = 0
\end{array}
\right\} \qquad (3.9)
$$

Properties A1 and A2 are consistent with the available wind tunnel data and usually (but not always) characterize flow around a body which is symmetric about its vertical plane. The symmetry of $RM$ is less obvious a priori. It can be shown from equations 3.6 and 3.7 that a symmetric and an antisymmetric function have distinctly different properties at the boundaries of $\mathcal{R}_o$ and within $\mathcal{R}_o$. The Ames roll-moment data are not consistent with either symmetry, but data from both reference 4 and 6 in appendices B and C show that it is antisymmetric and this is assumed here. It follows from equation 3.7 and property A2 above that $L$ and $PM$ are necessarily symmetric about this boundary, so that the complete symmetry properties about $\psi = 0$ are:

$$
\begin{pmatrix} D \\ Y \\ L \\ RM \\ PM \\ YM \end{pmatrix}_{(-\psi,\alpha)}
=
\begin{pmatrix} D \\ -Y \\ L \\ -RM \\ PM \\ -YM \end{pmatrix}_{(\psi,\alpha)}
\qquad (\psi,\alpha) \in \mathcal{D}_o \qquad (3.10)
$$

Symmetry about the $\mathcal{D}_o - \mathcal{D}_2$ boundary (about $\alpha = 0$) is obtained by combining equations 3.6 and 3.10;

$$
\begin{pmatrix} D \\ Y \\ L \\ RM \\ PM \\ YM \end{pmatrix}_{(\psi,-\alpha)}
=
\begin{pmatrix} D \\ Y \\ -L \\ -RM \\ -PM \\ YM \end{pmatrix}_{(\psi,\alpha)}
\qquad (\psi,\alpha) \in \mathcal{D}_o \qquad (3.11)
$$

Naturally, the force and moment components are zero at the boundaries about which they are antisymmetric, assuming continuity of the static aerodynamics throughout $\mathcal{D}$.

The aerodynamics at pairs of points within $\mathcal{D}_o$ can now be related. Referring to figure 3.6a, if $(\psi, \alpha)$ is any point in $\mathcal{D}_o$, and $(-\psi_1, \alpha_1)$ is its equivalent point in $\mathcal{D}_1$ from equation 3.7, then a relation between the aerodynamics at $(\psi, \alpha)$ and $(\psi_1, \alpha_1)$ is obtained by combining equation 3.7 and 3.10;

$$
\begin{pmatrix} D \\ Y \\ L \\ RM \\ PM \\ YM \end{pmatrix}_{(\psi_1,\alpha_1)}
=
\begin{pmatrix} D \\ -\cos\phi_w Y + \sin\phi_w L \\ \sin\phi_w Y + \cos\phi_w L \\ -RM \\ \cos\phi_w PM + \sin\phi_w YM \\ \sin\phi_w PM - \cos\phi_w YM \end{pmatrix}_{(\psi,\alpha)}
\qquad (\psi,\alpha) \in \mathcal{D}_o \qquad (3.12)
$$

18

where

$$\cot \phi_w = \tan \alpha \sin \psi = \tan \alpha_1 \sin \psi_1 \qquad \phi_w \in [0, 90°]$$
$$\sin \psi_1 = \sin \alpha \cos \psi \qquad \psi_1 \in [0, 90°]$$
$$\tan \alpha_1 = \tan \psi / \cos \alpha \qquad \alpha_1 \in [0, 90°]$$

Points related by equation 3.12 are termed "equivalent" hereafter. This relation is identical to that plotted in figure 3.5, except that values of $\psi_1$ are now positive. Referring to figure 3.6b, the regions $\mathcal{R}_2$ and $\overline{\mathcal{R}}_2$ are separated by the line of self-equivalent points (the line for which $(\psi_1, \alpha_1) = (\psi, \alpha)$ in eq. 3.12) given by

$$\psi^*(\alpha) = \tan^{-1}(\sin \alpha) \qquad \alpha \in [0, 90°] \tag{3.13}$$

Each point in $\mathcal{R}_2$ is equivalent to a point in $\overline{\mathcal{R}}_2$ and conversely. Therefore, the aerodynamics at any point in $\mathcal{D}_o$ (and any point in $\mathcal{D}$) can be given from the aerodynamics at a corresponding point in $\mathcal{R}_2$. Further, the left half of $\mathcal{D}_o$ (the region, $\psi \leq 45°$) contains $\mathcal{R}_2$ and is more than sufficient to define the aerodynamics throughout $\mathcal{D}$.

The available measurements are in the lower half of $\mathcal{D}_o$ (the region $\alpha \leq 45°$). This region is equivalent to the region $\mathcal{R}_1$ (fig. 3.6c) whose interior boundary is equivalent to the line $\alpha = 45°$ and is given from equation 3.12 by

$$\psi^{(45)}(\alpha) = \tan^{-1}(\cos \alpha), \qquad \alpha \in [0, 90°] \tag{3.14}$$

Unfortunately, this encloses only about one-third of the region $\alpha > 45°$ for which we have no measurements.

The boundaries of $\mathcal{R}_o, \mathcal{R}_1$ and $\mathcal{R}_2$ subdivide $\mathcal{D}_o$ into six regions, and it is useful for the analysis to denote these separately as shown in figure 3.6d. The figure includes formal definitions of these regions for use in the calculations of the next section. The region of measurements, $\mathcal{R}_o$, is subdivided into $S_1, S_2$ and $S_3$. Each point in $S_1$ is equivalent to a point in $S_2$ and the converse is true. Measurements at equivalent points within these two regions can be compared for their agreement with equation 3.12 and discrepancies are presumed to be due to measurement errors. Each point in $S_4$ is equivalent to a point in $S_3$ so that measurements in $S_3$ will provide measurements of the aerodynamics at corresponding points in $S_4$. Last, $S_5$ and $S_6$ are mutually equivalent, and the aerodynamics in these regions cannot be given from measurements in $\mathcal{R}_o$ using equation 3.12. Thus, the symmetry properties represented by equations 3.4, 3.5, and 3.8 are insufficient to define the aerodynamics everywhere in $\mathcal{D}$ from those in $\mathcal{R}_o$.

Although the aerodynamics in $S_5$ and $S_6$ cannot be determined from measurements in $\mathcal{R}_o$, the theory and data provide values along the boundaries of $S_5$ and $S_6$ and an equivalence relation which must be satisfied by any approximate model of the aerodynamics for this region.

Symmetry about the $\mathcal{D}_o$ - $\mathcal{D}_5$ boundary (about $\psi = 90°$) can be obtained by combining equation 3.8, which relates points in $\mathcal{D}_3$ and $\mathcal{D}_5$, with equation 3.6, which relates points in $\mathcal{D}_3$ and

**(a) EQUIVALENT POINTS IN $\mathcal{D}_0$**

$$\sin \psi_1 = \sin\alpha \cos\psi$$
$$\tan \alpha_1 = \tan\psi/\cos\alpha$$

**(b) THE LINE OF SELF-EQUIVALENT POINTS**

$$\psi^* = \tan^{-1}(\sin\alpha) \qquad \alpha \in [0, 90°]$$
$$\mathcal{R}_2 \triangleq \{(\psi, \alpha): \psi \in [0, \psi^*(\alpha)], \alpha \in [0, 90°]\}$$

**(c) $\mathcal{R}_1$: REGION EQUIVALENT TO $\mathcal{P}_0$**

$$\psi^{(45)} = \tan^{-1}(\cos\alpha) \qquad \alpha \in [0, 90°]$$
$$\mathcal{R}_1 \triangleq \{(\psi, \alpha) \quad \psi \in [0, \psi^{(45)}(\alpha)], \alpha \in [0, 90°]\}$$

**(d) SUBDIVISION OF $\mathcal{D}_0$ FOR EXTRAPOLATION CALCULATIONS**

$$S_1 \triangleq \{(\psi, \alpha): \psi \in [0, \psi^*(\alpha)], \alpha \in [0, 45°]\}$$
$$S_2 \triangleq \{(\psi, \alpha): \psi \in [\psi^*(\alpha), \psi^{(45)}(\alpha)], \alpha \in [0, 45°]\}$$
$$S_3 \triangleq \{(\psi, \alpha): \psi \in [\psi^{(45)}(\alpha), 90°], \alpha \in [, 45°]\}$$
$$S_4 \triangleq \{(\psi, \alpha): \psi \in [0, \psi^{(45)}(\alpha)], \alpha \in [45°, 90°]\}$$
$$S_5 \triangleq \{(\psi, \alpha): \psi \in [\psi^{(45)}(\alpha), \psi^*(\alpha)], \alpha \in [45°, 90°]\}$$
$$S_6 \triangleq \{(\psi, \alpha): \psi \in [\psi^*(\alpha), 90°], \alpha \in [45°, 90°]\}$$
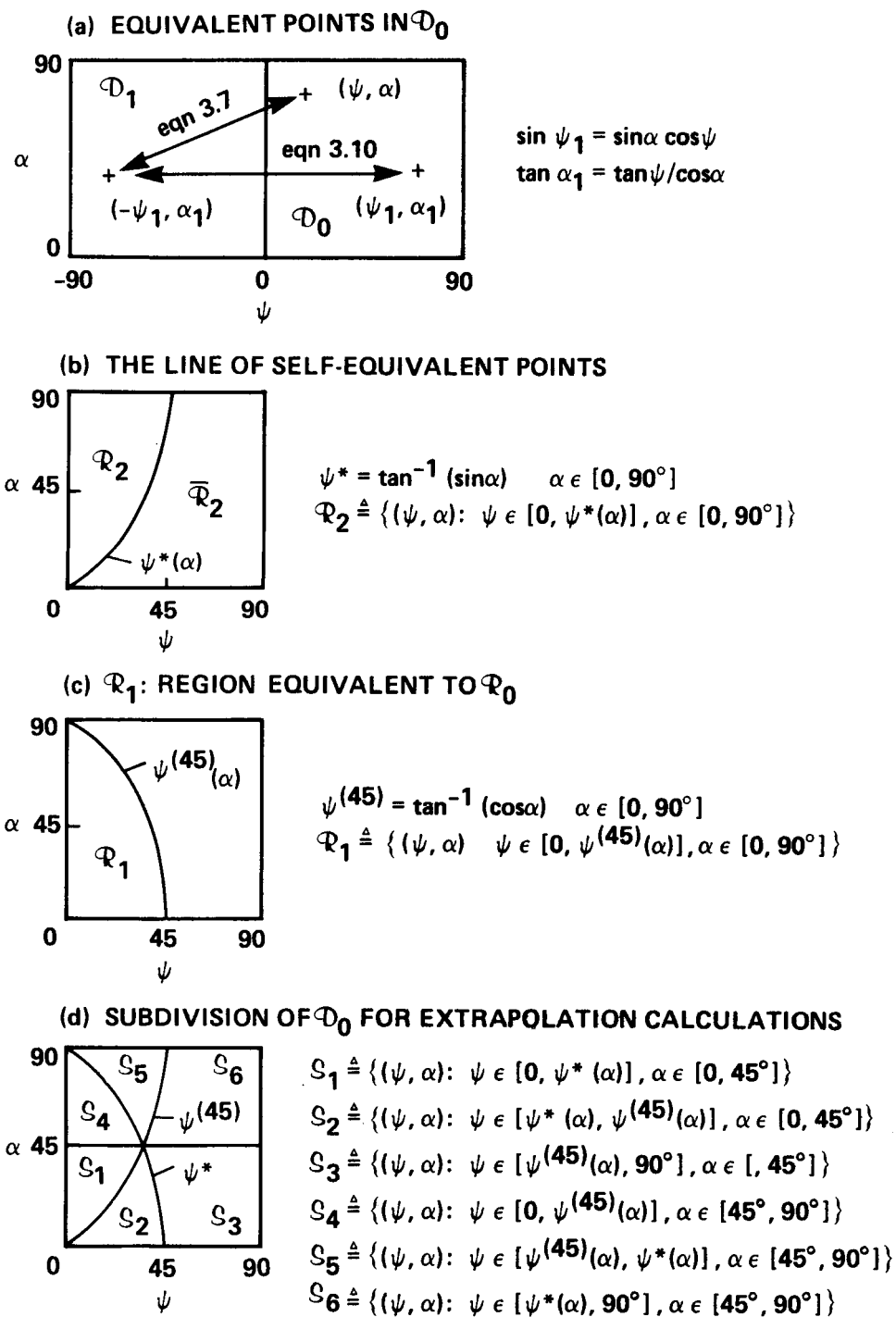
Figure 3.6.- Equivalent points and regions in $\mathcal{D}_0$.

$\mathcal{D}_o$;

$$\begin{pmatrix} D \\ Y \\ L \\ RM \\ PM \\ YM \end{pmatrix}_{(90-\Delta\psi,\alpha)} = \begin{pmatrix} D \\ -Y \\ -L \\ RM \\ -PM \\ -YM \end{pmatrix}_{(90+\Delta\psi,\alpha)} \qquad (3.15)$$

$Y, L, PM$ and $YM$ are antisymmetric in $\psi$ about $\psi = 90°$ and, therefore, zero on this boundary, while $D$ and $RM$ are symmetric. As previously noted with equation 3.7, all components are constant on this boundary; since $RM(90°, 0°) = 0$ (equation 3.11) we have

$$Y = L = RM = PM = YM = 0 \qquad at \quad \psi = 90° \qquad (3.16a)$$

$$D = D(90°, 0°) \qquad at \quad \psi = 90° \qquad (3.16b)$$

Last, symmetry about the boundary, $\alpha = 90°$, can be obtained by combining equation 3.10, which relates points in $\mathcal{D}_1$ and $\mathcal{D}_o$, with the second solution of equation 3.4 for the case $(m, n) = (1, 0)$, which relates points in $\mathcal{D}_1$ to points in the quadrant $(\psi, \alpha) \in [0°, 90°] * [90°, 180°]$;

$$\begin{pmatrix} D \\ Y \\ L \\ RM \\ PM \\ YM \end{pmatrix}_{(\psi, 90-\Delta\alpha)} = \begin{pmatrix} D \\ Y \\ -L \\ -RM \\ -PM \\ YM \end{pmatrix}_{(\psi, 90+\Delta\alpha)} \qquad (3.17)$$

The antisymmetric components, $L, RM$ and $PM$ are zero at $\alpha = 90°$. An evaluation of equation 3.12 on this boundary indicates that the symmetric components, $D, Y$ and $YM$ are either symmetric or antisymmetric in $\psi$ about $\psi = 45°$:

$$\left. \begin{array}{l} L = RM = PM = 0 \\ \\ \begin{pmatrix} D \\ Y \\ YM \end{pmatrix}_{(45-\Delta\psi)} = \begin{pmatrix} D \\ -Y \\ -YM \end{pmatrix}_{(45+\Delta\psi)} \qquad at \quad \alpha = 90° \end{array} \right\} \qquad (3.18)$$

Thus, $Y$ and $YM$ are zero at $\psi \in \{0, 45°, 90°\}$ along this boundary.

### 3.4 Summary

The geometric symmetry of the box results in a set of attitudes $\{(\psi_i, \alpha_i)\}$ corresponding to rotations of the box in the tunnel for which the measured aerodynamic components are identical or differ only by a sign (eqs. 3.4, 3.5 and 3.9). This permits determination of the aerodynamics at any point in the set from measurements at one point, and at any point in $\mathcal{D}$ from measurements at a corresponding point in $\mathcal{D}_o$ (eqs. 3.6, 3.7 and 3.8 or eqs. 3.8, 3.10 and 3.11), or at a corresponding point in the smaller region within $\mathcal{D}_o$ given by $0 \leq \psi \leq 45°$ (eqs. 3.8, 3.10 and 3.12).

Measurements confined to the region within $\mathcal{D}_o$ given by $0 \leq \alpha \leq 45°$ do not suffice to define the aerodynamics throughout $\mathcal{D}$; the aerodynamics at any point in $\mathcal{R}_o$ or $\mathcal{S}_4$ (fig. 3.6) and its related region in each other quadrant can be obtained from such measurements, but not at any point in $\mathcal{S}_5$ or $\mathcal{S}_6$ (fig. 3.6) and their related regions.

The exact aerodynamics and any model constructed from the available measurements must satisfy equation 3.12 and the zero boundary values specified by equations 3.10, 3.11, 3.16 and 3.18; that is, in $\mathcal{D}_o$;

$$
\left.
\begin{array}{ll}
1. & D \text{ satisfies equation 3.12.} \\
2. & L \text{ and } Y \text{ satisfy equation 3.12 and} \\
& Y = 0 \text{ if } \psi = 0 \text{ or } 90°, \\
& L = 0 \text{ if } \alpha = 0 \text{ or } 90°, \text{ or } \psi = 90°. \\
3. & RM \text{ satisfies equation 3.12 and} \\
& RM = 0 \text{ if } \psi = 0 \text{ or } 90°, \text{ or } \alpha = 0 \text{ or } 90°, \text{ or } \tan \psi = \sin \alpha. \\
4. & PM \text{ and } YM \text{ satisfy equation 3.12 and} \\
& PM = 0 \text{ if } \alpha = 0 \text{ or } 90° \text{ or } \psi = 90°, \text{ and} \\
& YM = 0 \text{ if } \psi = 0 \text{ or } 90°.
\end{array}
\right\} \qquad (3.19)
$$

The measurements of reference 3 are reviewed in the next section for their degree of agreement with these conditions, revised as needed to satisfy equation 3.19, and then extrapolated consistent with equation 3.19 throughout $\mathcal{D}_o$ to provide a comprehensive estimate of the box aerodynamics.

# 4. REVISION AND EXTRAPOLATION OF THE WIND TUNNEL DATA

The object of this section is to estimate the MILVAN's static aerodynamics throughout $D_0$ by fitting the Ames wind tunnel data in $R_0$ (fig. 2.2) to the theoretical model of the previous section. This is done by: 1) revising the data tables in $R_o$ to satisfy the theoretical equivalence relations and zero force and moment lines (eqs. 3.12 and 3.19); 2) extending this fit to $S_4$ using equation 3.12; and 3) defining approximation functions in $S_5$ and $S_6$ which satisfy the known boundary values from equation 3.19 and the previous two steps, and the equivalence relations (eq. 3.12), and whose functional behavior is smooth at the boundary with $S_3$ and $S_4$ and simple within $S_5$ and $S_6$. The results are given as new data tables which span $D_o$ and fit the theoretical model.

The Ames data in $R_o$ do not exactly satisfy equations 3.12 and 3.19. The discrepancies, which are large for some components, can result from measurement errors or differences between the assumptions underlying the theory and the test conditions. However, in all cases there is sufficient evidence from the Ames data or from independent wind tunnel tests (refs. 4-6) to show that the MILVAN's aerodynamics agree closely with the theory. Therefore, all significant discrepancies are assumed to be due to measurement errors and the estimate in $R_o$ is obtained by revising the data to fit the theoretical model. These revisions are small for drag, sideforce, and yaw moment, moderate for lift, and the roll- and pitching- moment data are entirely discarded and replaced by estimates obtained from independent data (roll) or from the remaining data and the theory (pitch). The resulting estimates are all compared with the available independent wind tunnel data, and good to fair agreement is obtained.

An analysis sufficient to identify the systematic and random tunnel errors in measuring forces, moments, and attitude angles or the data processing errors, which might account for the principal differences between the Ames data and the theory, is beyond our scope. The original tunnel records are no longer available for such an analysis nor was there any opportunity for further tunnel tests. In several cases, systematic measurement errors consistent with the observed discrepancies along the theoretical zero lines are noted as an aid to selecting plausible global behavior of the correction functions, but very little can be concluded from the data alone regarding actual error sources.

## 4.1 Drag

The drag data can be tested for their agreement with equation 3.12 over the regions $S_1$ and $S_2$ by calculating the difference between measurements at equivalent points:

$$\delta D(\psi, \alpha) = DC(\psi, \alpha) - DC(\psi_1, \alpha_1) \qquad (\psi, \alpha) \in S_1 \text{ or } S_2 \qquad (4.1)$$

where:
$$\sin \psi_1 = \sin \alpha \cos \psi$$
$$\tan \alpha_1 = \tan \psi / \cos \psi$$

and $DC$ is the corrected wind tunnel data from figure 2.2. These differences (fig. 4.1) are small everywhere in $S_1$ and $S_2$ with a maximum value corresponding to 5% of the measured drag.

An estimate of the drag in $S_1$ and $S_2$ which satisfies equation 3.12 is obtained by averaging the data at equivalent points:

$$\hat{D}(\psi, \alpha) = 0.5(DC(\psi, \alpha) + DC(\psi_1, \alpha_1)) \qquad (\psi, \alpha) \in S_1 \text{ or } S_2 \qquad (4.2)$$

23

This revises the drag data only slightly $(DC - \widehat{D} = 0.5\delta D)$.

To examine the appearance of measurement errors in these revisions first express the data, $DC$, as the sum of the actual drag, $D$, and the drag measurement error, $\widetilde{DC}$, and then obtain:

$$\left.\begin{aligned}
\widehat{D}(\psi, \alpha) &= D(\psi, \alpha) + 0.5(\widetilde{DC}(\psi, \alpha) + \widetilde{DC}(\psi_1, \alpha_1)) \\
\delta D(\psi, \alpha) &= \widetilde{DC}(\psi, \alpha) - \widetilde{DC}(\psi_1, \alpha_1)
\end{aligned}\right\} \tag{4.3}$$

Thus, $\widehat{D}$ retains the average measurement error at the two equivalent points while $\delta D$ is their difference. This difference is also a lower bound on measurement errors;

$$0.5|\delta D(\psi, \alpha)| \leq max\{|\widetilde{DC}(\psi, \alpha)|, |\widetilde{DC}(\psi_1, \alpha_1)|\} \tag{4.4}$$

Thus, the measurement errors are at least as large as $\delta D/2$ , and small values of $\delta D$ admit small errors, but do not preclude a large table bias or average error. However, a comparison of the drag estimate, $\widehat{D}$, with independent data from references 4-6 in figure 4.2 show only small differences which indicate the probable size of the measurement errors and the effects of differences in surface details of the wind tunnel models. A more comprehensive comparison with the data from reference 6 is made in appendix B (fig. B3) and shows similar good agreement throughout $\mathcal{R}_0$. Further, the data from references 4-6 were taken at negative heading so that these comparisons also confirm the symmetry of drag with $\psi$ about $\psi = 0$.

An estimate of the drag in $S_3$ and $S_4$ which satisfies equation 3.12 is obtained by averaging the drag measurements at $\psi = 90°$, denoted $\overline{D}_{90}$, and then

$$\widehat{D}(\psi, \alpha) = \begin{cases} DC(\psi, \alpha) & (\psi, \alpha) \in S_3 \quad \psi \neq 90° \\ \overline{D}_{90} & \psi = 90° \\ DC(\psi_1, \alpha_1) & (\psi, \alpha) \in S_4 \end{cases} \tag{4.5}$$

Note that the drag measurements (fig. 2.2) are very nearly constant at $\psi = 90°$, as expected from equation 3.12, and averaging to impose this boundary condition revises the data negligibly.

Last, drag must be extrapolated over $S_5$ and $S_6$ subject to equation 3.12. Consider, first, an extrapolation based on the theory that the drag of bluff bodies varies principally in proportion to the cross-sectional area of separated flow. This area is estimated here as the box area projected on the plane perpendicular to the air velocity vector:

$$A_p/S \equiv 0.4|\cos\psi\cos\alpha| + |\cos\psi\sin\alpha| + |\sin\psi| \tag{4.6}$$

where $S$ is the side area, $160ft^2$. A plot of the measurements versus $A_p$ (fig. 4.3) shows good correlation at low values of $A_p$ but much larger spread in the data at high values, and is nonlinear. However, when plotted versus the angle between the velocity vector and the box longitudinal axis;

$$\xi \equiv (\dot{\imath}_{w_o}, \dot{\imath}_{b_1}) = \cos^{-1}(\cos\psi\cos\alpha) \tag{4.7}$$

24

better correlation is obtained (fig. 4.3b). Thus, the drag measurements can be fitted with a monotonic function versus $\xi$ with moderate discrepancies, and this fit can be extrapolated to a global model for drag in only one variable;

$$\widehat{D}(\psi, \alpha) = \overline{D}(\xi(\psi, \alpha)) \qquad (\psi, \alpha) \in \mathcal{D}_0$$

where $\overline{D}(\xi)$ is the fitted function. It can be shown that both $A_p$ and $\xi$ are invariant at equivalent points $(A_p(\psi, \alpha) = A_p(\psi_1, \alpha_1)$ and $\xi(\psi, \alpha) = \xi(\psi_1, \alpha_1))$ so that global models obtained by fitting the data to either variable would satisfy equation 3.12.

The following estimate of drag over $S_5$ and $S_6$ is adopted based on the measured drag versus $\xi$ along the boundary $\alpha = 45°$;

$$\widehat{D}(\psi, \alpha) = \widehat{D}(\overline{\psi}(\psi, \alpha), 45) \qquad (\psi, \alpha) \in S_5 \text{ or } S_6 \tag{4.8}$$

where

$$\overline{\psi}(\psi, \alpha) = \cos^{-1}(\sqrt{2}\cos\xi(\psi, \alpha))$$

Here, $\widehat{D}(\psi, 45)$, $\xi$ are defined in equations 4.5 and 4.7 above, and $\overline{\psi}$ is an inversion of equation 4.7 at $\alpha = 45°$. This extrapolation satisfies equation 3.12 since it is a function of $\xi$ only. Further, it is continuous and "smooth" at the boundaries with $S_3$ and $S_4$ (that is, $\widehat{D}$ in eq. 4.8 matches $\widehat{D}$ in eq. 4.5 at these boundaries, and the functional behavior of $\widehat{D}$ does not change abruptly at these boundaries as can be seen in the contour plot in fig. 4.4), and the extrapolation assigns values which are within the range of the measured drag values.

The drag estimate defined by equations 4.2, 4.5 and 4.8 is given in figures 4.4 and 4.5. This estimate matches the measured behavior as closely as possible while satisfying equation 3.12.

## 4.2 Side force and lift

The side-force data and plots of figures 2.2 and 2.3 show small discrepancies from the expected zero crossings at the the boundaries, $\psi = 0, 90°$. These discrepancies are assumed to be measurement errors which are a sum of random and systematic errors in measuring angles and force. Plots of the data for these boundaries indicate they are systematic and qualitatively consistent with a bias of $1° - 2°$ in measuring yaw angle, $\Delta\psi$. This results in a side- force bias at the end points of the form; $b_y = \partial Y/\partial\psi\Delta\psi$. We assume these biases are continuous and affect measurements at other values of $\psi$, so a correction function, given as a linear combination of the end point discrepancies, is defined;

$$b_y(\psi, \alpha) = (1 - \frac{\psi}{90})\, YC(0, \alpha) + \frac{\psi}{90}\, YC(90, \alpha) \tag{4.9}$$

and then

$$YC1 = YC - b_y$$

This revision nulls $YC$ at $\psi = 0°$ and $90°$ and otherwise varies linearly in heading between its values at these end points. This variation approximately follows the variation of $\partial Y/\partial\psi$. A

comparison of the revised measurements with independent data from references 4-6 in figure 4.2 shows good numerical agreement at $\alpha = 0$, and a more comprehensive comparison in appendix B (fig. B4) shows good agreement throughout $\mathcal{R}_0$. This implies that the data from reference 3 do not contain a large systematic error at intermediate heading angles that was missed in the end-point data used to define the revision in equation 4.9.

The lift data in figures 2.2 and 2.3 show good agreement with the expected zero value at $\psi = 90°$, but agreement with the expected zero value along the $\alpha = 0$ boundary is poor; there the measured lift reaches $32Q$ lb at intermediate values of heading angle. This variation of measured lift with heading at $\alpha = 0$ is seen to be systematic and present consistently at $\alpha$ up to 30° in figure 2.3. It was noted that the box surfaces are not identical as assumed in the extrapolation theory of the previous section; the bottom, side, and front of the wind tunnel model were corrugated while the top and rear were smooth. This might result in a zero lift line different from $\alpha = 0$. However, reference 3 contains some data for a smooth-surfaced box which was compared with the data of figure 2.2 and shows the same variation of lift with $\psi$ at $\alpha = 0$ and generally small differences from the corrugated box lift over the region for which data are given. That is, the effect of the surface corrugation on lift is much smaller than the maximum lift measured at $\alpha = 0$. Further, data from reference 6 is available for both smooth and corrugated containers and these also show only small differences in lift, but good agreement with the expected zero-lift line at $\alpha = 0$ (appendix B, fig. B1). Finally, it is noted that the questionable lift variation in the Ames data was consistent with a sizeable systematic error in measuring angle of attack, $\Delta\alpha$, that is; the variation of lift at $\alpha = 0$ approximately follows the variation of $\partial L/\partial \alpha$ with yaw. A correction was defined from the nonzero boundary values as:

$$\left. \begin{array}{l} b_L(\psi, \alpha) = \frac{\psi}{90} LC(90, \alpha) + [LC(\psi, 0) - \frac{\psi}{90} LC(90, 0)](1 - \frac{\alpha}{45}) \\[2ex] LC1 = LC - b_L \end{array} \right\} \quad (4.10)$$

This revision nulls $LC$ at the boundaries $\psi = 90°$ and $\alpha = 0$. The second term varies linearly in $\alpha$ and approximately follows the variation of the lift slope, which declines monotonically with $\alpha$ to small values at $\alpha = 45°$. The resulting table of values of $LC1/Q$, contained small negative values, under 5 ft$^2$ , in the region $\psi > 60°$; these were assumed to be due to errors in estimating the systematic errors rather than present in the actual lift function, and were faired out of $LC1$ for the following calculations. The discrepancies from theoretical boundary values noted previously and the independent wind tunnel data suggest that lift is less accurately measured than side force in the Ames data.

The discrepancies between the revised data and values calculated from the data at the equivalent point are:

$$\begin{pmatrix} \delta Y \\ \delta L \end{pmatrix}_{(\psi, \alpha)} = \begin{pmatrix} YC1 \\ LC1 \end{pmatrix}_{(\psi, \alpha)} - \begin{pmatrix} -\cos\phi_w & \sin\phi_w \\ \sin\phi_w & \cos\phi_w \end{pmatrix} \begin{pmatrix} YC1 \\ LC1 \end{pmatrix}_{(\psi_1, \alpha_1)} \quad (4.11)$$

where $(\psi, \alpha) \in S_1$, $S_2$; $YC1, LC1$ are defined in equations 4.9, 4.10; and $(\psi_1, \alpha_1, \phi_w)$ are functions of $(\psi, \alpha)$ defined here and everywhere in this section by equation 3.12. A table of lift discrepancies is included in figure 4.1. The results show moderate discrepancies under $15Q$ at nearly

26

all gridpoints in $S_1$ and $S_2$. Plots of the two lift functions compared in equation 4.11 are given in figure 4.1c and show adequate agreement in curve shapes. The agreement of these data with equation 3.12 is somewhat poorer than for drag.

To abbreviate the notation hereafter, let $fc1, \hat{f}$, etc., be the two-dimensional force vectors $(YC1, LC1)^T$, $(\hat{Y}, \hat{L})^T$, etc., and let $U$ be the coefficient matrix for these components in equation 3.12 (repeated in eq. 4.11).

An estimate, $\hat{f}$, of these components which satisfies equation 3.19 can be given from $fc1$ by; 1) averaging $fc1$ at equivalent points in $S_1$ and $S_2$ to impose equation 3.12, 2) using equation 3.12 to define $\hat{f}$ in $S_4$ from $fc1$ in $S_3$, and by 3) interpolation of $\hat{f}$ in $S_5$, $S_6$, between its known values along the boundaries of this region, assuming linearity in $\alpha$, followed by averaging at equivalent points in $S_5$ and $S_6$ to impose equation 3.12;

$$\hat{f}(\psi, \alpha) = \begin{cases} 0.5(fc1(\psi, \alpha) + U\ fc1(\psi_1, \alpha_1)) & (\psi, \alpha) \in S_1,\ S_2 \\ fc1(\psi, \alpha) & (\psi, \alpha) \in S_3 \\ U\ fc1(\psi_1, \alpha_1) & (\psi, \alpha) \in S_4 \\ 0.5(fl(\psi, \alpha) + U\ fl(\psi_1, \alpha_1)) & (\psi, \alpha) \in S_5,\ S_6 \end{cases} \qquad (4.12)$$

where $fl$ is the linear function defined in $S_5$ and $S_6$ by;

$$fl(\psi, \alpha) = \hat{f}(\psi, \alpha_0) \frac{(90 - \alpha)}{(90 - \alpha_0)} \qquad (\psi, \alpha) \in S_5,\ S_6$$

$$\alpha_0 = \begin{cases} 45 & \psi \geq \psi^*(45) \\ \cos^{-1}(\tan(\psi)) & \psi < \psi^*(45) \end{cases}$$

Here, $\psi^*$ is defined by equation 3.13, $\psi^*(45°)$ corresponds to the meeting point of all regions $S_1 - S_6$ seen in figure 3.3, and $\{\alpha_0(\psi);\ 0 \leq \psi \leq 90°\}$ is the lower boundary of $S_5$ and $S_6$.

The estimate in $S_1$ and $S_2$ is obtained by averaging $fc1$ with the value calculated from $fc1$ at the equivalent point. The appearance of measurement errors in this estimate can be obtained by representing the revised data, $fc1$, as the sum of the exact force, $f$, and the error, $\widetilde{fc1}$, and then, assuming equation 3.12 is exact, $\hat{f}$ can be written as

$$\hat{f}(\psi, \alpha) = f(\psi, \alpha) + 0.5(\widetilde{fc1}(\psi, \alpha) + U\widetilde{fc1}(\psi_1, \alpha_1)) \qquad (\psi, \alpha) \in S_1,\ S_2 \qquad (4.13)$$

where $\hat{f}$ contains the average of the errors at the two points. Note that $U$ is orthogonal and does not change the magnitude of $\widetilde{fc1}(\psi_1, \alpha_1)$, but can distribute this magnitude in any ratio to the components $\hat{Y}$ and $\hat{L}$.

Alternatively, the estimate in $S_1$ and $S_2$ can be given solely from the side force data by solving equation 3.12 for $L(\psi, \alpha)$ in terms of $Y(\psi, \alpha)$, and $Y(\psi_1, \alpha_1)$;

$$\hat{Y}'(\psi, \alpha) = YC1(\psi, \alpha)$$

$$\hat{L}'(\psi, \alpha) = \cot \phi_w YC1(\psi, \alpha) + \csc \phi_w YC1(\psi_1, \alpha_1)$$

however, this lift estimate is ill-conditioned at small $\phi_w$, and the accuracy of $L'$ is degraded from the Y-measurement accuracy. An estimate based solely on the lift measurements can also be given analogously with a similar effect on estimation accuracy.

A comparison of the side force estimate at $\alpha = 0$ with independent data is included in figure 4.2, and a more comprehensive comparison of $\hat{f}$ with the data from reference 6 over the region $\mathcal{R}_0$ is given in appendix B (fig. B4). Good agreement is obtained for sideforce (differences are below $10Q$ at nearly all grid points). Lift differences are larger, in the range of $15Q$ to $30Q$ over much of $\mathcal{R}_0$, but these differences are the same size as the disagreement of the lift and side force data from reference 6 with equation 3.12, and are probably due primarily to lift measurement errors in the data from reference 6.

The extrapolation of $\hat{f}$ into $S_5$ and $S_6$ is carried out as follows. First, $\hat{f}$ is assumed zero on the upper boundary of $S_5$ and $S_6$ (at $\alpha = 90°$). For lift, this value is required by equation 3.18. For side force, this value is consistent with equation 3.18, which requires $Y = 0$ at the three points $\psi \in \{0, 45°, 90°\}$, and the expectation that $Y$ is small, if not zero, on this boundary. Second, $\hat{f}$ is known throughout $\mathcal{R}_0$ and $S_4$ from the measurements; this data can be plotted versus $\alpha$ and the resulting curve extrapolated to the known boundary value at $\alpha = 90°$ such that the extrapolation is both continuous and smooth at the lower boundary of $S_5$ and $S_6$. This first extrapolation does not necessarily satisfy equation 3.12, but equation 3.12 can be imposed by averaging the function with the value calculated from the function at the equivalent point. In the present computations $\hat{f}$ is extrapolated linearly in $\alpha$ and this was found sufficiently smooth and computationally convenient.

The estimates, $\hat{Y}$ and $\hat{L}$, defined by equations 4.9, 4.10 and 4.12 are given in figures 4.4 and 4.5. The maximum lift of the MILVAN occurs outside the domain of the original measurements and is predicted from the side-force data. Maximum values exceed $80Q$ lb at $\alpha = 60°$ and low values of $\psi$. The contour plots (fig. 4.4) show smoothly varying functional behavior throughout $\mathcal{D}_0$, and a comparison with the measurements plotted in figure 2.4 indicates that little qualitative change has been made to functional behavior over $\mathcal{R}_0$, while numerical changes are small for side force and more significant for lift, principally near $\alpha = 0$.

### 4.4 Roll moment

The roll moment data from references 4-6 (appendices B and C) indicate that $RM$ is an antisymmetric function and, in $\mathcal{R}_0$, it satisfies;

$$RM(\psi, \alpha) = -RM(\psi_1, \alpha_1)$$

$$RM = 0 \quad if \; \psi = 0, \; or \; \psi = 90°, \; or \; \alpha = 0$$

However, the Ames roll moment data (figs. 2.2-2.4) have large discrepancies from these properties. Large magnitudes occur along all boundaries where zero is expected, and the systematic trend versus $\psi$ to large negative values which occurs at $\alpha = 0$ is present at all $\alpha$.

To examine the symmetry of the Ames data further, the table can be separated over $S_1$ and $S_2$ into components which are symmetric and antisymmetric with respect to equation 3.12;

$$\left. \begin{array}{l} RMCS(\psi, \alpha) = 0.5(RMC(\psi, \alpha) + RMC(\psi_1, \alpha_1)) \\ RMCA(\psi, \alpha) = 0.5(RMC(\psi, \alpha) - RMC(\psi_1, \alpha_1)) \end{array} \right\} \tag{4.14}$$

28

where $RMCS$ and $RMCA$ are the symmetric and antisymmetric components of the data, $RMC$. Any arbitrary table of numbers can be separated in this way.

Assuming the exact function, $RM$, is antisymmetric and satisfies equation 3.12, the separation can be related to $RM$ and the measurement errors, $\widetilde{RMC}$, as follows

$$\left. \begin{array}{l} RMCS(\psi,\alpha) = 0.5(\widetilde{RMC}(\psi,\alpha) + \widetilde{RMC}(\psi_1,\alpha_1)) \\[2mm] RMCA(\psi,\alpha) = RM(\psi,\alpha) + 0.5(\widetilde{RMC}(\psi,\alpha) - \widetilde{RMC}(\psi_1,\alpha_1)) \end{array} \right\} \tag{4.15}$$

Here, $RMCS$ contains the average error, and $RMCA$ contains $RM$ and the antisymmetric component of the measurement errors. Note that a table bias $(\widetilde{RMC}(\psi,\alpha) \cong \widetilde{RMC}(\psi_1,\alpha_1))$ or nearly symmetric errors are self-canceling in $RMCA$.

The results (fig. 4.6) show that the measured antisymmetric function, $RMCA$, has large nonzero values to $100Q$ ft-lb along the boundaries, $\psi = 0$ and $\alpha = 0$, where zero is expected. Since these are among the largest values in the $RMCA$ table then $RMCA$ is predominantly the antisymmetric component of the measurement errors and any estimate of $RM$ from $RMCA$ would be completely uncertain, except for the zero values imposed by the theory. The average errors, $RMCS$, are also large, reaching $70Q$ ft-lb, and exceed the measured antisymmetric function at many points in the table. The average error is a lower bound on the measurement errors;

$$|RMCS(\psi,\alpha)| \leq max\{|\widetilde{RMC}(\psi,\alpha)|, \quad |\widetilde{RMC}(\psi_1,\alpha_1)|\} \tag{4.16}$$

Thus, the roll-moment data from reference 3 appear to be dominated by measurement errors.

Finally, we adopt the estimate

$$\widehat{RM}(\psi,\alpha) = 0 \qquad (\psi,\alpha) \in \mathcal{D}_0 \tag{4.17}$$

since 1) the data from reference 3 are uncertain, and 2) the data from reference 6 (appendix B) show much better agreement with the theory and indicate that roll moment is small throughout $\mathcal{R}_0$; therefore it will have little or no effect on load equilibrium and motion compared to the roll restoring torque exerted by a suspension.

### 4.5 Yaw and pitching moments

The yaw-moment data shows good agreement with its expected antisymmetry in $\psi$ about $\psi = 0$ and $90°$ (fig. 2.3). Numerical values (fig. 2.2) show moderate discrepancies from their expected zero values at these yaw angles. These appear to be systematic and were corrected similarly to the side-force data; the measurement errors were estimated as

$$b_{YM}(\psi,\alpha) = (1 - \frac{\psi}{90})YMC(0,\alpha) + \frac{\psi}{90}YMC(90,\alpha) \qquad (\psi,\alpha) \in \mathcal{R}_0 \tag{4.18}$$

and then

$$YMC1 = YMC - b_{YM}$$

This correction nulls $YMC$ at $\psi = 0$ and $90°$ and otherwise varies linearly between the apparent end-point errors. A comparison with data from references 4-6 at $\alpha = 0$ is included in figure 4.2 and shows good agreement in functional variation, with moderate numerical discrepancies (below $100Q$ ft-lb) among the three sources. A more comprehensive comparison with data from reference 6 in appendix B, figure B7, shows a similar degree of agreement throughout $\mathcal{R}_0$.

Pitching moment is predicted by the theory of section 3 to be antisymmetric in $\alpha$ about $\alpha = 0$, and in $\psi$ about $\psi = 90°$. The data in figures 2.2 and 2.3 show systematic departures from the predicted antisymmetries and large discrepancies from the predicted zero values along these boundaries. These discrepancies are also the largest measured values in the data table, and they are not due to the surface corrugations since the data for smooth and corrugated-surface boxes in reference 3 differ by amounts which are much smaller than these discrepancies. Independent data from references 4-6 in appendices B and C show small to moderate discrepancies from the expected zero-PM lines, and moderate discrepancies from the predicted relation with the $YM$ data when tested throughout the region $\mathcal{R}_0$.

Consequently it is assumed that the discrepancies of the $PM$ data in reference 3 from the theoretically predicted zero values are due to measurement errors and that these dominate the data at heading above $25°$. Therefore, the $PM$ data are discarded, and we estimate $PM$ and $YM$ entirely from the YM data and its extrapolation to the region $\alpha > 45°$ as follows:

$$\widehat{YM}(\psi,\alpha) = \begin{cases} YMC1(\psi,\alpha) & (\psi,\alpha) \in \mathcal{R}_0 \\ YMC1(\psi,45)(90-\alpha)/45 & (\psi,\alpha) \in \mathcal{S}_4 \end{cases}$$

$$\widehat{PM}(\psi,\alpha) = \cot\psi_w \widehat{YM}(\psi,\alpha) + \csc\phi_w \widehat{YM}(\psi_1,\alpha_1) \qquad (\psi,\alpha) \in \mathcal{R}_0, \mathcal{S}_4$$

$$(4.19)$$

$$\begin{pmatrix} \widehat{YM} \\ \widehat{PM} \end{pmatrix}_{(\psi,\alpha)} = .5\left[\begin{pmatrix} YMC1 \\ PMC1 \end{pmatrix}_{(\psi,\alpha)} + \begin{pmatrix} \cos\phi_w & \sin\phi_w \\ \sin\phi_w & -\cos\phi_w \end{pmatrix} \begin{pmatrix} YMC1 \\ PMC1 \end{pmatrix}_{(\psi_1,\alpha_1)}\right]$$

$$(\psi,\alpha) \in \mathcal{S}_5, \mathcal{S}_6$$

where, in $\mathcal{S}_5$ and $\mathcal{S}_6$
$$YMC1(\psi,\alpha) = YMC1(\psi,45)(90-\alpha)/45$$
$$PMC1(\psi,\alpha) = g(\psi,\alpha) = \text{faired extrapolation function}$$

The estimate of $PM$ in $\mathcal{R}_0$ and $\mathcal{S}_4$ is obtained from $YMC1$ at equivalent points using a relation obtained by rearranging equation 3.12. This relation is singular at $\phi_w = 0$, and otherwise can magnify the YM-estimation errors by the factor $\csc\phi_w$ so that $\widehat{PM}$ is necessarily less accurate than $\widehat{YM}$. However, the estimate given by equation 4.19 for the regions $\mathcal{R}_0$ and $\mathcal{S}_4$ is satisfactory since $\phi_w < 45°$ there and the error magnification is under 1.5. The resulting pitching-moment estimate, $\widehat{PM}$, is about as accurate as the yaw- moment estimate. This estimate differs completely from the original data in functional behavior (compare $PM$ in figs. 2.4 and 4.4), but a comparison with independent pitching-moment data from reference 6 over the region $\mathcal{R}_0$ (appendix B, fig. B7) shows the same degree of agreement as seen in the comparison of yaw moment estimates in figures 4.2 and B7.

The estimate in $S_5$ and $S_6$ uses the same extrapolation scheme employed for lift and side force in this region. Along the upper boundary, ($\alpha = 90°$), $PM$ is zero (eq. 3.18) and $YM$ is assumed zero based on its known zero value at three points on this boundary (eq. 3.18) and the expectation that its value is small elsewhere on this boundary, even if not zero. In addition, $\widehat{YM}$ and $\widehat{PM}$ are known throughout $\mathcal{R}_0$ and $S_4$ from equation 4.19(a), and can be plotted versus $\alpha$ and then extrapolated across $S_5$ and ,$S_6$ to the known boundary values at $\alpha = 90°$. This extrapolation, denoted $YMC1$ and $PMC1$ in equation 4.19(b), is made with little knowledge of the actual functional behavior, such as local extremes, in $S_5$ and $S_6$. Therefore, a curve is faired between the known boundary values subject to; a) continuity and smoothness (continuous derivatives) at the lower boundary, and b) the minimum number of curve reversals needed to connect the boundary values. In the application of this conceptual scheme, $YM$ was extrapolated linearly in $\alpha$ while $PM$, which rises toward a maximum near $\alpha = 45°$, required some nonlinearity in the faired extrapolation function (denoted as $g(\psi, \alpha)$ in equation 4.19 without further definition and implemented as a tabulated function obtained from manually faired graphs in the actual work) to obtain smoothness at the boundary. The resulting initial extrapolation, $YMC1$ and $PMC1$, was then averaged at equivalent points in $S_5$ and $S_6$ to impose equation 3.12. The results are included in figures 4.4 and 4.5.

$\alpha$

| $\alpha$ | 0.0 | 4.0 | 8.0 | 12.0 | 16.0 | 20.0 | 25.0 | 30.0 | 35.0 | 40.0 | 45.0 | 50.0 | 60.0 | 75.0 | 90.0 |
|---|---|---|---|---|---|---|---|---|---|---|---|---|---|---|---|
| 0.0 | 0.0 | -3.5 | -2.3 | -0.6 | 2.6 | 2.1 | 2.6 | 2.6 | 5.8 | -0.9 | -6.5 | | | | |
| 2.0 | 1.8 | -2.4 | -1.5 | -0.3 | 3.0 | 2.4 | 3.4 | 3.7 | 6.2 | 0.5 | | | | | |
| 4.0 | 3.5 | 0.0 | 0.5 | 0.0 | 4.0 | 4.0 | 3.8 | 4.9 | 5.9 | 1.6 | | | | | |
| 6.0 | 2.6 | -0.1 | 0.5 | -0.1 | 2.9 | 3.1 | 4.3 | 4.8 | 5.5 | 2.0 | | | | | |
| 8.0 | 2.3 | -0.5 | 0.0 | 0.1 | 2.1 | 2.6 | 3.8 | 4.4 | 5.0 | 2.3 | | | | | |
| 10.0 | 1.4 | -0.5 | 0.1 | 0.1 | 2.5 | 3.5 | 5.0 | 4.4 | 4.9 | 3.3 | | | | | |
| 12.0 | 0.6 | -0.1 | -0.1 | 0.0 | 2.7 | 4.9 | 6.2 | 4.5 | 6.5 | 4.8 | | | | | |
| 16.0 | -2.6 | -4.1 | -2.2 | -2.5 | 0.1 | 3.6 | 7.7 | 6.9 | 7.8 | 6.8 | | | | | |
| 20.0 | -2.1 | -4.1 | -2.9 | -5.0 | -2.2 | 1.0 | 5.0 | 4.6 | 8.6 | 7.7 | | | | | |
| 25.0 | -2.6 | -4.3 | -4.2 | -6.6 | -5.9 | -1.5 | 2.0 | 1.9 | 6.4 | 7.3 | | | | | |
| 30.0 | -2.6 | -5.3 | -4.7 | -4.9 | -6.4 | -2.5 | -0.5 | 0.7 | 4.0 | 4.1 | | | | | |
| 35.0 | -5.8 | -6.0 | -4.7 | -7.1 | -8.6 | -3.7 | -1.8 | 0.2 | 2.8 | | | | | | |
| 40.0 | 0.9 | -2.5 | -3.9 | -6.8 | -7.6 | -7.6 | -3.5 | -1.0 | 1.2 | | | | | | |
| 45.0 | 6.5 | 4.2 | -1.9 | -7.4 | -10.1 | -6.3 | -1.7 | -1.4 | 0.1 | | | | | | |

(a) $\delta D/Q$: Drag Difference.

$\alpha$

| $\alpha$ | 0.0 | 4.0 | 8.0 | 12.0 | 16.0 | 20.0 | 25.0 | 30.0 | 35.0 | 40.0 | 45.0 | 50.0 | 60.0 | 75.0 | 90.0 |
|---|---|---|---|---|---|---|---|---|---|---|---|---|---|---|---|
| 0.0 | 0.0 | 0.0 | 0.0 | 0.0 | 0.0 | 0.0 | 0.0 | 0.0 | 0.0 | 0.0 | 0.0 | 0.0 | | | |
| 2.0 | -1.3 | -1.0 | -2.3 | -1.4 | -0.4 | -2.6 | -0.9 | 0.7 | 5.0 | 6.0 | | | | | |
| 4.0 | -3.5 | -3.2 | -2.7 | -2.9 | -0.1 | -4.5 | -1.9 | 1.7 | 10.7 | 12.2 | | | | | |
| 6.0 | -4.2 | -4.1 | -5.5 | -5.9 | -3.4 | -6.4 | -0.3 | 3.9 | 13.5 | 13.0 | | | | | |
| 8.0 | -5.0 | -5.3 | -10.0 | -10.2 | -8.5 | -9.3 | -0.6 | 7.1 | 17.2 | 12.4 | | | | | |
| 10.0 | -6.3 | -6.7 | -9.0 | -10.7 | -11.3 | -10.1 | -2.6 | 4.9 | 16.2 | 9.4 | | | | | |
| 12.0 | -5.4 | -8.0 | -8.4 | -10.8 | -12.7 | -9.7 | -4.2 | 2.7 | 9.8 | 6.5 | | | | | |
| 16.0 | -5.6 | -2.3 | -4.4 | -8.9 | -14.0 | -10.3 | -1.0 | -2.9 | 3.3 | 3.9 | | | | | |
| 20.0 | -6.5 | -4.9 | -7.7 | -9.8 | -11.6 | -9.0 | -5.9 | -6.4 | -0.9 | 2.1 | | | | | |
| 25.0 | -11.4 | -9.7 | -9.8 | -8.0 | -7.4 | -9.5 | -11.1 | -7.3 | -3.2 | 1.8 | | | | | |
| 30.0 | -11.2 | -10.3 | -10.2 | -5.4 | -4.1 | -5.8 | -12.0 | -4.9 | -1.6 | 1.2 | | | | | |
| 35.0 | -13.7 | -7.8 | -7.6 | -7.1 | -1.5 | -2.7 | -5.1 | -2.5 | 0.4 | | | | | | |
| 40.0 | -11.6 | -6.8 | -5.5 | -3.0 | -3.0 | -4.6 | -4.7 | -1.0 | -1.0 | | | | | | |
| 45.0 | -11.6 | -4.8 | -5.5 | -5.4 | -6.4 | -4.0 | -1.8 | 0.3 | 0.9 | | | | | | |
| $\psi$ | 0.0 | 4.0 | 8.0 | 12.0 | 16.0 | 20.0 | 25.0 | 30.0 | 35.0 | 40.0 | 45.0 | 50.0 | 60.0 | 75.0 | 90.0 |

(b) $\delta L/Q$: Lift Difference.



(c) Lift comparison.

Notes:

$\delta D(\psi, \alpha) = DC(\psi, \alpha) - DC(\psi_1, \alpha_1)$

$\delta L = LC1 - L1$

$L1(\psi, \alpha) = \sin \phi_w \, YC1(\psi_1, \alpha_1)$
$\qquad + \cos \phi_w LC1(\psi_1, \alpha_1)$

$YC1 = YC - b_Y; \quad LC1 = LC - b_L$

Figure 4.1.- Differences between data at equivalent points; force components.

Figure 4.2.- Comparison of estimate from Ames data with independent data; $\alpha = 0°$.
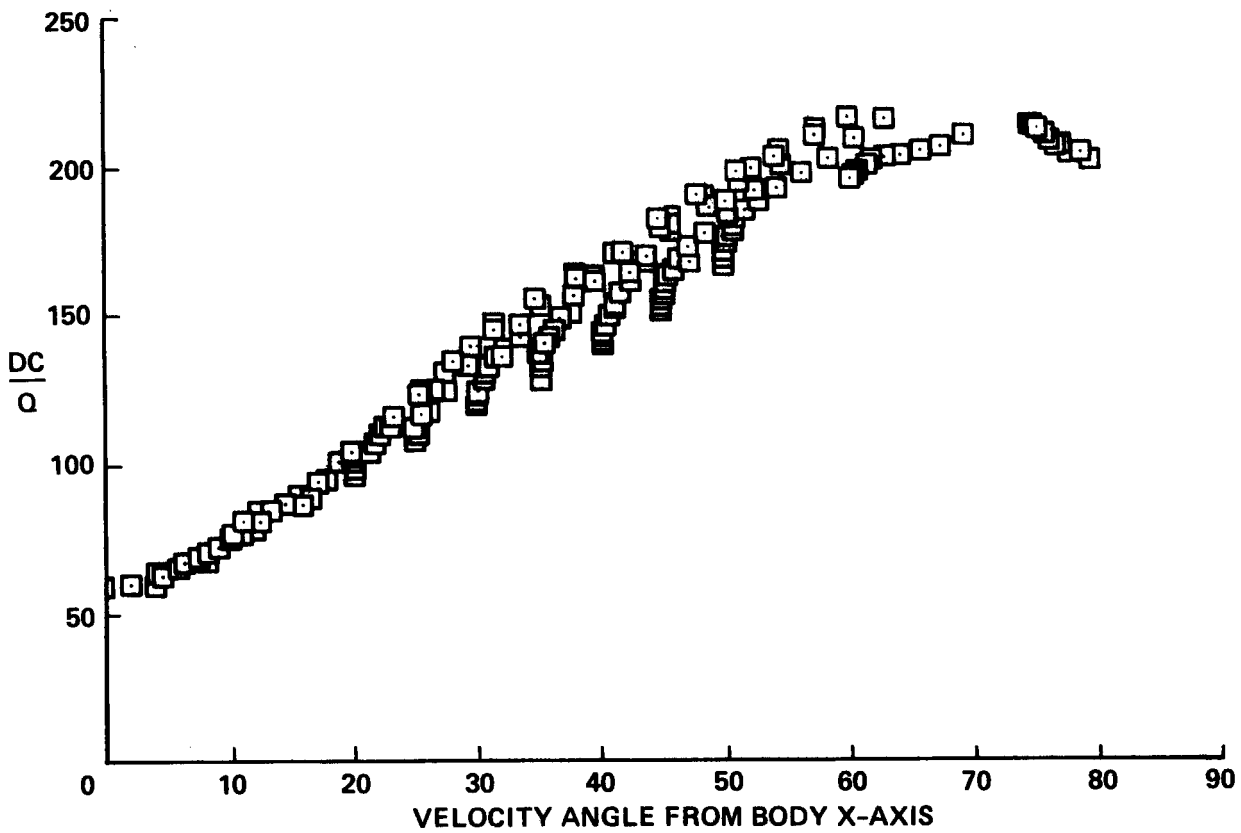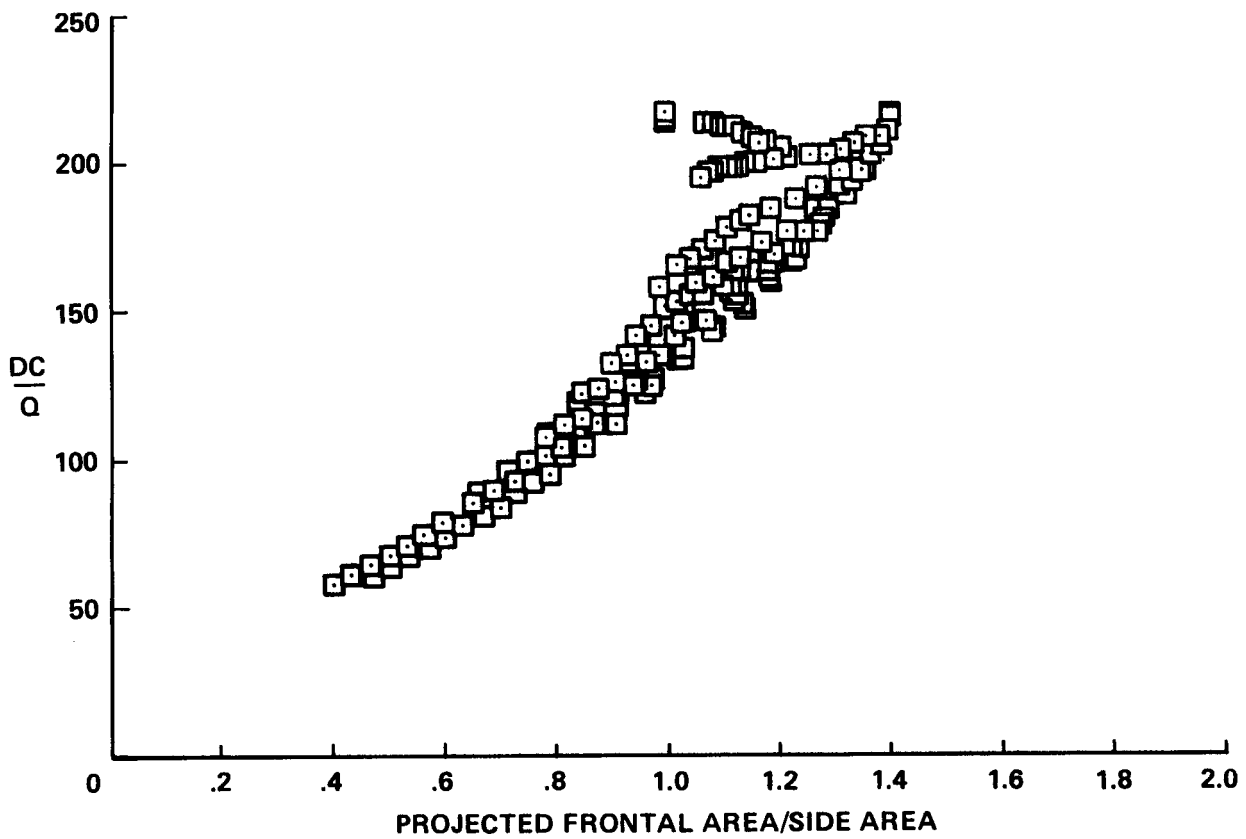
Figure 4.3.- Correlation of drag measurements with frontal area and velocity angle.
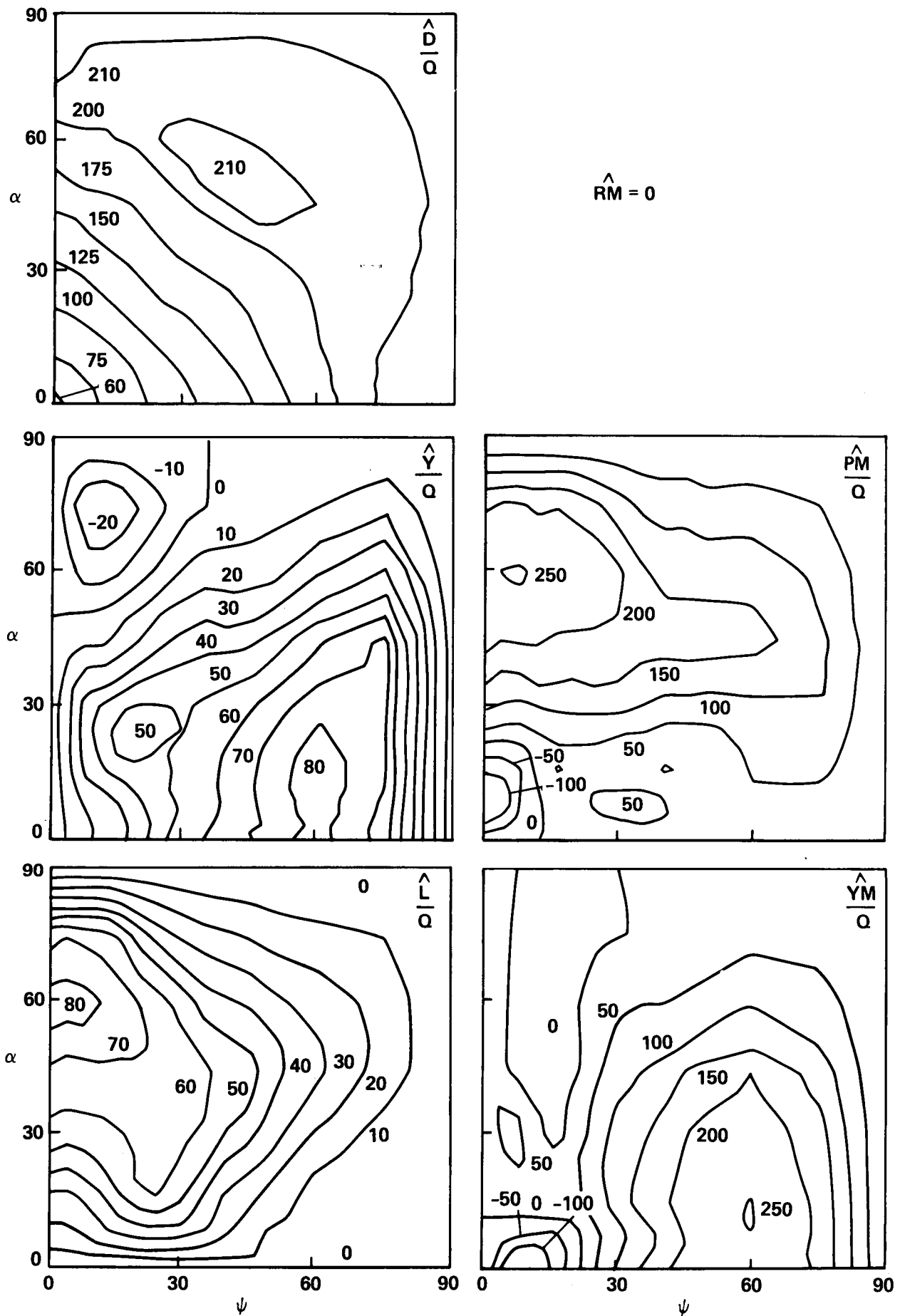
Figure 4.4.- Estimated MILVAN aerodynamics: contour plots.

$$\widehat{D}/Q$$

| $\alpha$ | 0.0 | 4.0 | 8.0 | 12.0 | 16.0 | 20.0 | 25.0 | 30.0 | 35.0 | 40.0 | 45.0 | 50.0 | 60.0 | 75.0 | 90.0 |
|---|---|---|---|---|---|---|---|---|---|---|---|---|---|---|---|
| 0.0 | 57.9 | 62.1 | 69.3 | 77.8 | 87.0 | 95.7 | 108.3 | 120.3 | 129.5 | 141.4 | 154.0 | 165.5 | 195.1 | 213.4 | 216.5 |
| 2.0 | 60.0 | 63.8 | 71.0 | 78.9 | 87.9 | 97.1 | 109.7 | 121.5 | 131.7 | 142.7 | 152.1 | 167.7 | 195.9 | 212.8 | 216.5 |
| 4.0 | 62.1 | 66.1 | 73.3 | 80.0 | 89.0 | 99.1 | 111.0 | 122.8 | 133.6 | 144.0 | 153.6 | 170.3 | 197.5 | 213.1 | 216.5 |
| 6.0 | 65.5 | 69.8 | 76.9 | 83.3 | 91.8 | 101.7 | 114.2 | 125.1 | 136.3 | 145.8 | 156.3 | 173.4 | 198.0 | 212.3 | 216.5 |
| 8.0 | 69.3 | 73.3 | 80.3 | 87.0 | 95.0 | 104.7 | 117.4 | 128.0 | 139.4 | 148.7 | 161.0 | 177.6 | 198.4 | 212.1 | 216.5 |
| 10.0 | 73.6 | 76.6 | 83.8 | 90.7 | 99.2 | 108.9 | 121.7 | 131.6 | 142.7 | 152.1 | 165.0 | 180.2 | 199.1 | 212.5 | 216.5 |
| 12.0 | 77.8 | 80.0 | 87.1 | 94.4 | 103.4 | 113.4 | 126.0 | 135.8 | 146.1 | 155.2 | 168.1 | 182.1 | 199.8 | 211.5 | 216.5 |
| 16.0 | 87.0 | 89.0 | 95.3 | 103.4 | 112.2 | 123.0 | 135.3 | 143.9 | 152.1 | 160.3 | 172.9 | 184.8 | 200.8 | 210.0 | 216.5 |
| 20.0 | 95.7 | 99.2 | 105.2 | 113.7 | 123.4 | 133.1 | 143.8 | 150.1 | 158.1 | 165.2 | 176.8 | 187.3 | 200.9 | 208.5 | 216.5 |
| 25.0 | 108.3 | 111.3 | 118.5 | 127.2 | 136.2 | 145.1 | 154.3 | 160.5 | 167.8 | 173.5 | 184.2 | 192.4 | 202.1 | 206.5 | 216.5 |
| 30.0 | 120.3 | 123.1 | 129.4 | 138.5 | 145.3 | 153.8 | 162.7 | 170.2 | 177.6 | 183.1 | 191.3 | 197.2 | 202.9 | 206.0 | 216.5 |
| 35.0 | 129.5 | 134.4 | 141.5 | 148.4 | 154.0 | 162.8 | 171.4 | 182.3 | 188.2 | 193.4 | 198.7 | 201.6 | 204.6 | 204.1 | 216.5 |
| 40.0 | 141.4 | 144.6 | 151.7 | 158.0 | 163.7 | 170.5 | 181.2 | 190.7 | 197.2 | 202.4 | 208.5 | 208.6 | 206.1 | 204.2 | 216.5 |
| 45.0 | 154.0 | 157.7 | 164.8 | 167.7 | 171.6 | 179.8 | 189.8 | 198.3 | 205.8 | 210.2 | 215.9 | 214.7 | 209.6 | 201.1 | 216.5 |
| 50.0 | 165.5 | 173.2 | 180.5 | 183.0 | 187.0 | 191.9 | 199.5 | 207.3 | 212.3 | 215.7 | 214.7 | 212.6 | 208.0 | 202.5 | 216.5 |
| 60.0 | 195.1 | 197.9 | 199.2 | 199.3 | 200.8 | 203.9 | 211.6 | 213.6 | 212.4 | 211.1 | 209.6 | 208.0 | 204.4 | 205.6 | 216.5 |
| 75.0 | 213.4 | 210.0 | 205.7 | 204.7 | 204.4 | 204.1 | 203.7 | 203.1 | 202.6 | 201.9 | 201.1 | 202.5 | 205.6 | 210.9 | 216.5 |
| 90.0 | 216.5 | 216.5 | 216.5 | 216.5 | 216.5 | 216.5 | 216.5 | 216.5 | 216.5 | 216.5 | 216.5 | 216.5 | 216.5 | 216.5 | 216.5 |

$$\widehat{Y}/Q$$

| $\alpha$ | 0.0 | 4.0 | 8.0 | 12.0 | 16.0 | 20.0 | 25.0 | 30.0 | 35.0 | 40.0 | 45.0 | 50.0 | 60.0 | 75.0 | 90.0 |
|---|---|---|---|---|---|---|---|---|---|---|---|---|---|---|---|
| 0.0 | 0.0 | 10.5 | 17.8 | 23.0 | 27.2 | 35.8 | 47.9 | 57.2 | 60.9 | 66.6 | 69.0 | 77.8 | 83.9 | 66.0 | 0.0 |
| 2.0 | 0.0 | 10.6 | 17.6 | 22.1 | 26.6 | 34.8 | 46.6 | 54.8 | 59.7 | 64.3 | 70.8 | 75.1 | 84.1 | 65.5 | 0.0 |
| 4.0 | 0.0 | 10.6 | 17.4 | 23.6 | 26.5 | 34.5 | 45.3 | 53.3 | 58.9 | 62.1 | 67.0 | 72.2 | 83.4 | 65.1 | 0.0 |
| 6.0 | 0.0 | 12.0 | 19.2 | 24.4 | 28.4 | 36.3 | 45.1 | 52.4 | 58.2 | 61.7 | 67.9 | 74.4 | 85.1 | 66.5 | 0.0 |
| 8.0 | 0.0 | 13.2 | 20.7 | 25.5 | 30.0 | 37.7 | 45.5 | 51.7 | 58.2 | 61.8 | 68.0 | 75.6 | 85.3 | 67.5 | 0.0 |
| 10.0 | 0.0 | 14.0 | 23.7 | 28.0 | 33.4 | 40.3 | 46.7 | 52.0 | 57.5 | 61.8 | 68.4 | 75.6 | 85.5 | 68.2 | 0.0 |
| 12.0 | 0.0 | 15.4 | 26.6 | 30.6 | 36.7 | 42.7 | 48.1 | 52.8 | 57.9 | 62.6 | 69.2 | 76.4 | 87.2 | 69.5 | 0.0 |
| 16.0 | 0.0 | 17.9 | 31.9 | 39.0 | 45.2 | 47.7 | 47.9 | 52.2 | 56.7 | 62.3 | 68.7 | 75.0 | 86.1 | 70.9 | 0.0 |
| 20.0 | 0.0 | 20.9 | 34.9 | 44.2 | 51.8 | 52.3 | 49.2 | 51.6 | 57.1 | 61.0 | 68.2 | 74.1 | 84.8 | 73.1 | 0.0 |
| 25.0 | 0.0 | 21.7 | 36.5 | 46.6 | 54.8 | 55.5 | 51.5 | 49.8 | 54.8 | 57.9 | 63.8 | 69.7 | 81.2 | 71.0 | 0.0 |
| 30.0 | 0.0 | 21.6 | 34.8 | 42.2 | 48.4 | 51.6 | 50.9 | 48.9 | 52.9 | 54.8 | 59.7 | 65.5 | 77.5 | 72.3 | 0.0 |
| 35.0 | 0.0 | 18.0 | 26.4 | 28.5 | 34.0 | 41.5 | 44.0 | 45.7 | 47.1 | 50.0 | 53.5 | 59.5 | 70.8 | 74.1 | 0.0 |
| 40.0 | 0.0 | 11.5 | 18.3 | 17.9 | 23.2 | 30.7 | 36.3 | 39.7 | 41.8 | 43.1 | 45.4 | 52.1 | 64.7 | 72.5 | 0.0 |
| 45.0 | 0.0 | 3.6 | 6.7 | 6.9 | 12.8 | 19.9 | 28.4 | 32.5 | 35.3 | 35.6 | 38.3 | 45.6 | 59.5 | 73.3 | 0.0 |
| 50.0 | 0.0 | 0.8 | 1.9 | 3.2 | 7.7 | 13.8 | 21.9 | 26.0 | 31.7 | 31.6 | 34.0 | 40.5 | 52.9 | 65.2 | 0.0 |
| 60.0 | 0.0 | -6.5 | -15.2 | -14.2 | -10.2 | -4.2 | 2.6 | 18.2 | 23.8 | 23.7 | 25.5 | 30.4 | 39.7 | 48.9 | 0.0 |
| 75.0 | 0.0 | -16.6 | -29.1 | -30.8 | -24.0 | -11.7 | -0.3 | 9.1 | 11.9 | 11.9 | 12.8 | 15.2 | 19.8 | 24.4 | 0.0 |
| 90.0 | 0.0 | 0.0 | 0.0 | 0.0 | 0.0 | 0.0 | 0.0 | 0.0 | 0.0 | 0.0 | 0.0 | 0.0 | 0.0 | 0.0 | 0.0 |

$$\widehat{L}/Q$$

| $\alpha$ | 0.0 | 4.0 | 8.0 | 12.0 | 16.0 | 20.0 | 25.0 | 30.0 | 35.0 | 40.0 | 45.0 | 50.0 | 60.0 | 75.0 | 90.0 |
|---|---|---|---|---|---|---|---|---|---|---|---|---|---|---|---|
| 0.0 | 0.0 | 0.0 | 0.0 | 0.0 | 0.0 | 0.0 | 0.0 | 0.0 | 0.0 | 0.0 | 0.0 | 0.0 | 0.0 | 0.0 | 0.0 |
| 2.0 | 5.5 | 5.6 | 6.2 | 7.7 | 8.7 | 10.1 | 10.6 | 10.4 | 8.7 | 6.3 | 6.6 | 2.3 | 2.3 | 1.2 | 0.0 |
| 4.0 | 10.5 | 10.6 | 13.3 | 15.5 | 17.9 | 20.6 | 21.0 | 20.8 | 17.8 | 12.6 | 12.8 | 5.1 | 3.6 | 1.2 | 0.0 |
| 6.0 | 14.2 | 14.1 | 17.6 | 21.6 | 25.5 | 28.4 | 29.9 | 28.8 | 23.9 | 16.8 | 14.0 | 6.6 | 3.6 | 1.2 | 0.0 |
| 8.0 | 17.8 | 17.6 | 21.0 | 27.1 | 32.3 | 35.2 | 37.1 | 36.1 | 29.2 | 21.1 | 14.2 | 7.6 | 3.6 | 1.2 | 0.0 |
| 10.0 | 19.8 | 20.7 | 23.9 | 29.6 | 36.6 | 40.8 | 42.6 | 40.3 | 32.2 | 24.2 | 16.3 | 10.1 | 3.6 | 1.2 | 0.0 |
| 12.0 | 23.0 | 23.8 | 26.4 | 32.1 | 40.8 | 46.2 | 47.7 | 44.2 | 32.8 | 25.1 | 19.3 | 13.2 | 3.6 | 1.2 | 0.0 |
| 16.0 | 27.2 | 26.9 | 31.6 | 39.6 | 48.8 | 55.9 | 59.4 | 50.4 | 37.0 | 27.0 | 22.4 | 17.5 | 3.6 | 1.2 | 0.0 |
| 20.0 | 35.8 | 35.1 | 39.6 | 46.6 | 53.9 | 60.8 | 63.7 | 55.8 | 43.3 | 32.7 | 27.1 | 21.3 | 7.3 | 1.2 | 0.0 |
| 25.0 | 47.9 | 45.7 | 47.9 | 52.5 | 55.9 | 60.3 | 63.8 | 60.7 | 51.9 | 41.0 | 35.3 | 27.9 | 13.0 | 1.2 | 0.0 |
| 30.0 | 57.2 | 53.6 | 54.2 | 57.8 | 59.2 | 61.3 | 62.5 | 62.6 | 56.5 | 47.9 | 42.4 | 33.6 | 18.3 | 4.1 | 0.0 |
| 35.0 | 60.9 | 59.5 | 60.1 | 60.5 | 63.8 | 64.7 | 65.5 | 64.1 | 60.3 | 53.5 | 49.0 | 38.3 | 23.8 | 8.7 | 0.0 |
| 40.0 | 66.6 | 62.4 | 64.1 | 65.7 | 66.4 | 66.9 | 67.6 | 65.3 | 61.0 | 55.0 | 51.6 | 41.0 | 27.6 | 12.0 | 0.0 |
| 45.0 | 69.0 | 66.0 | 67.7 | 68.3 | 67.6 | 68.2 | 67.4 | 65.0 | 61.6 | 56.9 | 53.3 | 43.2 | 31.9 | 16.3 | 0.0 |
| 50.0 | 77.8 | 74.6 | 76.7 | 75.7 | 73.5 | 71.8 | 68.5 | 63.2 | 54.8 | 50.5 | 47.4 | 38.4 | 28.4 | 14.5 | 0.0 |
| 60.0 | 83.9 | 84.8 | 83.9 | 80.2 | 76.3 | 70.8 | 64.5 | 52.7 | 41.1 | 37.9 | 35.5 | 28.8 | 21.3 | 10.8 | 0.0 |
| 75.0 | 66.0 | 69.2 | 66.9 | 65.6 | 58.7 | 46.3 | 34.5 | 26.4 | 20.6 | 19.0 | 17.8 | 14.4 | 10.6 | 5.4 | 0.0 |
| 90.0 | 0.0 | 0.0 | 0.0 | 0.0 | 0.0 | 0.0 | 0.0 | 0.0 | 0.0 | 0.0 | 0.0 | 0.0 | 0.0 | 0.0 | 0.0 |
| $\psi$ | 0.0 | 4.0 | 8.0 | 12.0 | 16.0 | 20.0 | 25.0 | 30.0 | 35.0 | 40.0 | 45.0 | 50.0 | 60.0 | 75.0 | 90.0 |

(a) Force components.

Figure 4.5.- Estimated MILVAN aerodynamics.

36

$$\widehat{RM}/Q = 0$$

$$\widehat{PM}/Q$$

| $\alpha$ | | | | | | | | | | | | | | | |
|---|---|---|---|---|---|---|---|---|---|---|---|---|---|---|---|
| 0.0 | 0.0 | 0.0 | 0.0 | 0.0 | 0.0 | 0.0 | 0.0 | 0.0 | 0.0 | 0.0 | 0.0 | 0.0 | 0.0 | 0.0 | 0.0 |
| 2.0 | -52.0 | -38.0 | -12.6 | -1.9 | 8.2 | 16.1 | 20.4 | 23.4 | 24.6 | 21.1 | 11.4 | 11.2 | 10.2 | 7.2 | 0.0 |
| 4.0 | -104.0 | -75.8 | -24.9 | -3.6 | 16.5 | 32.2 | 40.6 | 46.7 | 48.8 | 41.5 | 22.3 | 22.0 | 20.5 | 14.3 | 0.0 |
| 6.0 | -128.3 | -106.6 | -35.4 | -4.2 | 20.2 | 36.8 | 49.8 | 57.4 | 60.5 | 53.1 | 30.5 | 33.2 | 31.1 | 21.7 | 0.0 |
| 8.0 | -152.5 | -137.0 | -45.0 | -3.9 | 24.0 | 39.9 | 55.7 | 61.9 | 62.1 | 50.8 | 25.5 | 33.2 | 41.8 | 29.1 | 0.0 |
| 10.0 | -140.0 | -129.2 | -48.5 | 0.1 | 30.7 | 41.0 | 53.9 | 60.0 | 62.2 | 48.9 | 21.3 | 31.9 | 45.2 | 36.6 | 0.0 |
| 12.0 | -127.6 | -121.0 | -51.5 | 4.8 | 38.1 | 40.7 | 45.7 | 46.5 | 47.0 | 32.3 | 16.9 | 30.9 | 48.6 | 43.9 | 0.0 |
| 16.0 | -80.0 | -81.8 | -53.8 | 15.4 | 51.9 | 44.7 | 30.3 | 20.9 | 21.5 | -3.7 | 5.1 | 25.5 | 55.1 | 58.2 | 0.0 |
| 20.0 | -26.7 | -29.6 | -19.2 | 14.1 | 41.5 | 40.4 | 32.7 | 14.7 | 12.5 | 7.5 | 12.0 | 25.1 | 58.7 | 68.5 | 0.0 |
| 25.0 | 50.6 | 39.4 | 40.0 | 62.0 | 74.2 | 75.7 | 71.8 | 59.8 | 52.4 | 38.4 | 37.9 | 45.0 | 65.2 | 81.1 | 0.0 |
| 30.0 | 108.2 | 93.4 | 87.3 | 107.1 | 112.9 | 113.5 | 115.3 | 111.1 | 95.6 | 77.8 | 75.0 | 77.4 | 87.7 | 94.5 | 0.0 |
| 35.0 | 151.6 | 132.9 | 135.5 | 154.1 | 150.4 | 145.5 | 150.5 | 147.8 | 128.3 | 117.5 | 117.7 | 109.6 | 110.9 | 104.1 | 0.0 |
| 40.0 | 184.9 | 164.6 | 169.5 | 180.9 | 174.1 | 169.1 | 167.7 | 161.9 | 151.0 | 146.1 | 149.1 | 145.1 | 137.8 | 105.5 | 0.0 |
| 45.0 | 223.4 | 201.7 | 207.5 | 207.3 | 195.6 | 188.2 | 185.4 | 177.1 | 171.8 | 168.6 | 174.8 | 173.0 | 167.9 | 114.2 | 0.0 |
| 50.0 | 239.1 | 230.1 | 237.8 | 227.7 | 218.8 | 215.5 | 212.4 | 199.2 | 170.4 | 163.8 | 164.5 | 165.5 | 155.6 | 99.8 | 0.0 |
| 60.0 | 240.0 | 251.5 | 255.3 | 241.8 | 239.1 | 234.5 | 239.9 | 207.9 | 158.7 | 132.8 | 132.8 | 127.7 | 133.7 | 90.0 | 0.0 |
| 75.0 | 192.5 | 200.5 | 204.3 | 192.8 | 197.8 | 186.9 | 158.6 | 124.9 | 94.0 | 82.6 | 83.0 | 69.0 | 71.8 | 51.4 | 0.0 |
| 90.0 | 0.0 | 0.0 | 0.0 | 0.0 | 0.0 | 0.0 | 0.0 | 0.0 | 0.0 | 0.0 | 0.0 | 0.0 | 0.0 | 0.0 | 0.0 |

$$\widehat{YM}/Q$$

| $\alpha$ | | | | | | | | | | | | | | | |
|---|---|---|---|---|---|---|---|---|---|---|---|---|---|---|---|
| 0.0 | 0.0 | -104.0 | -152.5 | -127.6 | -80.0 | -26.7 | 50.6 | 108.2 | 151.6 | 184.9 | 223.4 | 239.1 | 240.0 | 192.5 | 0.0 |
| 2.0 | 0.0 | -93.8 | -150.0 | -127.2 | -82.0 | -28.6 | 44.2 | 100.1 | 142.1 | 175.5 | 214.2 | 233.1 | 241.9 | 191.9 | 0.0 |
| 4.0 | 0.0 | -75.7 | -137.9 | -122.1 | -82.5 | -30.0 | 38.6 | 93.2 | 131.9 | 165.4 | 204.4 | 226.7 | 243.6 | 190.2 | 0.0 |
| 6.0 | 0.0 | -48.6 | -93.7 | -95.1 | -73.6 | -29.2 | 39.6 | 89.7 | 129.7 | 160.5 | 200.5 | 228.5 | 247.2 | 191.5 | 0.0 |
| 8.0 | 0.0 | -23.9 | -45.4 | -54.5 | -60.6 | -24.4 | 34.2 | 81.9 | 128.2 | 158.3 | 201.3 | 232.9 | 248.7 | 192.3 | 0.0 |
| 10.0 | 0.0 | -12.6 | -21.0 | -22.0 | -25.4 | -5.5 | 46.6 | 87.2 | 134.3 | 165.5 | 207.1 | 236.0 | 251.5 | 193.0 | 0.0 |
| 12.0 | 0.0 | -2.0 | -3.2 | 2.8 | 8.8 | 5.1 | 58.4 | 97.3 | 144.7 | 175.5 | 214.2 | 239.4 | 252.3 | 192.2 | 0.0 |
| 16.0 | 0.0 | 18.6 | 26.3 | 38.8 | 50.1 | 33.4 | 77.9 | 125.2 | 166.6 | 192.0 | 220.5 | 239.9 | 250.9 | 190.0 | 0.0 |
| 20.0 | 0.0 | 35.0 | 41.3 | 40.1 | 45.7 | 34.2 | 85.4 | 125.1 | 162.3 | 186.4 | 215.3 | 234.1 | 244.4 | 185.7 | 0.0 |
| 25.0 | 0.0 | 43.5 | 55.7 | 35.3 | 19.5 | 34.2 | 86.9 | 121.1 | 150.8 | 176.5 | 209.1 | 227.5 | 237.3 | 179.3 | 0.0 |
| 30.0 | 0.0 | 50.1 | 58.5 | 22.5 | -17.2 | 15.2 | 73.9 | 119.5 | 141.5 | 165.8 | 199.1 | 218.9 | 232.2 | 173.8 | 0.0 |
| 35.0 | 0.0 | 53.2 | 52.0 | 9.8 | -19.7 | 13.8 | 66.0 | 106.7 | 128.2 | 152.4 | 184.7 | 199.2 | 222.3 | 161.9 | 0.0 |
| 40.0 | 0.0 | 44.9 | 32.6 | -36.5 | -30.1 | 5.3 | 50.9 | 87.1 | 109.8 | 134.1 | 166.5 | 182.8 | 209.7 | 140.5 | 0.0 |
| 45.0 | 0.0 | 17.3 | -11.4 | -46.5 | -40.9 | -13.7 | 38.0 | 72.4 | 98.0 | 119.4 | 148.9 | 167.5 | 198.7 | 129.8 | 0.0 |
| 50.0 | 0.0 | 15.4 | -10.1 | -41.4 | -36.4 | -12.2 | 33.8 | 64.4 | 82.4 | 86.1 | 105.6 | 127.6 | 150.4 | 102.6 | 0.0 |
| 60.0 | 0.0 | 11.5 | -7.6 | -31.0 | -27.3 | -9.1 | 25.3 | 42.4 | 49.5 | 49.5 | 56.6 | 67.9 | 97.5 | 71.7 | 0.0 |
| 75.0 | 0.0 | 5.8 | -3.8 | -15.5 | -12.3 | -12.6 | -9.3 | -3.8 | 3.1 | 9.8 | 16.6 | 21.1 | 35.9 | 30.2 | 0.0 |
| 90.0 | 0.0 | 0.0 | 0.0 | 0.0 | 0.0 | 0.0 | 0.0 | 0.0 | 0.0 | 0.0 | 0.0 | 0.0 | 0.0 | 0.0 | 0.0 |
| $\psi$ | 0.0 | 4.0 | 8.0 | 12.0 | 16.0 | 20.0 | 25.0 | 30.0 | 35.0 | 40.0 | 45.0 | 50.0 | 60.0 | 75.0 | 90.0 |

(b) Moment components.

Figure 4.5.- Concluded.

## RMCA/Q

| α | 0.0 | 4.0 | 8.0 | 12.0 | 16.0 | 20.0 | 25.0 | 30.0 | 35.0 | 40.0 | 45.0 |
|---|---|---|---|---|---|---|---|---|---|---|---|
| 0.0 | 0.0 | 0.6 | -4.7 | -23.0 | -11.0 | -40.8 | -42.2 | -44.2 | -54.0 | -81.6 | -103.4 |
| 2.0 | -8.5 | -4.9 | 14.9 | -10.1 | -6.0 | -13.2 | -35.3 | -22.8 | -40.3 | -75.8 | |
| 4.0 | -0.6 | 0.0 | -2.1 | -23.5 | -5.5 | -7.2 | -20.5 | -34.2 | -42.5 | -78.6 | |
| 6.0 | 2.6 | 1.0 | -10.0 | -5.3 | 8.8 | 4.6 | -16.6 | -25.2 | -33.8 | -91.0 | |
| 8.0 | 4.7 | 2.3 | -0.1 | 8.3 | 27.2 | 21.0 | 9.2 | -23.9 | -61.6 | -104.0 | |
| 10.0 | 13.6 | 13.5 | -11.3 | 4.3 | 11.8 | 14.3 | 8.8 | -24.1 | -60.5 | -96.8 | |
| 12.0 | 23.0 | 22.7 | -9.6 | 2.2 | 21.2 | -1.0 | 3.1 | -26.6 | -74.8 | -88.1 | |
| 16.0 | 11.0 | 5.0 | -26.0 | -18.1 | 0.0 | 4.8 | 4.4 | -7.6 | -41.6 | -45.1 | |
| 20.0 | 40.8 | 4.5 | -22.5 | 3.2 | -5.9 | -1.7 | 6.3 | 9.7 | -9.1 | -31.1 | |
| 25.0 | 42.2 | 19.4 | -10.0 | -2.4 | -6.2 | -1.0 | 5.4 | 16.2 | 10.3 | -26.4 | |
| 30.0 | 44.2 | 32.6 | 17.6 | 25.3 | -19.3 | -12.5 | -3.6 | -9.5 | -0.6 | -23.4 | |
| 35.0 | 54.0 | 33.9 | 59.6 | 64.9 | 16.1 | -25.4 | 16.5 | 0.0 | 13.5 | | |
| 40.0 | 81.6 | 83.2 | 92.5 | 36.5 | 20.9 | 12.6 | -3.5 | -22.8 | -2.0 | | |
| 45.0 | 103.4 | 136.3 | 115.8 | 77.2 | 47.0 | 37.2 | 37.8 | 41.4 | 2.0 | | |

## RMCS/Q

| α | 0.0 | 4.0 | 8.0 | 12.0 | 16.0 | 20.0 | 25.0 | 30.0 | 35.0 | 40.0 | 45.0 |
|---|---|---|---|---|---|---|---|---|---|---|---|
| 0.0 | 13.3 | -3.6 | 18.0 | 17.3 | 37.2 | 38.4 | 25.5 | 32.7 | 27.2 | -1.0 | -19.1 |
| 2.0 | -3.4 | -1.1 | 23.9 | 13.4 | 27.9 | 32.9 | 18.8 | 45.7 | 17.9 | -8.7 | |
| 4.0 | -3.6 | 11.9 | -6.8 | -16.7 | 14.1 | 5.9 | 20.2 | 25.6 | -7.0 | -24.6 | |
| 6.0 | 7.8 | 2.3 | -33.0 | -21.6 | 5.0 | 0.6 | 11.6 | 19.1 | -1.4 | -44.7 | |
| 8.0 | 18.0 | -7.2 | -41.9 | -31.4 | -0.5 | 2.4 | 25.0 | 3.1 | -17.5 | -56.9 | |
| 10.0 | 17.4 | -11.2 | -44.6 | -18.1 | -14.7 | 1.4 | 17.3 | -2.4 | -5.6 | -49.0 | |
| 12.0 | 17.3 | -16.7 | -32.5 | 0.5 | 1.0 | -1.9 | 8.9 | 7.5 | -13.0 | -57.0 | |
| 16.0 | 37.2 | 13.5 | -5.8 | -2.7 | -23.5 | -17.2 | -11.4 | 1.9 | 7.0 | -51.5 | |
| 20.0 | 38.4 | 4.1 | -1.2 | 0.6 | -25.2 | -33.1 | -24.1 | -25.8 | -5.1 | -37.3 | |
| 25.0 | 25.5 | 18.2 | 20.3 | 2.5 | -19.4 | -22.9 | -23.1 | -27.2 | -28.8 | -42.3 | |
| 30.0 | 32.7 | 24.9 | -3.2 | 14.5 | -31.4 | -27.5 | -32.9 | -27.3 | -47.0 | -51.0 | |
| 35.0 | 27.2 | -8.7 | -4.9 | 18.6 | -0.7 | -40.4 | -21.3 | -52.4 | -72.0 | | |
| 40.0 | -1.0 | -37.8 | -46.2 | -53.2 | -27.7 | -29.1 | -58.6 | -89.8 | -70.2 | | |
| 45.0 | -19.1 | -65.4 | -52.8 | -47.8 | -56.4 | -58.1 | -66.8 | -62.1 | -66.7 | | |

| ψ | 0.0 | 4.0 | 8.0 | 12.0 | 16.0 | 20.0 | 25.0 | 30.0 | 35.0 | 40.0 | 45.0 | 50.0 | 60.0 | 75.0 | 90.0 |

Figure 4.6.- Roll moment data separated into symmetric and antisymmetric components.

# 5. DISCUSSION AND CONCLUSIONS

Thus far, the results consist of a table of wind-axes force and moment components in the base domain, $\mathcal{D}_0$, (fig. 4.5) together with formulas in section 3 (eqs. 3.8, 3.10 and 3.11) for extrapolation to the complete domain of interest for simulations. These formulas are collected together in figure 5.1. For any point $(\psi, \alpha)$ the force and moment components are given from the data at a corresponding point $(\psi_0, \alpha_0)$ in $\mathcal{D}_0$ by a relation which depends on the quadrant of $(\psi, \alpha)$. The form of this relation together with the correspondence of points and the coefficient matrix for each quadrant are listed in figure 5.1. The coefficent matrices are all diagonal and represent rotations of 180° about one or another axis. A simulation routine is readily written from this information.

A body axis formulation is often preferred in simulations. The required data tables are not given here but can be generated routinely from the data in figure 4.5 by the transformation

$$f_b(\psi, \alpha) = T_{b,w}(\psi, \alpha) f_w(\psi, \alpha) \tag{5.1}$$

where

$$T_{b,w}(\psi, \alpha) = E_2(\alpha) E_3(\psi) = \begin{pmatrix} \cos\alpha\cos\psi & \cos\alpha\sin\psi & -\sin\alpha \\ -\sin\psi & \cos\psi & 0 \\ \sin\alpha\cos\psi & \sin\alpha\sin\psi & \cos\alpha \end{pmatrix}$$

and $\underline{f}$ refers to either the force or moment vector. The corresponding extrapolation formulas can be obtained by applying equation 5.1 to the extrapolation formulas for wind axes. The results are included in figure 5.1; these have the same form as for wind axes, but the coefficient matrices are modified for quadrants with $|\psi| > 90°$.

In addition, sideslip angle is customarily used in simulations in place of heading relative to wind axes. This can be accommodated by revising signs in the data tables for either wind or body axes in accordance with equation 3.10 and then equations 3.8, 3.10 and 3.11 and the formulas of figure 5.1, with $\beta$ replacing $\psi$, govern the extrapolation to all quadrants. Another possibility is to formulate the model in vector form without special notation for each scalar component; for this, the signs of $D$ and $L$ in the data table are changed, and then the formulas of figure 5.1 apply unchanged for both wind and body axes; e.g., for wind axes

$$\begin{pmatrix} FA_w \\ MA_w \end{pmatrix}_{(\psi, \alpha)} = S \begin{pmatrix} FA_w \\ MA_w \end{pmatrix}_{(\psi_0, \alpha_0)}$$

where $\underline{FA}$ and $\underline{MA}$ are the aerodynamic force and moment vectors.

Various indications of the accuracy of the data and the present estimate are noted in the text and summarized next. First, differences in repeated measurements indicate the presence of random measurement errors and unsteady flow effects not averaged out in the data processing. Second, discrepancies of the data from the zero lines and from the relations between the data at equivalent points predicted by the theory of section 3 reveal the presence of systematic errors because of sensors, test conditions, and data processing, and from differences between the assumptions of the theory and the test conditions. Third, differences in data and results from the independent data of reference 6 reflect errors in the data from both sources, and provide an independent

indication of the systematic errors. The data from reference 6 do not show the large-to-gross discrepancies from theory found in the Ames data for $L$, $RM$ and $PM$, but are not otherwise in closer agreement with theory. The effects of nonidentical model surfaces are present in the second and third comparisons, but these effects were measured in both wind tunnel studies and were found to be small.

The drag data show good repeatability and good agreement with the expected symmetry at equivalent points in the region for which this can be tested (in $S_1$ and $S_2$), and the drag estimate agrees closely with the data from reference 6. The side-force data show good repeatability and agreement with the expected zero lines and with the data from reference 6. The lift data show good repeatability, good agreement with the zero-line at $\psi = 90°$ but significant discrepancy from the zero line at $\alpha = 0°$ for intermediate heading and, when these disagreements are corrected, the results show good agreement with the theoretical relation of lift and sideforce measurements at equivalent points. The lift estimate shows only fair agreement with the lift data from reference 6, but the difference is likely dominated by inaccuracies in the lift data from reference 6. The roll data show poor repeatability and no agreement with any symmetry property or with the data from reference 6, and the pitching moment data show poor repeatability and gross disagreement from the expected zero lines at $\alpha = 0$, and $\psi = 90°$. In both cases, the largest values in the data table are presumed measurement errors and these data are considered unusable. Finally, the yaw moment data show good repeatability and agree well with the expected zero lines at $\psi = 0$ or 90°, and the estimates of both $PM$ and $YM$ obtained from the $YM$ data show fair agreement with the data from reference 6. In summary, it appears from these comparisons that the accuracy of the estimate is good for drag and side force and fair for the remaining components in the regions for which the comparisons can be made.

A more definitive assessment of the inaccuracies in the data from reference 3 and a more accurate correction of that data than the revisions of section 4 requires a study and identification of the principal underlying tunnel and data processing errors. Unfortunately, the possibility of such a study is limited since the measurement and data processing records have been discarded. A review of the equations relating the six wind axes components of the aerodynamics to the six tunnel scale outputs for the Ames 7 x 10 ft tunnel indicated that the gross trends of $RM$ and $PM$ versus $\psi$ seen in figure 2.3 (which are also the systematic discrepancies of these data from the theory) are consistent with a significant error in the vertical coordinate of the model support point in the data processing. This results in RM and PM errors proportional to side force and drag, respectively, and has no effect on any other component. A correction of the $RM$ and $PM$ data based on this model of one error source reduced the discrepancies, but large discrepancies remained apparently because of significant additional systematic and random errors.

Factors which limit the accuracy of the present estimate of the MILVAN's static aerodynamics are; 1) random and unidentified systematic tunnel errors in the available data, 2) the sparseness of the heading-angle measurement grid in the region $45° \leq \psi \leq 90°$, which may result in significant interpolation error in generating $Y$ and $YM$ from the data table, as well as a lack of independent comparison data to confirm the estimate in this region, and 3) the lack of data for the region $\alpha > 45°$. Model uncertainty is greatest in the region $\alpha > 45°$. The analysis of symmetry shows

that the aerodynamics in most of this region are unrelated to the aerodynamics in the region of available measurements. The present model is defined in the subregion $S_4$ from the measurements in $S_3$, but this could only be done for the force components, and otherwise, the model for $\alpha > 45°$ is defined by fairing curves between theoretical or measured boundary values. Thus, it appears that the present global model is subject to small to moderate uncertainties depending on component and region of the domain, and that improvements in accuracy require new measurements with improvements in measurement accuracy, tunnel error corrections, and measurement grid density and domain.

Finally, the following conclusions are drawn:

1. The symmetry of a rectangular box permits determination of its static aerodynamics at any attitude from its aerodynamics at a corresponding point in a restricted attitude domain in $D_0$. The smallest such domain is

$$\{(\psi, \alpha); \ 0 \leq \psi < \tan^{-1}(\sin \alpha), \ 0 \leq \alpha \leq 90°\}$$

This is included in the region $0 \leq \psi \leq 45°$ of $D_0$, which is more than sufficient to define the aerodynamics globally. However, the measurement grid of the Ames data encloses the region $0 \leq \alpha \leq 45°$ of $D_0$. This suffices to define the aerodynamics everywhere except in

$$\{(\psi, \alpha); \ \tan^{-1}(\cos \alpha) < \psi < 90°, \ 45° < \alpha \leq 90°\}$$

and its equivalent regions in other quadrants of $D$; that is, except in about two-thirds of the region of $D$ with $|\alpha| > 45°$.

2. For all components, zero lines and/or relationships between data at equivalent points are determined by the symmetry of the box. This feature permits comprehensive testing of the wind tunnel data for consistency with these properties throughout the attitude domain. Discrepancies indicate the presence and size of measurement errors in the data.

3. For the Ames data, discrepancies are small for drag, side force, and yaw moment, large for lift, and gross for roll and pitching moment. Limited data from a University of Maryland study agree more consistently with the theory, and discrepancies range from small to moderate in size, depending on the component. In addition, repeated measurements in the the Ames data show small differences for the force components and yaw moment, and large differences for the *RM* and *PM* data.

4. The accuracy of the global model estimated from the Ames data varies with component and over the domain. Accuracy is judged to decrease by component in the order drag, side-force, and yaw moment, lift, pitching moment, and roll moment. Accuracy over the domain is best at small angles, $|\alpha|$, $|\psi| < 45°$ where most of the measurements are concentrated, and poorer elsewhere because of larger yaw measurement grid intervals ($10°$ to $15°$), or the absence of measurements.

5. The existing data provide adequate accuracy for the most significant components of the aerodynamics in the region surrounding the minimum drag attitude of the MILVAN and suffice for a global model of moderate accuracy. Gains in the accuracy over that obtained here require new measurements with improved measurement grids.

$$
\begin{pmatrix} D \\ Y \\ L \\ RM \\ PM \\ YM \end{pmatrix}_{(\psi,\alpha)} = S \begin{pmatrix} D \\ Y \\ L \\ RM \\ PM \\ YM \end{pmatrix}_{(\psi_0,\alpha_0)}
\qquad
\begin{array}{c} -180^\circ \leq \psi \leq 180^\circ \\ -90^\circ \leq \alpha \leq 90^\circ \\ 0 \leq \psi_o, \ \alpha_o \leq 90^\circ \end{array}
$$

| $\mathcal{D}_i$ | QUADARANT $\alpha$ | QUADARANT $\psi$ | POINT IN $\mathcal{D}_o$ $\alpha_o$ | POINT IN $\mathcal{D}_o$ $\psi_o$ | COEFFICIENT MATRIX, S Wind axes | COEFFICIENT MATRIX, S Body axes |
|---|---|---|---|---|---|---|
| $\mathcal{D}_6$ | $\alpha > 0$ | $-180 \leq \psi \leq -90$ | $\alpha$ | $180 + \psi$ | $S_2$ | $S_6$ |
| $\mathcal{D}_1$ | $\alpha > 0$ | $-90 \leq \psi \leq 0$ | $\alpha$ | $-\psi$ | $S_1$ | $S_1$ |
| $\mathcal{D}_o$ | $\alpha > 0$ | $0 \leq \psi \leq 90$ | $\alpha$ | $\psi$ | $I$ | $I$ |
| $\mathcal{D}_5$ | $\alpha > 0$ | $90 \leq \psi \leq 180$ | $\alpha$ | $-180 + \psi$ | $S_3$ | $S_5$ |
| $\mathcal{D}_7$ | $\alpha < 0$ | $-180 \leq \psi \leq -90$ | $-\alpha$ | $180 + \psi$ | $I$ | $S_7$ |
| $\mathcal{D}_3$ | $\alpha < 0$ | $-90 \leq \psi \leq 0$ | $-\alpha$ | $-\psi$ | $S_3$ | $S_3$ |
| $\mathcal{D}_2$ | $\alpha < 0$ | $0 \leq \psi \leq 90$ | $-\alpha$ | $\psi$ | $S_2$ | $S_2$ |
| $\mathcal{D}_4$ | $\alpha < 0$ | $90 \leq \psi \leq 180$ | $-\alpha$ | $180 - \psi$ | $S_1$ | $S_4$ |

$$S_1 = diag\{1,-1,1,-1,1,-1\} = diag\{-E_2(\pi), E_2(\pi)\}$$

$$S_2 = diag\{1,1,-1,-1,-1,1\} = diag\{-E_3(\pi), E_3(\pi)\}$$

$$S_3 = diag\{1,-1,-1,1,-1,-1\} = diag\{E_1(\pi), E_1(\pi)\}$$

$$S_4 = diag\{-1,1,1,1,-1,-1\} = diag\{-E_1(\pi), E_1(\pi)\}$$

$$S_5 = diag\{-1,1,-1,-1,1,-1\} = diag\{E_2(\pi), E_2(\pi)\}$$

$$S_6 = diag\{-1,-1,-1,1,1,1\} = diag\{-I, I\}$$

$$S_7 = diag\{-1,-1,1,-1,-1,1\} = diag\{E_3(\pi), E_3(\pi)\}$$

Figure 5.1.- Equations for the extrapolation of data in $\mathcal{D}_o$ to any point in $\mathcal{D}$.

# APPENDIX A.-AMES RESEARCH CENTER WIND TUNNEL DATA

The reference table of wind tunnel data used in the text is obtained by combining the data provided in reference 3 for all points in the reference domain,

$$\mathcal{R}_o = \{(\psi, \alpha) : \quad \psi \in [0°, 90°], \quad \alpha \in [0°, 90°]\} \tag{A1}$$

This combining can be done in two steps as described below.

## A1. Basic Measurements

First, reference 3 provides two tables of measurements of the force and moment components in wind axes, and these must be combined. The two tables are obtained from measurement sequences made with fixed angle of attack (yaw-sweep data) and fixed yaw angle (pitch-sweep data), respectively. These data are quoted in figure A1 for all points which fall in $\mathcal{R}_o$. As seen from the grids in figure A1, the two tables together cover all of $\mathcal{R}_o$ and have a common region over which two sets of measurements are available, but at nonidentical grid points.

These data can be combined by; 1) defining a reference grid as the union of the two grids, and 2) averaging the two tables in the common region, using table interpolation if a reference grid point is absent from one or both tables. This treatment uses all available data, halves the discrepancy between the two tables, and the combined grid provides better function definition than either individual grid.

Errors in the data are assumed to be a superposition of repeatable systematic errors which can vary with attitude, and random errors which are independent from measurement to measurement and are assumed to have similar statistics for both tables; that is, the error in a measurement of $f$ at $(\psi, \alpha)$ can be written as:

$$\tilde{f}(\psi, \alpha) = \tilde{f}_o(\psi, \alpha) + \eta \tag{A2}$$

where $\tilde{f}$, $\tilde{f}_o$, $\eta$ are the total, systematic, and random errors in the data, respectively. These errors can arise from multiple causes originating in the sensors, tunnel flow, test apparatus, and data processing, but the principal sources cannot be identified here since the test conditions are no longer accessible and the analysis is confined to the measurements. In the tunnel tests, the scale readings varied continually because of unsteady flow effects, and the measured static aerodynamics were obtained by averaging numerous readings. Similar unsteady effects and their treatment by averaging occurred in all investigations; the magnitudes of these effects have not been reported, but we assume they are small, and that the static aerodynamics correspond to the unique mean values of indefintely long records of each component. In the Ames data, averaging reduces the standard deviation of the random errors remaining in the measured values.

The reference grid and a table indicating the number of measurements from reference 3 at each grid point is given in figure A2. At points with two measurements, averaging reduces the standard deviation of the independent errors, but retains the systematic errors present in both tables. At the remaining grid points in the common region one or both tables must be interpolated; this adds an approximation error to one or both values, and adds the average approximation error to the inaccuracy of the averaged measurements. This approximation error is small for sufficiently small interpolation intervals, or it may be small compared to the independent measurement errors.

For unfavorable conditions (large intervals and strong function nonlinearity) the averaging scheme may not provide the best accuracy at points with one measurement.

The differences between the two sets of measurements are also given in figure A2 along with some statistics of the difference tables (means, standard deviations, and the table extremes) which describe the apparent random-measurement- error processes. All three force components and the yaw moment show small differences under $10Q$ lb, $30Q$ ft-lb, respectively. This excellent repeatability implies small random and interpolation errors. The roll- and pitching- moment differences are much larger; these exceed $25Q$ ft-lb over a large part of the common domain and reach maximum values exceeding $100Q$ ft-lb. These two tables were also separated according to the number of measurements at each point (not shown) to verify that the largest differences occurred at grid points with two measurements and were not introduced by the interpolation. Further, these differences appear to be random with very small mean values; differences exceeding $25Q$ ft-lb are distributed throughout the grid, and no systematic behavior is discernible.

The composite table is shown in figure A3. The reference grid for yaw has intervals of $10°$ to $15°$ for $\psi > 45°$. This is sparse compared to the grid density below $45°$ and results in a coarse linearization of the aerodynamic functions with respect to $\psi$ in this region. Several of these ($Y$, $L$, and $YM$) are strongly nonlinear here, as can be seen in figure 2.3 of the text. This region is of particular interest in the case of single-point suspensions for which the MILVAN adopts a broadside attitude in equilibrium. The measurement grid density is greatest and the functions are best defined near $\psi = 0°$ which corresponds to the MILVAN'S equilibrium position with a two-point suspension.

## A2. Interference Tares

Second, the interference tares must be determined and subtracted from the basic measurements. Reference 3 provides two tables of data obtained from yaw-sweep and pitch-sweep measuring sequences, respectively. These are quoted in figure A4 for all points in $\mathcal{R}_o$.

The following factors affect the treatment. As seen from the grids in figure A4, the measurements do not cover all of $\mathcal{R}_o$; the yaw-sweep data covers $\mathcal{R}_0$ for $\alpha \leq 20°$ and the pitch-sweep data covers $\mathcal{R}_o$ for $\psi \leq 45°$. In addition, the pitch-sweep data were taken without an image of the pitch-angle control arm so that these data measure the interference effects incompletely. Further, both tables were considered in reference 3 to be sufficiently erratic that their use was open to individual interpretation and was, therefore, left unsettled. The erratic measurements were attributed to random variations in the separation characteristics of the flow around the box. A review of the size of the yaw-sweep data indicates generally small values for drag and side-force interference, moderate values for lift and yaw moment, and large effects in roll and pitch moment. Thus, the interference tares are not small enough to discard as negligible effects.

The first approach was the straightforward one of using the best available measurement or estimate; that is, the interference function was taken to be the yaw-sweep data for $\alpha \leq 20°$, the pitch-sweep data for ($20° < \alpha < 45°, \psi \leq 45°$), and zero in the remainder of $\mathcal{R}_o$ where no measurements were made. However, this approach 1) amplified the randomness of the basic measurements by adding the random measurement errors of the tare data, and 2) disturbed the systematic trends in the basic data by adding a function with distinctly different trends in the

44

three regions of $\mathcal{R}_o$ where it is differently defined. If the tare data are accurate measurements of an interference function which varies rapidly with $(\psi, \alpha)$, then this treatment would tend to smooth the basic data. However, the results appeared to be a sum of independent random processes and are consistent with the hypothesis that the rapid variations in both sets of measurements are due to random measurement errors.

In the approach adopted, the tare data were viewed as the superposition of a function which varies smoothly in $(\psi, \alpha)$ and a random, independent measurement error;

$$\widehat{\Delta f}(\psi, \alpha) = \Delta f(\psi, \alpha) + \eta \tag{A3}$$

where $f$ refers to any aerodynamic component, and $\widehat{\Delta f}$, $\Delta f$ and $\eta$ are the data, the actual interference plus systematic measurement errors similar to those in the basic data, and the random-measurement errors with statistics similar to those of the random errors in the basic data, respectively. The data were therefore plotted and reviewed for systematic trends; that is, for consistent patterns versus $\psi, \alpha$ with only a few extremes.

The yaw-sweep data are plotted in figure A5. For the force components, the data plotted versus $\psi$ (fig. A5a) show consistent trends which can be estimated by averaging over $\alpha$, but the data plotted versus $\alpha$ (fig. A5b) show no consistent trend nor any progression of curve shapes for different values of $\psi$. For most values of $\psi$, these curves can be interpreted as random measurement errors about a constant value independent of $\alpha$. Straight-line least squares fits to the data showed nearly zero slopes at most values of $\psi$. Further, the pitch-sweep data over the larger range, $0° \leq \alpha \leq 45°$, did not indicate the presence of any significant $\alpha$-dependent interference effect which might have been missed in reviewing the yaw-sweep data over $0° \leq \alpha \leq 20°$. Thus, the systematic variation of these tares can be estimated as independent of $\alpha$ and given by averaging the yaw-sweep data over $\alpha$. The results, after minor smoothing of local curve reversals, are given in figure A6. The drag and side-force tares are seen to be small, below $10Q$ lb everywhere, while the lift interference reaches somewhat larger values at large yaw angles.

Figure A6 includes some statistical properties of the difference from the original tare measurements; these differences are viewed here as the apparent random tare measurement errors, and also indicate the degree to which the tare data have been modified by our interpretation. The mean errors are zero by construction, and the standard deviations and extreme errors indicate measurement errors for the force components which are a moderate fraction of the tare data and small in absolute magnitude. Assuming the same random measurement error processes effect all sets of measurements then the statistics given in figure A6 should be close to those previously calculated in figure A2 from the differences in repeated measurements of the aerodynamics. A comparison of the two sets of statistics shows good agreement for the force components.

The roll moment interference tare appears to be predominantly samples of a random variable. There is no discernible trend with $\psi$ (fig. A5a). Individual curves show reversals to local extremes and sign reversals at most grid points, and the data, when averaged over $\alpha$, show the same properties again. Further, the data plotted versus $\alpha$ (fig. A5b) also show no discernible trend. Consequently, the roll-moment interference was estimated as the mean of the yaw-sweep data, $-6Q$ ft-lb, independent of either $\psi$ or $\alpha$. This is a nearly negligible value compared to the

table extremes $(-72.4, 63.6Q$ ft-lb). Thus, the roll moment interference tare table is interpreted to be almost entirely samples of a random process or random measurement errors, which is statistically consistent with the differences in repeated roll moment measurements given in figure A2. Evidently, the systematic roll moment interference is much smaller than the random measurement errors.

The pitching-moment interference data shows a consistent trend vs $\psi$, and a consistent, increasing trend with $\alpha$ at $\psi = 0°$ and low yaw angles. This trend declines to a nearly fixed value at $\psi = 45°$ and the data become erratic above 45°. Thus, systematic variations in both $\psi, \alpha$ are discerned. For $\alpha \leq 20°$ the yaw-sweep data are used after smoothing of some local curve reversals. For the region $\alpha > 20°$, the pitch-sweep data were reviewed; when plotted versus $\alpha$ these showed variations which 1) paralleled the yaw sweep data but were offset by a fixed bias, and 2) were constant for $\alpha > 20°$. Consequently, the interference tare was estimated as fixed for $\alpha \geq 20°$. The results are given in figure A6, and show large tares through most of $\mathcal{R}_o$. The error statistics indicate a smaller, moderate-sized error process (the large extreme error, $116Q$ ft-lb, seen in figure A6 is an isolated value in the error table).

Last, the yaw moment tares versus $\psi$ (fig. A5a) are nearly independent of $\alpha$ for $\psi$ near 0° and above 60°. Elsewhere, there is some consistent variation with $\alpha$ (fig. A5b) but the spread is small enough in magnitude to treat by averaging over $\alpha$. The results are given in figure A6, and show modest tare magnitudes, and a random-measurement error process of about the same size.

## A3. Reference Table

The basic data with the estimated interference tares subtracted are given in the text (fig. 2.2) along with plots versus $\psi$ and contour plots (figs. 2.3, 2.4).

$$D/Q$$

| $\alpha$ | 0.0 | 4.0 | 8.0 | 12.0 | 16.0 | 20.0 | 25.0 | 30.0 | 35.0 | 45.0 | 60.0 | 75.0 | 90.0 |
|---|---|---|---|---|---|---|---|---|---|---|---|---|---|
| 0.0 | 59.6 | 62.3 | 70.1 | 80.7 | 91.9 | 100.5 | 113.9 | 128.5 | 139.5 | 160.6 | 198.3 | 214.9 | 224.2 |
| 2.0 | 63.1 | 64.5 | 71.9 | 81.6 | 92.9 | 101.5 | 115.8 | 130.2 | 141.8 | 161.7 | 199.1 | 212.7 | 223.8 |
| 4.0 | 66.4 | 69.2 | 76.2 | 82.8 | 95.0 | 105.1 | 117.1 | 132.1 | 143.0 | 163.0 | 201.7 | 212.6 | 226.4 |
| 6.0 | 69.0 | 73.0 | 79.4 | 86.2 | 96.5 | 107.2 | 120.9 | 134.4 | 145.3 | 164.9 | 202.1 | 211.4 | 226.2 |
| 8.0 | 73.0 | 76.0 | 81.8 | 90.6 | 99.2 | 110.5 | 123.7 | 137.7 | 148.4 | 170.6 | 202.2 | 211.5 | 224.6 |
| 10.0 | 76.6 | 78.9 | 85.7 | 94.4 | 104.2 | 115.0 | 128.7 | 140.5 | 151.3 | 175.6 | 202.9 | 212.8 | 225.1 |
| 12.0 | 80.5 | 82.3 | 89.1 | 98.1 | 109.0 | 120.8 | 133.8 | 144.4 | 156.1 | 178.7 | 203.4 | 211.5 | 225.0 |
| 16.0 | 87.9 | 88.8 | 97.1 | 106.6 | 116.4 | 129.2 | 144.4 | 154.0 | 162.1 | 182.1 | 203.9 | 209.6 | 224.4 |
| 20.0 | 96.7 | 99.8 | 107.0 | 115.2 | 128.1 | 138.6 | 151.9 | 157.6 | 168.5 | 185.2 | 203.7 | 207.9 | 225.5 |
| 25.0 | 110.1 | 112.2 | 120.5 | 128.6 | 139.5 | 149.7 | 161.2 | 167.5 | 177.6 | 193.8 | 205.4 | 205.6 | 224.7 |
| 30.0 | 122.6 | 123.2 | 130.0 | 141.0 | 146.6 | 155.7 | 166.9 | 177.2 | 186.9 | 202.0 | 206.6 | 206.4 | 226.6 |
| 35.0 | 129.0 | 133.4 | 140.9 | 148.2 | 153.3 | 164.7 | 174.8 | 188.8 | 196.4 | 208.2 | 208.4 | 204.2 | 224.9 |
| 40.0 | 144.2 | 145.3 | 151.6 | 158.0 | 163.5 | 170.5 | 183.7 | 196.6 | 204.6 | 218.0 | 209.9 | 204.3 | 223.2 |
| 45.0 | 159.6 | 161.8 | 165.6 | 167.4 | 170.1 | 180.4 | 193.2 | 204.0 | 212.7 | 225.4 | 213.4 | 201.2 | 224.0 |

$$Y/Q$$

| $\alpha$ | 0.0 | 4.0 | 8.0 | 12.0 | 16.0 | 20.0 | 25.0 | 30.0 | 35.0 | 45.0 | 60.0 | 75.0 | 90.0 |
|---|---|---|---|---|---|---|---|---|---|---|---|---|---|
| 0.0 | -3.5 | 11.9 | 22.1 | 28.5 | 31.2 | 41.7 | 57.1 | 68.8 | 74.8 | 83.2 | 86.4 | 76.9 | 1.3 |
| 2.0 | -2.6 | 12.7 | 22.7 | 26.3 | 29.6 | 39.9 | 55.9 | 65.5 | 72.5 | 79.4 | 87.8 | 76.4 | 0.9 |
| 4.0 | -2.9 | 12.1 | 22.8 | 32.7 | 29.9 | 40.7 | 55.1 | 65.9 | 71.9 | 76.5 | 88.5 | 77.5 | 2.7 |
| 6.0 | -3.3 | 13.8 | 25.8 | 32.4 | 32.5 | 43.2 | 53.5 | 64.3 | 68.3 | 76.5 | 90.1 | 78.1 | 2.1 |
| 8.0 | -4.1 | 14.7 | 27.5 | 33.4 | 34.0 | 44.2 | 54.1 | 63.1 | 68.3 | 75.5 | 89.5 | 79.1 | 3.1 |
| 10.0 | -4.2 | 14.4 | 31.1 | 34.9 | 38.0 | 48.0 | 56.3 | 63.8 | 66.5 | 76.3 | 90.0 | 79.9 | 3.7 |
| 12.0 | -5.8 | 14.8 | 32.5 | 35.1 | 39.7 | 49.2 | 57.3 | 62.6 | 68.0 | 76.4 | 92.2 | 80.7 | 3.0 |
| 16.0 | -6.2 | 13.7 | 35.7 | 45.7 | 52.1 | 55.0 | 53.0 | 58.1 | 63.3 | 75.4 | 90.4 | 82.6 | 4.5 |
| 20.0 | -13.2 | 16.9 | 36.9 | 48.0 | 58.8 | 56.7 | 49.5 | 52.4 | 58.5 | 72.9 | 87.6 | 84.5 | 3.0 |
| 25.0 | -13.6 | 14.4 | 32.7 | 47.6 | 58.7 | 62.8 | 58.0 | 51.7 | 58.6 | 68.3 | 85.3 | 81.7 | 4.8 |
| 30.0 | -12.1 | 11.0 | 24.4 | 37.4 | 48.3 | 53.8 | 56.7 | 53.3 | 56.9 | 63.1 | 80.5 | 82.3 | 2.0 |
| 35.0 | -5.4 | 10.1 | 17.4 | 26.3 | 34.8 | 46.0 | 48.8 | 50.9 | 51.9 | 58.3 | 73.4 | 83.0 | -0.6 |
| 40.0 | -3.2 | 4.7 | 15.2 | 18.3 | 25.3 | 34.7 | 41.1 | 45.2 | 47.3 | 51.0 | 67.7 | 81.2 | -1.2 |
| 45.0 | -0.5 | -0.2 | 6.5 | 6.9 | 13.8 | 22.1 | 32.7 | 37.9 | 38.9 | 42.5 | 59.8 | 78.0 | -6.6 |

$$L/Q$$

| $\alpha$ | 0.0 | 4.0 | 8.0 | 12.0 | 16.0 | 20.0 | 25.0 | 30.0 | 35.0 | 45.0 | 60.0 | 75.0 | 90.0 |
|---|---|---|---|---|---|---|---|---|---|---|---|---|---|
| 0.0 | 4.0 | 3.6 | 6.0 | 8.7 | 9.8 | 16.3 | 24.4 | 33.4 | 38.8 | 38.8 | 5.0 | -16.6 | -6.2 |
| 2.0 | 9.0 | 9.3 | 10.1 | 15.7 | 18.2 | 24.1 | 33.2 | 43.3 | 48.7 | 44.9 | 1.1 | -16.6 | -5.5 |
| 4.0 | 12.1 | 12.5 | 17.8 | 22.3 | 27.4 | 32.6 | 40.7 | 52.4 | 58.8 | 48.5 | -0.5 | -18.1 | -8.0 |
| 6.0 | 15.6 | 15.3 | 21.2 | 27.5 | 34.0 | 40.1 | 52.3 | 61.0 | 65.9 | 50.3 | 0.3 | -18.5 | -5.4 |
| 8.0 | 18.7 | 17.6 | 21.0 | 30.0 | 36.9 | 44.1 | 57.9 | 68.2 | 71.7 | 49.0 | 1.1 | -18.7 | -5.0 |
| 10.0 | 18.9 | 19.5 | 24.1 | 30.9 | 38.8 | 48.7 | 60.7 | 70.9 | 75.6 | 50.4 | 2.7 | -19.4 | -4.9 |
| 12.0 | 23.4 | 21.5 | 26.0 | 31.9 | 42.1 | 54.2 | 63.0 | 73.1 | 69.1 | 53.7 | 4.6 | -20.5 | -4.8 |
| 16.0 | 26.5 | 27.7 | 33.1 | 41.2 | 49.1 | 61.6 | 77.2 | 72.7 | 68.5 | 54.0 | 8.2 | -19.6 | -5.1 |
| 20.0 | 34.8 | 34.4 | 40.1 | 48.0 | 56.8 | 69.5 | 79.8 | 74.7 | 69.3 | 55.5 | 11.1 | -18.1 | -4.5 |
| 25.0 | 44.2 | 42.3 | 47.3 | 53.8 | 59.0 | 64.0 | 73.3 | 76.9 | 74.6 | 61.8 | 16.8 | -12.9 | -4.0 |
| 30.0 | 53.0 | 48.8 | 52.1 | 59.0 | 63.1 | 65.7 | 68.2 | 76.5 | 75.7 | 65.9 | 21.7 | -9.8 | -3.5 |
| 35.0 | 53.9 | 55.8 | 57.7 | 60.1 | 67.1 | 69.1 | 72.9 | 76.2 | 77.6 | 68.9 | 26.4 | -5.7 | -3.3 |
| 40.0 | 60.1 | 58.8 | 62.3 | 66.8 | 68.5 | 69.3 | 73.7 | 76.0 | 75.1 | 69.7 | 31.0 | -0.6 | -1.1 |
| 45.0 | 61.9 | 62.9 | 65.2 | 67.3 | 66.9 | 69.1 | 72.6 | 73.2 | 73.0 | 68.0 | 34.2 | 3.0 | -1.9 |
| $\psi$ | 0.0 | 4.0 | 8.0 | 12.0 | 16.0 | 20.0 | 25.0 | 30.0 | 35.0 | 45.0 | 60.0 | 75.0 | 90.0 |

(a) Pitch-sweep data; force components.

Figure A1.- Wind tunnel data; force and moment measurements.

$\alpha$ — RM/Q

| $\alpha$ | | | | | | | | | | | | | |
|---|---|---|---|---|---|---|---|---|---|---|---|---|
| 0.0 | -3.1 | -11.1 | -21.5 | -18.3 | 33.2 | -18.1 | -10.9 | -21.6 | -58.5 | -158.0 | -151.4 | -75.5 | -67.0 |
| 2.0 | -31.1 | -21.2 | 49.8 | 6.5 | 40.8 | 33.4 | -9.2 | 42.8 | -47.7 | -162.9 | -169.8 | -74.9 | -60.4 |
| 4.0 | 6.8 | 10.7 | -25.1 | -73.6 | 30.3 | -1.4 | 24.5 | -24.9 | -100.0 | -171.7 | -183.8 | -62.9 | -59.7 |
| 6.0 | 11.1 | -5.2 | -81.2 | -39.4 | 20.9 | 5.4 | -5.7 | -10.8 | -43.2 | -253.0 | -229.3 | -77.3 | -101.9 |
| 8.0 | 10.8 | -20.4 | -67.1 | -24.6 | 26.7 | 35.6 | 51.9 | -31.1 | -102.9 | -188.3 | -224.7 | -104.4 | -107.5 |
| 10.0 | 16.2 | -12.7 | -93.8 | -12.7 | -19.9 | 26.8 | 35.7 | -45.7 | -91.1 | -186.7 | -208.7 | -99.1 | -127.7 |
| 12.0 | 23.3 | -11.9 | -65.1 | 13.5 | 43.2 | -3.7 | 7.2 | -34.2 | -148.6 | -173.6 | -277.0 | -107.6 | -94.9 |
| 16.0 | 16.4 | 0.0 | -42.6 | -46.9 | -22.9 | -9.4 | -31.0 | -13.8 | -70.6 | -151.6 | -253.7 | -110.1 | -113.5 |
| 20.0 | 77.6 | -23.9 | -38.1 | -6.0 | -41.4 | -44.8 | -37.8 | -22.2 | -15.3 | -113.7 | -216.3 | -135.3 | -77.0 |
| 25.0 | 53.5 | 29.1 | 15.3 | -23.9 | -34.7 | -11.3 | -19.3 | 3.0 | -5.7 | -149.2 | -243.0 | -85.2 | -152.9 |
| 30.0 | 71.1 | 63.8 | 8.7 | 45.1 | -88.8 | -32.0 | -38.3 | -33.3 | -45.8 | -156.5 | -216.8 | -83.0 | -77.3 |
| 35.0 | 75.2 | 19.2 | 48.7 | 77.5 | 9.4 | -71.8 | -10.8 | -58.4 | -64.5 | -189.4 | -199.1 | -73.2 | -66.8 |
| 40.0 | 74.6 | 39.4 | 40.3 | -22.7 | -12.8 | -22.5 | -60.1 | -118.6 | -78.2 | -198.3 | -223.8 | -67.9 | -64.6 |
| 45.0 | 78.3 | 64.9 | 57.0 | 23.4 | -15.4 | -26.9 | -35.0 | -26.7 | -70.7 | -158.4 | -208.2 | -72.0 | -35.4 |

$\alpha$ — PM/Q

| $\alpha$ | | | | | | | | | | | | | |
|---|---|---|---|---|---|---|---|---|---|---|---|---|
| 0.0 | -33.6 | -25.9 | -26.4 | -26.4 | 0.0 | -0.5 | -9.2 | -11.5 | -25.1 | -33.3 | -235.4 | -249.4 | -232.8 |
| 2.0 | -104.4 | -76.7 | -52.0 | -18.6 | 10.0 | 7.0 | 9.1 | 22.8 | 0.5 | -28.9 | -243.1 | -264.4 | -195.3 |
| 4.0 | -105.0 | -101.3 | -82.5 | -34.3 | 7.7 | 28.5 | 29.3 | 60.4 | 39.3 | -2.5 | -253.1 | -217.8 | -202.9 |
| 6.0 | -106.5 | -111.8 | -77.8 | -15.5 | -3.2 | 21.6 | 45.6 | 79.4 | 62.1 | 13.4 | -256.6 | -235.8 | -222.6 |
| 8.0 | -112.1 | -118.7 | -64.3 | -39.0 | -0.6 | -7.1 | 25.3 | 47.8 | 53.5 | 0.0 | -261.7 | -207.6 | -211.2 |
| 10.0 | -102.2 | -109.0 | -66.7 | -52.8 | -10.6 | -30.4 | 9.8 | 64.0 | 44.6 | -72.7 | -234.2 | -234.5 | -211.7 |
| 12.0 | -69.1 | -68.1 | -56.7 | -58.9 | -35.7 | -21.0 | 33.3 | 32.3 | 31.8 | -101.1 | -237.4 | -232.6 | -192.7 |
| 16.0 | -19.5 | -24.3 | -2.9 | -8.0 | 6.8 | 8.9 | 7.7 | -21.6 | -39.1 | -92.7 | -233.0 | -203.9 | -201.7 |
| 20.0 | 33.3 | 20.6 | 39.8 | 23.7 | 27.1 | 29.7 | 6.5 | -19.9 | -48.1 | -52.9 | -233.2 | -180.7 | -215.8 |
| 25.0 | 115.1 | 71.0 | 41.1 | 62.0 | 100.6 | 55.6 | 28.8 | -2.4 | -21.0 | -30.6 | -213.5 | -202.0 | -225.8 |
| 30.0 | 147.1 | 119.2 | 110.3 | 74.1 | 108.7 | 104.3 | 77.9 | 25.4 | -36.9 | -44.0 | -194.6 | -209.7 | -236.4 |
| 35.0 | 192.1 | 184.3 | 179.3 | 149.4 | 163.2 | 111.1 | 119.0 | 49.5 | -2.7 | -7.1 | -154.6 | -176.0 | -263.1 |
| 40.0 | 202.9 | 220.5 | 162.4 | 166.9 | 151.7 | 146.9 | 127.2 | 51.2 | 50.5 | -17.3 | -101.9 | -230.0 | -250.5 |
| 45.0 | 206.5 | 190.3 | 201.1 | 188.5 | 179.2 | 150.1 | 98.0 | 63.2 | 43.8 | -3.8 | -96.3 | -130.3 | -176.0 |

$\alpha$ — YM/Q

| $\alpha$ | | | | | | | | | | | | | |
|---|---|---|---|---|---|---|---|---|---|---|---|---|
| 0.0 | 29.5 | -60.7 | -96.7 | -69.4 | -18.5 | 35.9 | 111.0 | 166.3 | 207.3 | 274.2 | 289.8 | 241.9 | 36.8 |
| 2.0 | 27.7 | -54.0 | -101.0 | -74.3 | -23.0 | 32.2 | 102.1 | 156.1 | 196.9 | 264.8 | 289.6 | 239.0 | 34.0 |
| 4.0 | 23.5 | -33.7 | -87.7 | -70.8 | -25.4 | 29.2 | 94.8 | 148.7 | 185.6 | 255.8 | 292.1 | 238.4 | 37.1 |
| 6.0 | 18.9 | -12.8 | -55.0 | -58.7 | -25.0 | 24.4 | 95.9 | 143.7 | 178.6 | 245.3 | 294.5 | 236.8 | 35.9 |
| 8.0 | 16.2 | 5.3 | -12.1 | -17.1 | -14.4 | 29.6 | 86.6 | 132.5 | 175.3 | 246.5 | 295.4 | 236.7 | 37.5 |
| 10.0 | 14.3 | 15.5 | 19.6 | 25.2 | 28.1 | 52.1 | 98.4 | 130.0 | 176.7 | 251.8 | 298.8 | 237.9 | 36.9 |
| 12.0 | 12.8 | 24.8 | 38.6 | 52.4 | 69.0 | 58.2 | 109.3 | 137.5 | 186.9 | 260.1 | 298.6 | 236.3 | 36.5 |
| 16.0 | 8.4 | 41.1 | 63.4 | 79.4 | 96.2 | 85.1 | 123.7 | 168.7 | 211.0 | 262.7 | 295.5 | 236.6 | 41.4 |
| 20.0 | 2.2 | 59.2 | 78.6 | 82.2 | 102.3 | 86.6 | 136.1 | 167.2 | 205.8 | 256.0 | 286.4 | 231.4 | 41.6 |
| 25.0 | -0.9 | 62.4 | 93.4 | 77.0 | 72.6 | 90.4 | 139.4 | 160.7 | 190.4 | 250.8 | 279.2 | 224.2 | 42.5 |
| 30.0 | -1.7 | 64.0 | 87.0 | 57.5 | 23.8 | 57.8 | 115.2 | 160.5 | 180.6 | 238.9 | 276.4 | 219.0 | 43.1 |
| 35.0 | -1.2 | 67.3 | 79.6 | 42.7 | 20.3 | 56.5 | 106.6 | 146.7 | 167.7 | 224.0 | 268.7 | 211.1 | 46.7 |
| 40.0 | 8.2 | 68.2 | 69.3 | 5.4 | 18.7 | 56.7 | 100.0 | 135.4 | 157.4 | 213.6 | 263.4 | 196.5 | 52.9 |
| 45.0 | 16.0 | 48.1 | 32.5 | 2.1 | 14.3 | 43.8 | 92.8 | 126.0 | 150.4 | 200.0 | 255.0 | 187.2 | 53.0 |
| $\psi$ | 0.0 | 4.0 | 8.0 | 12.0 | 16.0 | 20.0 | 25.0 | 30.0 | 35.0 | 45.0 | 60.0 | 75.0 | 90.0 |

(b) Pitch-sweep data; Moment components.

Figure A1.- Continued.

$\alpha$ | | | | | | $D/Q$ | | | | | | | | |

| $\alpha$ | | | | | | | $D/Q$ | | | | | | | | |
|---|---|---|---|---|---|---|---|---|---|---|---|---|---|---|---|
| 0.0 | 61.0 | 62.3 | 69.9 | 81.2 | 91.9 | 100.6 | 113.9 | 127.4 | 138.9 | 149.6 | 159.9 | 171.3 | 199.5 | 212.2 | 226.1 |
| 4.0 | 66.1 | 66.9 | 74.5 | 84.0 | 94.2 | 104.7 | 117.3 | 131.3 | 143.8 | 154.4 | 163.2 | 178.1 | 200.9 | 213.8 | 227.0 |
| 8.0 | 72.8 | 74.1 | 82.5 | 90.3 | 100.1 | 109.1 | 123.5 | 135.5 | 148.9 | 158.0 | 170.3 | 187.5 | 202.2 | 212.9 | 226.2 |
| 16.0 | 88.3 | 89.2 | 94.8 | 104.6 | 115.2 | 128.0 | 142.5 | 153.4 | 163.6 | 173.2 | 182.6 | 193.7 | 205.4 | 210.6 | 226.2 |
| 30.0 | 120.1 | 121.7 | 127.7 | 137.9 | 144.8 | 157.0 | 166.6 | 176.6 | 185.9 | 193.7 | 199.6 | 204.3 | 206.8 | 205.8 | 224.9 |

| $\alpha$ | | | | | | | $Y/Q$ | | | | | | | | |
|---|---|---|---|---|---|---|---|---|---|---|---|---|---|---|---|
| 0.0 | -4.5 | 10.5 | 19.3 | 26.9 | 33.1 | 42.1 | 57.9 | 67.9 | 72.4 | 80.7 | 81.1 | 84.4 | 92.4 | 79.4 | 4.8 |
| 4.0 | -2.1 | 13.2 | 21.4 | 29.7 | 32.5 | 42.0 | 56.2 | 65.0 | 69.0 | 74.3 | 75.6 | 80.5 | 93.2 | 80.8 | 7.5 |
| 8.0 | -3.4 | 13.2 | 25.8 | 31.0 | 35.2 | 45.7 | 55.5 | 61.8 | 68.2 | 73.0 | 76.9 | 85.9 | 94.3 | 82.9 | 6.1 |
| 16.0 | -8.3 | 14.4 | 33.2 | 45.3 | 53.5 | 54.7 | 53.3 | 59.2 | 63.6 | 71.4 | 75.8 | 82.4 | 93.9 | 86.4 | 6.3 |
| 30.0 | -12.8 | 13.1 | 27.0 | 39.4 | 47.5 | 55.0 | 57.0 | 51.9 | 57.9 | 59.1 | 62.9 | 68.0 | 80.4 | 84.5 | 4.9 |

| $\alpha$ | | | | | | | $L/Q$ | | | | | | | | |
|---|---|---|---|---|---|---|---|---|---|---|---|---|---|---|---|
| 0.0 | 4.2 | 3.6 | 6.0 | 8.2 | 10.7 | 16.2 | 23.7 | 31.9 | 39.5 | 45.3 | 39.8 | 28.3 | 5.7 | -16.6 | -5.5 |
| 4.0 | 12.5 | 11.9 | 17.0 | 21.3 | 27.1 | 34.0 | 44.0 | 51.3 | 60.4 | 62.2 | 50.7 | 30.6 | 0.4 | -16.1 | -4.3 |
| 8.0 | 18.1 | 17.9 | 21.1 | 28.6 | 37.2 | 45.0 | 57.8 | 68.0 | 72.7 | 68.9 | 49.9 | 33.7 | 1.4 | -16.2 | -4.0 |
| 16.0 | 26.7 | 28.1 | 33.7 | 41.4 | 49.8 | 63.4 | 76.4 | 73.5 | 67.8 | 61.3 | 52.8 | 42.9 | 8.7 | -18.4 | -2.0 |
| 30.0 | 51.2 | 49.7 | 50.6 | 59.4 | 61.9 | 66.5 | 69.6 | 77.2 | 77.5 | 73.5 | 66.0 | 54.2 | 23.2 | -8.6 | -0.3 |

| $\alpha$ | | | | | | | $RM/Q$ | | | | | | | | |
|---|---|---|---|---|---|---|---|---|---|---|---|---|---|---|---|
| 0.0 | 17.7 | -6.9 | 36.1 | -5.2 | 7.2 | 1.2 | -34.4 | -13.4 | -7.2 | -68.9 | -98.9 | -167.4 | -227.0 | -151.0 | -104.1 |
| 4.0 | -27.2 | 1.2 | -4.7 | -18.9 | -25.2 | -13.3 | -37.0 | -4.3 | -11.0 | -82.5 | -166.2 | -137.9 | -247.3 | -159.1 | -160.8 |
| 8.0 | 22.5 | -1.5 | -29.0 | -33.7 | 14.7 | -0.7 | 4.4 | -22.5 | -67.3 | -188.2 | -201.7 | -199.1 | -272.9 | -185.5 | -116.6 |
| 16.0 | 68.0 | 25.1 | -33.1 | -6.7 | -36.1 | -27.5 | 5.1 | -9.7 | -10.6 | -94.0 | -138.9 | -179.7 | -298.9 | -164.0 | -123.8 |
| 30.0 | 70.8 | 39.2 | 8.1 | 22.4 | -24.5 | -60.0 | -46.6 | -52.3 | -61.4 | -59.7 | -151.4 | -172.6 | -264.5 | -138.6 | -141.7 |

| $\alpha$ | | | | | | | $PM/Q$ | | | | | | | | |
|---|---|---|---|---|---|---|---|---|---|---|---|---|---|---|---|
| 0.0 | -60.5 | -27.8 | -41.2 | -22.3 | 14.6 | 2.0 | -1.9 | -14.5 | -1.6 | -15.4 | -28.0 | -61.9 | -250.1 | -257.1 | -210.7 |
| 4.0 | -81.1 | -67.9 | -31.5 | -9.0 | 35.7 | 55.3 | 50.5 | 63.5 | 41.5 | 18.9 | 11.8 | -29.4 | -236.4 | -264.4 | -234.8 |
| 8.0 | -97.2 | -91.0 | -55.2 | -12.5 | 9.5 | 25.4 | 35.4 | 61.4 | 82.0 | 65.0 | 33.9 | -223.6 | -263.9 | -262.3 | -206.0 |
| 16.0 | -5.1 | 5.4 | 23.1 | 1.9 | 41.3 | 44.1 | 59.1 | -13.1 | -31.0 | -87.8 | -111.5 | -186.2 | -256.7 | -237.3 | -244.1 |
| 30.0 | 163.5 | 141.3 | 156.6 | 108.5 | 127.4 | 76.7 | 70.6 | 38.3 | -2.2 | -0.9 | -19.0 | -78.1 | -186.0 | -213.2 | -245.5 |

| $\alpha$ | | | | | | | $YM/Q$ | | | | | | | | |
|---|---|---|---|---|---|---|---|---|---|---|---|---|---|---|---|
| 0.0 | 30.7 | -60.2 | -97.6 | -68.1 | -13.4 | 40.9 | 111.6 | 165.8 | 206.0 | 242.7 | 273.5 | 296.0 | 291.7 | 237.0 | 38.5 |
| 4.0 | 24.5 | -42.0 | -88.0 | -65.4 | -20.3 | 33.0 | 96.9 | 147.5 | 183.4 | 219.9 | 251.1 | 280.9 | 297.1 | 239.3 | 44.8 |
| 8.0 | 14.8 | 6.3 | 5.7 | 1.1 | -1.9 | 30.0 | 83.4 | 129.0 | 175.2 | 205.1 | 244.6 | 289.7 | 296.9 | 240.6 | 42.3 |
| 16.0 | 5.2 | 39.0 | 57.9 | 76.0 | 94.7 | 76.6 | 121.1 | 167.8 | 205.7 | 236.9 | 258.1 | 285.1 | 295.4 | 233.3 | 38.4 |
| 30.0 | 1.5 | 66.2 | 86.9 | 54.6 | 22.9 | 58.8 | 114.2 | 158.6 | 181.2 | 208.2 | 237.1 | 264.6 | 278.7 | 224.0 | 46.2 |
| $\psi$ | 0.0 | 4.0 | 8.0 | 12.0 | 16.0 | 20.0 | 25.0 | 30.0 | 35.0 | 40.0 | 45.0 | 50.0 | 60.0 | 75.0 | 90.0 |

(c) Yaw-sweep data.

Figure A1.- Concluded.

| $\alpha$ | | | | | | | | | | | | | | | |
|---|---|---|---|---|---|---|---|---|---|---|---|---|---|---|---|
| 0.0 | 2 | 2 | 2 | 2 | 2 | 2 | 2 | 2 | 2 | 1 | 2 | 1 | 2 | 2 | 2 |
| 2.0 | 1 | 1 | 1 | 1 | 1 | 1 | 1 | 1 | 1 | 0 | 1 | 0 | 1 | 1 | 1 |
| 4.0 | 2 | 2 | 2 | 2 | 2 | 2 | 2 | 2 | 2 | 1 | 2 | 1 | 2 | 2 | 2 |
| 6.0 | 1 | 1 | 1 | 1 | 1 | 1 | 1 | 1 | 1 | 0 | 1 | 0 | 1 | 1 | 1 |
| 8.0 | 2 | 2 | 2 | 2 | 2 | 2 | 2 | 2 | 2 | 1 | 2 | 1 | 2 | 2 | 2 |
| 10.0 | 1 | 1 | 1 | 1 | 1 | 1 | 1 | 1 | 1 | 0 | 1 | 0 | 1 | 1 | 1 |
| 12.0 | 1 | 1 | 1 | 1 | 1 | 1 | 1 | 1 | 1 | 0 | 1 | 0 | 1 | 1 | 1 |
| 16.0 | 2 | 2 | 2 | 2 | 2 | 2 | 2 | 2 | 2 | 1 | 2 | 1 | 2 | 2 | 2 |
| 20.0 | 1 | 1 | 1 | 1 | 1 | 1 | 1 | 1 | 1 | 0 | 1 | 0 | 1 | 1 | 1 |
| 25.0 | 1 | 1 | 1 | 1 | 1 | 1 | 1 | 1 | 1 | 0 | 1 | 0 | 1 | 1 | 1 |
| 30.0 | 2 | 2 | 2 | 2 | 2 | 2 | 2 | 2 | 2 | 1 | 2 | 1 | 2 | 2 | 2 |
| 35.0 | 1 | 1 | 1 | 1 | 1 | 1 | 1 | 1 | 1 | 1 | 1 | 1 | 1 | 1 | 1 |
| 40.0 | 1 | 1 | 1 | 1 | 1 | 1 | 1 | 1 | 1 | 1 | 1 | 1 | 1 | 1 | 1 |
| 45.0 | 1 | 1 | 1 | 1 | 1 | 1 | 1 | 1 | 1 | 1 | 1 | 1 | 1 | 1 | 1 |
| $\psi$ | 0. | 4. | 8. | 12. | 16. | 20. | 25. | 30. | 35. | 40. | 45. | 50. | 60. | 75. | 90. |

(a) Number of measurements each grid point.

Figure A2.- Differences between yaw- and pitch-sweep data.

| $\alpha$ | | | | | | D/Q | | | | | | | | | |
|---|---|---|---|---|---|---|---|---|---|---|---|---|---|---|---|
| 0.0 | -1.4 | 0.0 | 0.2 | -0.5 | 0.0 | -0.1 | 0.0 | 1.1 | 0.6 | 0.4 | 0.7 | 1.9 | -1.2 | 2.7 | -1.9 |
| 2.0 | -0.5 | -0.1 | -0.3 | -1.0 | -0.2 | -1.2 | 0.2 | 0.8 | 0.4 | -0.3 | 0.1 | -0.5 | -1.1 | -0.3 | -2.8 |
| 4.0 | 0.3 | 2.3 | 1.7 | -1.2 | 0.8 | 0.4 | -0.2 | 0.8 | -0.8 | -1.4 | -0.2 | -2.2 | 0.8 | -1.2 | -0.6 |
| 6.0 | -0.5 | 2.5 | 0.9 | -1.0 | -0.7 | 0.3 | 0.5 | 1.0 | -1.1 | -1.1 | -1.9 | -5.5 | 0.6 | -2.0 | -0.4 |
| 8.0 | 0.2 | 1.9 | -0.7 | 0.3 | -0.9 | 1.4 | 0.2 | 2.2 | -0.5 | 1.5 | 0.3 | -6.4 | 0.0 | -1.4 | -1.6 |
| 10.0 | -0.1 | 1.0 | 0.1 | 0.5 | 0.3 | 1.2 | 0.4 | 0.5 | -1.3 | 1.7 | 2.2 | -4.4 | -0.1 | 0.5 | -1.1 |
| 12.0 | -0.1 | 0.7 | 0.4 | 0.6 | 1.3 | 2.3 | 0.8 | -0.1 | -0.1 | 1.8 | 2.2 | -3.7 | -0.4 | -0.3 | -1.2 |
| 16.0 | -0.4 | -0.4 | 2.3 | 2.0 | 1.2 | 1.2 | 1.9 | 0.6 | -1.5 | -1.1 | -0.5 | -4.3 | -1.5 | -1.0 | -1.8 |
| 20.0 | -0.7 | 1.3 | 2.8 | 1.1 | 4.4 | 2.3 | 2.5 | -2.4 | -1.5 | -2.2 | -2.3 | -5.4 | -2.1 | -1.3 | -0.3 |
| 25.0 | 1.4 | 2.1 | 4.6 | 2.6 | 5.3 | 3.1 | 3.2 | -0.8 | -0.3 | -0.7 | 0.3 | -2.8 | -0.9 | -1.9 | -0.7 |
| 30.0 | 2.5 | 1.5 | 2.3 | 3.1 | 1.8 | -1.3 | 0.3 | 0.6 | 1.0 | 0.8 | 2.4 | -0.8 | -0.2 | 0.6 | 1.7 |

| $\alpha$ | | | | | | Y/Q | | | | | | | | | |
|---|---|---|---|---|---|---|---|---|---|---|---|---|---|---|---|
| 0.0 | 1.0 | 1.4 | 2.8 | 1.6 | -1.9 | -0.4 | -0.8 | 0.9 | 2.4 | -1.7 | 2.1 | -0.1 | -6.0 | -2.5 | -3.5 |
| 2.0 | 0.7 | 0.8 | 2.4 | -2.0 | -3.2 | -2.1 | -1.2 | -1.0 | 1.8 | -1.5 | 1.1 | -0.3 | -5.0 | -3.7 | -5.3 |
| 4.0 | -0.8 | -1.1 | 1.4 | 3.0 | -2.6 | -1.3 | -1.1 | 0.9 | 2.9 | -0.1 | 0.9 | 0.0 | -4.7 | -3.3 | -4.8 |
| 6.0 | -0.5 | 0.6 | 2.2 | 2.1 | -1.4 | -0.7 | -2.4 | 0.9 | -0.3 | -1.3 | 0.3 | -2.2 | -3.7 | -3.8 | -4.7 |
| 8.0 | -0.7 | 1.5 | 1.7 | 2.4 | -1.2 | -1.5 | -1.4 | 1.3 | 0.1 | -1.1 | -1.4 | -5.7 | -4.8 | -3.8 | -3.0 |
| 10.0 | 0.4 | 0.9 | 3.5 | 0.3 | -1.8 | 0.0 | 1.3 | 2.6 | -0.5 | -1.2 | -0.3 | -4.2 | -4.2 | -3.9 | -2.5 |
| 12.0 | 0.1 | 1.0 | 3.0 | -3.1 | -4.7 | -1.0 | 2.9 | 2.1 | 2.1 | 0.0 | 0.0 | -2.5 | -1.9 | -4.0 | -3.2 |
| 16.0 | 2.1 | -0.7 | 2.5 | 0.4 | -1.4 | 0.3 | -0.3 | -1.1 | -0.3 | -2.1 | -0.4 | -2.0 | -3.5 | -3.8 | -1.8 |
| 20.0 | -3.6 | 2.9 | 5.5 | 4.4 | 7.0 | 1.9 | -4.9 | -4.7 | -3.5 | -2.2 | 0.8 | -0.5 | -2.4 | -1.4 | -2.9 |
| 25.0 | -2.4 | 0.8 | 3.5 | 6.1 | 9.1 | 7.9 | 2.3 | -2.8 | -1.3 | 0.0 | 0.8 | 0.8 | 0.1 | -3.5 | -0.6 |
| 30.0 | 0.7 | -2.1 | -2.6 | -2.0 | 0.8 | -1.2 | -0.3 | 1.4 | -1.0 | 0.9 | 0.2 | 0.9 | 0.1 | -2.2 | -2.9 |

| $\alpha$ | | | | | | L/Q | | | | | | | | | |
|---|---|---|---|---|---|---|---|---|---|---|---|---|---|---|---|
| 0.0 | -0.2 | 0.0 | 0.0 | 0.5 | -0.9 | 0.1 | 0.7 | 1.5 | -0.7 | -6.5 | -1.0 | -0.8 | -0.7 | 0.0 | -0.7 |
| 2.0 | 0.6 | 1.6 | -1.4 | 0.9 | -0.7 | -1.0 | -0.7 | 1.7 | -1.3 | -6.9 | -0.3 | 0.9 | -1.9 | -0.3 | -0.6 |
| 4.0 | -0.4 | 0.6 | 0.8 | 1.0 | 0.3 | -1.4 | -3.3 | 1.1 | -1.6 | -8.5 | -2.2 | 1.6 | -0.9 | -2.0 | -3.7 |
| 6.0 | 0.3 | 0.4 | 2.1 | 2.5 | 1.8 | 0.6 | 1.4 | 1.3 | -0.7 | -7.5 | 0.0 | 1.5 | -0.6 | -2.3 | -1.2 |
| 8.0 | 0.6 | -0.3 | -0.1 | 1.4 | -0.3 | -0.9 | 0.1 | 0.2 | -1.0 | -8.6 | -0.9 | -0.7 | -0.3 | -2.5 | -1.0 |
| 10.0 | -1.4 | -1.0 | -0.1 | -0.9 | -1.6 | -0.9 | -1.8 | 1.5 | 4.1 | -4.0 | -0.2 | -1.5 | -0.5 | -2.6 | -1.4 |
| 12.0 | 1.0 | -1.5 | -1.4 | -3.1 | -1.4 | 0.0 | -4.1 | 2.3 | -1.2 | -3.7 | 2.3 | -1.0 | -0.4 | -3.2 | -1.8 |
| 16.0 | -0.2 | -0.4 | -0.6 | -0.2 | -0.7 | -1.8 | 0.8 | -0.8 | 0.7 | 0.0 | 1.2 | -4.2 | -0.5 | -1.2 | -3.1 |
| 20.0 | 1.1 | 0.1 | 1.6 | 1.5 | 3.5 | 5.2 | 5.3 | 0.1 | -1.3 | -2.4 | -1.1 | -5.4 | -1.7 | -2.5 | -3.0 |
| 25.0 | 1.8 | 0.3 | 2.7 | 0.8 | 1.4 | -1.4 | 1.3 | 1.0 | 0.6 | -0.9 | 0.5 | -3.4 | -1.2 | -0.8 | -3.1 |
| 30.0 | 1.8 | -0.9 | 1.5 | -0.4 | 1.2 | -0.8 | -1.4 | -0.7 | -1.8 | -2.7 | -0.1 | -3.0 | -1.5 | -1.2 | -3.2 |
| $\psi$ | 0.0 | 4.0 | 8.0 | 12.0 | 16.0 | 20.0 | 25.0 | 30.0 | 35.0 | 40.0 | 45.0 | 50.0 | 60.0 | 75.0 | 90.0 |

DIFFERENCE STATISTICS

| | MIN | MAX | MEAN | STD DEV |
|---|---|---|---|---|
| D/Q | -6.4 | 5.3 | .1 | 1.7 |
| Y/Q | -6.0 | 9.1 | -.5 | 2.6 |
| L/Q | -8.6 | 5.3 | -.6 | 2.1 |

(b) Force differences.

Figure A2.- Continued.

$\alpha$             *RM/Q*

| $\alpha$ | | | | | | | | | | | | | | | |
|---|---|---|---|---|---|---|---|---|---|---|---|---|---|---|
| 0.0 | -20.8 | -4.2 | -57.6 | -13.1 | 26.0 | -19.3 | 23.5 | -8.2 | -51.3 | -39.3 | -59.1 | 11.6 | 75.6 | 75.5 | 37.1 |
| 2.0 | -26.4 | -18.4 | 34.1 | 18.6 | 49.8 | 39.5 | 26.5 | 51.7 | -38.6 | -29.6 | -30.3 | -12.6 | 67.4 | 80.2 | 72.0 |
| 4.0 | 34.0 | 9.5 | -20.4 | -54.7 | 55.5 | 11.9 | 61.5 | -20.6 | -89.0 | -53.4 | -5.5 | -37.8 | 63.5 | 96.2 | 101.1 |
| 6.0 | 13.5 | -5.0 | -64.3 | -13.1 | 26.1 | 12.4 | 10.6 | 2.6 | -4.0 | -12.8 | -69.1 | -76.6 | 30.8 | 95.0 | 36.8 |
| 8.0 | -11.7 | -18.9 | -38.1 | 9.1 | 12.0 | 36.3 | 47.5 | -8.6 | -35.6 | 42.6 | 13.4 | -1.3 | 48.2 | 81.1 | 9.1 |
| 10.0 | -17.7 | -17.9 | -63.8 | 14.3 | -21.9 | 34.2 | 31.1 | -26.4 | -38.0 | 25.8 | -0.7 | 0.2 | 70.7 | 81.0 | -9.3 |
| 12.0 | -22.0 | -23.7 | -34.0 | 33.7 | 53.9 | 10.4 | 2.4 | -18.1 | -109.7 | -20.0 | -3.3 | -18.7 | 8.9 | 67.2 | 25.3 |
| 16.0 | -51.6 | -25.1 | -9.5 | -40.2 | 13.2 | 18.1 | -36.1 | -4.1 | -60.0 | -17.1 | -12.7 | -5.9 | 45.2 | 53.9 | 10.3 |
| 20.0 | 8.8 | -53.0 | -16.8 | -7.6 | -8.6 | -8.0 | -28.1 | -0.3 | 9.8 | 19.7 | 28.8 | 29.8 | 72.8 | 21.4 | 51.9 |
| 25.0 | -16.3 | -5.1 | 21.9 | -35.9 | -6.1 | 37.1 | 8.8 | 40.1 | 37.6 | -5.5 | -2.3 | -5.3 | 33.8 | 62.5 | -17.6 |
| 30.0 | 0.3 | 24.6 | 0.6 | 22.7 | -64.3 | 28.0 | 8.3 | 19.0 | 15.6 | -41.5 | -5.1 | -4.0 | 47.7 | 55.6 | 64.4 |

$\alpha$             *PM/Q*

| $\alpha$ | | | | | | | | | | | | | | | |
|---|---|---|---|---|---|---|---|---|---|---|---|---|---|---|
| 0.0 | 26.9 | 1.9 | 14.8 | -4.1 | -14.6 | -2.5 | -7.3 | 3.0 | -23.5 | -13.8 | -5.3 | -38.8 | 14.7 | 7.7 | -22.1 |
| 2.0 | -33.6 | -28.8 | -15.6 | -3.0 | -15.2 | -21.6 | -15.2 | -1.7 | -19.4 | -15.9 | -20.8 | -54.7 | 0.1 | -3.6 | 27.4 |
| 4.0 | -23.9 | -33.4 | -51.0 | -25.3 | -28.0 | -26.8 | -21.2 | -3.1 | -2.2 | -0.5 | -14.3 | -56.6 | -16.7 | 46.6 | 31.9 |
| 6.0 | -17.3 | -32.3 | -34.5 | -4.8 | -25.8 | -18.7 | 2.6 | 17.0 | 0.3 | -4.2 | -9.5 | 49.9 | -6.5 | 27.6 | -2.2 |
| 8.0 | -14.9 | -27.7 | -9.1 | -26.5 | -10.1 | -32.5 | -10.1 | -13.6 | -28.5 | -38.3 | -33.9 | 136.4 | 2.2 | 54.7 | -5.2 |
| 10.0 | -28.0 | -42.1 | -31.1 | -43.9 | -28.1 | -60.5 | -31.5 | 21.2 | -9.2 | -40.8 | -70.3 | 87.7 | 27.9 | 21.5 | 3.8 |
| 12.0 | -18.0 | -25.3 | -40.7 | -53.6 | -61.1 | -55.8 | -14.0 | 8.1 | 6.3 | -23.2 | -62.3 | 58.4 | 22.9 | 17.2 | 32.4 |
| 16.0 | -14.4 | -29.7 | -26.0 | -9.9 | -34.5 | -35.2 | -51.4 | -8.5 | -8.1 | 21.9 | 18.8 | 46.7 | 23.7 | 33.4 | 42.4 |
| 20.0 | -9.8 | -23.6 | -21.4 | -8.7 | -38.8 | -23.7 | -55.9 | -21.5 | -25.3 | 12.5 | 32.2 | 42.3 | 3.3 | 49.7 | 28.7 |
| 25.0 | 11.8 | -21.8 | -67.8 | -8.4 | 3.9 | -9.5 | -37.7 | -22.3 | -8.5 | 6.1 | 21.4 | 25.1 | -2.3 | 19.8 | 19.2 |
| 30.0 | -16.4 | -22.1 | -46.3 | -34.4 | -18.7 | 27.6 | 7.3 | -12.9 | -34.7 | -39.5 | -25.0 | -16.1 | -8.6 | 3.5 | 9.1 |

$\alpha$             *YM/Q*

| $\alpha$ | | | | | | | | | | | | | | | |
|---|---|---|---|---|---|---|---|---|---|---|---|---|---|---|
| 0.0 | -1.2 | -0.5 | 0.9 | -1.3 | -5.1 | -5.0 | -0.6 | 0.5 | 1.3 | -1.9 | 0.7 | -16.6 | -1.9 | 4.9 | -1.7 |
| 2.0 | 0.1 | -2.9 | -8.2 | -7.6 | -6.1 | -4.8 | -2.2 | -0.6 | 2.2 | -0.5 | 2.5 | -15.4 | -4.8 | 0.8 | -7.7 |
| 4.0 | -1.0 | 8.3 | 0.3 | -5.4 | -5.1 | -3.8 | -2.1 | 1.2 | 2.2 | 0.8 | 4.7 | -13.0 | -5.0 | -0.9 | -7.7 |
| 6.0 | -0.8 | 5.1 | -13.8 | -26.5 | -13.9 | -7.1 | 5.8 | 5.4 | -0.7 | -0.5 | -2.6 | -23.6 | -2.5 | -3.2 | -7.7 |
| 8.0 | 1.4 | -1.0 | -17.8 | -18.2 | -12.5 | -0.4 | 3.2 | 3.5 | 0.1 | 5.8 | 1.9 | -26.9 | -1.5 | -3.9 | -4.8 |
| 10.0 | 1.9 | 1.0 | 0.9 | 5.4 | 5.9 | 10.4 | 5.6 | -8.7 | -6.1 | 1.2 | 3.8 | -21.1 | 2.3 | -0.9 | -4.4 |
| 12.0 | 2.8 | 2.1 | 6.8 | 13.9 | 22.6 | 4.9 | 7.1 | -10.9 | -3.6 | 2.5 | 8.8 | -14.5 | 2.5 | -0.7 | -3.8 |
| 16.0 | 3.2 | 2.1 | 5.5 | 3.4 | 1.5 | 8.5 | 2.6 | 0.9 | 5.3 | 0.0 | 4.6 | -11.5 | 0.1 | 3.3 | 3.0 |
| 20.0 | -1.9 | 12.4 | 12.4 | 12.3 | 28.1 | 15.1 | 17.0 | 2.0 | 7.1 | 2.2 | 3.9 | -13.1 | -4.2 | 0.8 | 1.0 |
| 25.0 | -3.7 | 5.9 | 16.9 | 14.8 | 24.1 | 25.2 | 22.7 | -1.2 | 0.4 | 2.2 | 6.2 | -11.7 | -5.5 | -3.1 | -0.9 |
| 30.0 | -3.2 | -2.2 | 0.1 | 2.9 | 0.9 | -1.0 | 1.0 | 1.9 | -0.6 | 1.6 | 1.8 | -13.2 | -2.3 | -5.0 | -3.1 |

| $\psi$ | 0.0 | 4.0 | 8.0 | 12.0 | 16.0 | 20.0 | 25.0 | 30.0 | 35.0 | 40.0 | 45.0 | 50.0 | 60.0 | 75.0 | 90.0 |
|---|---|---|---|---|---|---|---|---|---|---|---|---|---|---|---|

### TABLE STATISTICS

| | MIN | MAX | MEAN | STD DEV |
|---|---|---|---|---|
| RM | -109.7 | 101.1 | 5.5 | 39.1 |
| PM | -70.3 | 136.4 | -8.8 | 29.5 |
| YM | -26.9 | 28.1 | -.2 | 8.5 |

(c) Moment differences.

Figure A2.- Concluded.

| $\alpha$ | $D/Q$ | | | | | | | | | | | | | | |
|---|---|---|---|---|---|---|---|---|---|---|---|---|---|---|---|
| 0.0 | 60.3 | 62.3 | 70.0 | 80.9 | 91.9 | 100.6 | 113.9 | 128.0 | 139.2 | 149.8 | 160.3 | 172.2 | 198.9 | 213.6 | 225.2 |
| 2.0 | 63.3 | 64.6 | 72.1 | 82.1 | 93.0 | 102.1 | 115.7 | 129.8 | 141.6 | 151.9 | 161.6 | 174.4 | 199.7 | 212.9 | 225.2 |
| 4.0 | 66.3 | 68.1 | 75.3 | 83.4 | 94.6 | 104.9 | 117.2 | 131.7 | 143.4 | 153.7 | 163.1 | 177.0 | 201.3 | 213.2 | 226.7 |
| 6.0 | 69.2 | 71.8 | 79.0 | 86.7 | 96.8 | 107.1 | 120.7 | 133.9 | 145.8 | 155.7 | 165.8 | 180.1 | 201.8 | 212.4 | 226.4 |
| 8.0 | 72.9 | 75.1 | 82.2 | 90.5 | 99.7 | 109.8 | 123.6 | 136.6 | 148.6 | 158.8 | 170.5 | 184.3 | 202.2 | 212.2 | 225.4 |
| 10.0 | 76.6 | 78.4 | 85.6 | 94.1 | 104.0 | 114.4 | 128.5 | 140.2 | 151.9 | 162.6 | 174.5 | 186.9 | 202.9 | 212.6 | 225.7 |
| 12.0 | 80.5 | 82.0 | 88.9 | 97.8 | 108.3 | 119.7 | 133.4 | 144.4 | 156.2 | 166.5 | 177.6 | 188.8 | 203.6 | 211.6 | 225.6 |
| 16.0 | 88.1 | 89.0 | 96.0 | 105.6 | 115.8 | 128.6 | 143.4 | 153.7 | 162.9 | 172.7 | 182.4 | 191.5 | 204.6 | 210.1 | 225.3 |
| 20.0 | 97.0 | 99.1 | 105.6 | 114.7 | 125.9 | 137.4 | 150.6 | 158.8 | 169.2 | 178.0 | 186.3 | 194.0 | 204.8 | 208.6 | 225.7 |
| 25.0 | 109.4 | 111.1 | 118.2 | 127.3 | 136.9 | 148.2 | 159.6 | 167.9 | 177.8 | 186.0 | 193.7 | 199.1 | 205.9 | 206.6 | 225.0 |
| 30.0 | 121.3 | 122.4 | 128.9 | 139.4 | 145.7 | 156.4 | 166.8 | 176.9 | 186.4 | 194.1 | 200.8 | 203.9 | 206.7 | 206.1 | 225.8 |
| 35.0 | 129.0 | 133.4 | 140.9 | 148.2 | 153.3 | 164.7 | 174.8 | 188.8 | 196.4 | 202.3 | 208.2 | 208.3 | 208.4 | 204.2 | 224.9 |
| 40.0 | 144.2 | 145.3 | 151.6 | 158.0 | 163.5 | 170.5 | 183.7 | 196.6 | 204.6 | 211.3 | 218.0 | 215.3 | 209.9 | 204.3 | 223.2 |
| 45.0 | 159.6 | 161.8 | 165.6 | 167.4 | 170.1 | 180.4 | 193.2 | 204.0 | 212.7 | 219.1 | 225.4 | 221.4 | 213.4 | 201.2 | 224.0 |

| $\alpha$ | $Y/Q$ | | | | | | | | | | | | | | |
|---|---|---|---|---|---|---|---|---|---|---|---|---|---|---|---|
| 0.0 | -4.0 | 11.2 | 20.7 | 27.7 | 32.2 | 41.9 | 57.5 | 68.4 | 73.6 | 79.8 | 82.2 | 84.3 | 89.4 | 78.2 | 3.1 |
| 2.0 | -3.0 | 12.3 | 21.5 | 27.3 | 31.2 | 41.0 | 56.5 | 66.0 | 71.6 | 76.7 | 78.9 | 82.3 | 90.3 | 78.3 | 3.5 |
| 4.0 | -2.5 | 12.7 | 22.1 | 31.2 | 31.2 | 41.4 | 55.7 | 65.5 | 70.5 | 74.3 | 76.1 | 80.5 | 90.8 | 79.2 | 5.1 |
| 6.0 | -3.0 | 13.5 | 24.7 | 31.4 | 33.2 | 43.5 | 54.7 | 63.9 | 68.5 | 73.0 | 76.4 | 82.1 | 91.9 | 80.0 | 4.4 |
| 8.0 | -3.8 | 13.9 | 26.6 | 32.2 | 34.6 | 45.0 | 54.8 | 62.5 | 68.3 | 72.5 | 76.2 | 83.0 | 91.9 | 81.0 | 4.6 |
| 10.0 | -4.4 | 13.9 | 29.4 | 34.7 | 38.9 | 48.0 | 55.6 | 62.5 | 66.8 | 72.0 | 76.5 | 82.9 | 92.1 | 81.8 | 4.9 |
| 12.0 | -5.8 | 14.3 | 31.0 | 36.6 | 42.0 | 49.7 | 55.9 | 61.5 | 67.0 | 72.2 | 76.4 | 82.9 | 93.2 | 82.7 | 4.6 |
| 16.0 | -7.3 | 14.1 | 34.5 | 45.5 | 52.8 | 54.9 | 53.2 | 58.7 | 63.5 | 70.4 | 75.6 | 81.4 | 92.2 | 84.5 | 5.4 |
| 20.0 | -11.4 | 15.5 | 34.2 | 45.8 | 55.3 | 55.7 | 51.9 | 54.8 | 60.2 | 66.8 | 72.5 | 78.0 | 88.8 | 85.2 | 4.5 |
| 25.0 | -12.4 | 14.0 | 31.0 | 44.6 | 54.2 | 58.8 | 56.8 | 53.1 | 59.3 | 63.5 | 67.9 | 73.6 | 85.3 | 83.4 | 5.1 |
| 30.0 | -12.5 | 12.1 | 25.7 | 38.4 | 47.9 | 54.4 | 56.9 | 52.6 | 57.4 | 59.5 | 63.0 | 68.5 | 80.5 | 83.4 | 3.5 |
| 35.0 | -5.4 | 10.1 | 17.4 | 26.3 | 34.8 | 46.0 | 48.8 | 50.9 | 51.9 | 55.1 | 58.3 | 63.3 | 73.4 | 83.0 | -0.6 |
| 40.0 | -3.2 | 4.7 | 15.2 | 18.3 | 25.3 | 34.7 | 41.1 | 45.2 | 47.3 | 49.2 | 51.0 | 56.6 | 67.7 | 81.2 | -1.2 |
| 45.0 | -0.5 | -0.2 | 6.5 | 6.9 | 13.8 | 22.1 | 32.7 | 37.9 | 38.9 | 40.7 | 42.5 | 48.3 | 59.8 | 78.0 | -6.6 |

| $\alpha$ | $L/Q$ | | | | | | | | | | | | | | |
|---|---|---|---|---|---|---|---|---|---|---|---|---|---|---|---|
| 0.0 | 4.1 | 3.6 | 6.0 | 8.4 | 10.3 | 16.3 | 24.1 | 32.7 | 39.2 | 42.0 | 39.3 | 27.9 | 5.3 | -16.6 | -5.8 |
| 2.0 | 8.7 | 8.5 | 10.8 | 15.2 | 18.6 | 24.6 | 33.5 | 42.5 | 49.3 | 50.3 | 45.1 | 29.9 | 2.1 | -16.5 | -5.2 |
| 4.0 | 12.3 | 12.2 | 17.4 | 21.8 | 27.3 | 33.3 | 42.4 | 51.9 | 59.6 | 57.9 | 49.6 | 31.4 | 0.0 | -17.1 | -6.2 |
| 6.0 | 15.5 | 15.1 | 20.1 | 26.2 | 33.1 | 39.8 | 51.6 | 60.3 | 66.2 | 61.8 | 50.3 | 32.9 | 0.6 | -17.3 | -4.8 |
| 8.0 | 18.4 | 17.8 | 21.1 | 29.3 | 37.1 | 44.5 | 57.9 | 68.1 | 72.2 | 64.6 | 49.5 | 33.4 | 1.3 | -17.5 | -4.5 |
| 10.0 | 19.6 | 20.0 | 24.2 | 31.4 | 39.6 | 49.2 | 61.6 | 70.1 | 73.5 | 65.0 | 50.5 | 35.3 | 3.0 | -18.1 | -4.2 |
| 12.0 | 22.9 | 22.3 | 26.7 | 33.5 | 42.8 | 54.2 | 65.1 | 71.9 | 69.7 | 63.3 | 52.5 | 37.8 | 4.8 | -18.9 | -3.9 |
| 16.0 | 26.6 | 27.9 | 33.4 | 41.3 | 49.5 | 62.5 | 76.8 | 73.1 | 68.2 | 61.3 | 53.4 | 40.8 | 8.4 | -19.0 | -3.5 |
| 20.0 | 34.3 | 34.3 | 39.3 | 47.3 | 55.0 | 66.9 | 77.1 | 74.6 | 69.9 | 63.6 | 56.0 | 43.4 | 12.0 | -16.9 | -3.0 |
| 25.0 | 43.3 | 42.1 | 45.9 | 53.4 | 58.3 | 64.7 | 72.7 | 76.4 | 74.3 | 68.7 | 61.5 | 48.5 | 17.4 | -12.5 | -2.5 |
| 30.0 | 52.1 | 49.3 | 51.3 | 59.2 | 62.5 | 66.1 | 68.9 | 76.8 | 76.6 | 72.2 | 66.0 | 52.7 | 22.5 | -9.2 | -1.9 |
| 35.0 | 53.9 | 55.8 | 57.7 | 60.1 | 67.1 | 69.1 | 72.9 | 76.2 | 77.6 | 73.3 | 68.9 | 54.7 | 26.4 | -5.7 | -3.3 |
| 40.0 | 60.1 | 58.8 | 62.3 | 66.8 | 68.5 | 69.3 | 73.7 | 76.0 | 75.1 | 72.4 | 69.7 | 56.8 | 31.0 | -0.6 | -1.1 |
| 45.0 | 61.9 | 62.9 | 65.2 | 67.3 | 66.9 | 69.1 | 72.6 | 73.2 | 73.0 | 70.5 | 68.0 | 56.7 | 34.2 | 3.0 | -1.9 |
| $\psi$ | 0.0 | 4.0 | 8.0 | 12.0 | 16.0 | 20.0 | 25.0 | 30.0 | 35.0 | 40.0 | 45.0 | 50.0 | 60.0 | 75.0 | 90.0 |

(a) Force components.

Figure A3.- Combined yaw- and pitch-sweep data.

| $\alpha$ | | | | | | $RM/Q$ | | | | | | | | | |
|---|---|---|---|---|---|---|---|---|---|---|---|---|---|---|---|
| 0.0 | 7.3 | -9.0 | 7.3 | -11.8 | 20.2 | -8.4 | -22.7 | -17.5 | -32.8 | -88.6 | -128.4 | -161.6 | -189.2 | -113.3 | -85.6 |
| 2.0 | -17.9 | -12.0 | 32.8 | -2.8 | 15.9 | 13.7 | -22.5 | 17.0 | -28.4 | -90.5 | -147.7 | -158.9 | -203.5 | -115.0 | -96.4 |
| 4.0 | -10.2 | 5.9 | -14.9 | -46.3 | 2.5 | -7.3 | -6.3 | -14.6 | -55.5 | -109.2 | -168.9 | -156.8 | -215.6 | -111.0 | -110.3 |
| 6.0 | 4.4 | -2.7 | -49.0 | -32.9 | 7.8 | -0.8 | -11.0 | -12.1 | -41.2 | -141.7 | -218.5 | -206.8 | -244.7 | -124.8 | -120.3 |
| 8.0 | 16.6 | -10.9 | -48.0 | -29.2 | 20.7 | 17.4 | 28.2 | -26.8 | -85.1 | -166.9 | -195.0 | -199.8 | -248.8 | -144.9 | -112.1 |
| 10.0 | 25.0 | -3.8 | -61.9 | -19.8 | -8.9 | 9.7 | 20.1 | -32.5 | -72.1 | -151.8 | -186.4 | -194.1 | -244.1 | -139.6 | -123.1 |
| 12.0 | 34.3 | 0.0 | -48.1 | -3.4 | 16.3 | -8.9 | 6.0 | -25.2 | -93.8 | -151.1 | -172.0 | -198.7 | -281.5 | -141.2 | -107.6 |
| 16.0 | 42.2 | 12.6 | -37.8 | -26.8 | -29.5 | -18.5 | -12.9 | -11.8 | -40.6 | -102.6 | -145.3 | -182.7 | -276.3 | -137.1 | -118.7 |
| 20.0 | 73.2 | 2.6 | -29.7 | -2.2 | -37.1 | -40.8 | -23.7 | -22.0 | -20.2 | -74.3 | -128.1 | -162.8 | -252.7 | -146.0 | -103.0 |
| 25.0 | 61.7 | 31.6 | 4.3 | -5.9 | -31.7 | -29.8 | -23.7 | -17.0 | -24.5 | -74.7 | -148.1 | -177.8 | -259.9 | -116.4 | -144.1 |
| 30.0 | 71.0 | 51.5 | 8.4 | 33.8 | -56.7 | -46.0 | -42.5 | -42.8 | -53.6 | -80.4 | -153.9 | -174.6 | -240.7 | -110.8 | -109.5 |
| 35.0 | 75.2 | 19.2 | 48.7 | 77.5 | 9.4 | -71.8 | -10.8 | -58.4 | -64.5 | -126.9 | -189.4 | -192.6 | -199.1 | -73.2 | -66.8 |
| 40.0 | 74.6 | 39.4 | 40.3 | -22.7 | -12.8 | -22.5 | -68.1 | -118.6 | -78.2 | -138.3 | -198.3 | -206.8 | -223.8 | -67.9 | -64.6 |
| 45.0 | 78.3 | 64.9 | 57.0 | 23.4 | -15.4 | -26.9 | -35.0 | -26.7 | -70.7 | -114.5 | -158.4 | -175.0 | -208.2 | -72.0 | -35.4 |

| $\alpha$ | | | | | | $PM/Q$ | | | | | | | | | |
|---|---|---|---|---|---|---|---|---|---|---|---|---|---|---|---|
| 0.0 | -47.0 | -26.9 | -33.8 | -24.4 | 7.3 | 0.8 | -5.5 | -13.0 | -13.4 | -22.3 | -30.6 | -81.3 | -242.8 | -253.3 | -221.8 |
| 2.0 | -87.6 | -62.3 | -44.2 | -17.1 | 17.6 | 17.8 | 16.7 | 23.6 | 10.2 | -6.2 | -18.5 | -73.0 | -243.2 | -262.6 | -209.0 |
| 4.0 | -93.1 | -84.6 | -57.0 | -21.6 | 21.7 | 41.9 | 39.9 | 62.0 | 40.4 | 18.6 | 4.7 | -57.7 | -244.8 | -241.1 | -218.9 |
| 6.0 | -97.8 | -95.6 | -60.6 | -13.1 | 9.7 | 31.0 | 44.3 | 70.9 | 61.9 | 39.9 | 18.1 | -101.6 | -253.4 | -249.6 | -221.5 |
| 8.0 | -104.7 | -104.8 | -59.8 | -25.8 | 4.4 | 9.1 | 30.4 | 54.6 | 67.8 | 45.9 | 17.0 | -155.4 | -262.8 | -234.9 | -208.6 |
| 10.0 | -88.2 | -88.0 | -51.2 | -30.9 | 3.4 | -0.2 | 25.6 | 53.4 | 49.2 | 6.4 | -37.6 | -170.4 | -248.2 | -245.3 | -213.6 |
| 12.0 | -60.1 | -55.5 | -36.4 | -32.1 | -5.2 | 6.9 | 40.3 | 28.2 | 28.6 | -23.0 | -70.0 | -175.7 | -248.9 | -241.2 | -208.9 |
| 16.0 | -12.3 | -9.4 | 10.1 | -3.0 | 24.0 | 26.5 | 33.4 | -17.4 | -35.0 | -76.9 | -102.1 | -162.8 | -244.9 | -220.6 | -222.9 |
| 20.0 | 38.2 | 32.4 | 50.5 | 28.0 | 46.5 | 41.6 | 34.4 | -9.2 | -35.4 | -56.7 | -69.0 | -134.2 | -234.9 | -205.6 | -230.2 |
| 25.0 | 109.2 | 81.9 | 75.0 | 66.2 | 98.6 | 60.3 | 47.6 | 8.8 | -16.7 | -28.9 | -41.3 | -104.1 | -212.4 | -211.9 | -235.4 |
| 30.0 | 155.3 | 130.3 | 133.5 | 91.3 | 118.1 | 90.5 | 74.3 | 31.9 | -19.6 | -20.7 | -31.5 | -86.2 | -190.3 | -211.4 | -240.9 |
| 35.0 | 192.1 | 184.3 | 179.3 | 149.4 | 163.2 | 111.1 | 119.0 | 49.5 | -2.7 | -4.9 | -7.1 | -56.3 | -154.6 | -176.0 | -263.1 |
| 40.0 | 202.9 | 220.5 | 162.4 | 166.9 | 151.7 | 146.9 | 127.2 | 51.2 | 50.5 | 16.6 | -17.3 | -45.5 | -101.9 | -230.0 | -250.5 |
| 45.0 | 206.5 | 190.3 | 201.1 | 188.5 | 179.2 | 150.1 | 98.0 | 63.2 | 43.8 | 20.0 | -3.8 | -34.6 | -96.3 | -130.3 | -176.0 |

| $\alpha$ | | | | | | $YM/Q$ | | | | | | | | | |
|---|---|---|---|---|---|---|---|---|---|---|---|---|---|---|---|
| 0.0 | 30.1 | -60.5 | -97.2 | -68.8 | -15.9 | 38.4 | 111.3 | 166.1 | 206.7 | 241.7 | 273.9 | 287.7 | 290.8 | 239.4 | 37.7 |
| 2.0 | 27.7 | -52.6 | -96.9 | -70.5 | -19.9 | 34.6 | 103.2 | 156.4 | 195.8 | 231.1 | 263.6 | 280.8 | 292.0 | 238.6 | 37.8 |
| 4.0 | 24.0 | -37.9 | -87.8 | -68.1 | -22.9 | 31.1 | 95.9 | 148.1 | 184.5 | 220.3 | 253.5 | 274.4 | 294.6 | 238.9 | 40.9 |
| 6.0 | 19.3 | -15.3 | -48.1 | -45.4 | -18.0 | 28.0 | 93.0 | 141.0 | 179.0 | 212.2 | 246.6 | 273.5 | 295.8 | 238.4 | 39.7 |
| 8.0 | 15.5 | 5.8 | -3.2 | -8.0 | -8.1 | 29.8 | 85.0 | 130.8 | 175.3 | 208.0 | 245.6 | 276.3 | 296.1 | 238.7 | 39.9 |
| 10.0 | 13.4 | 15.0 | 19.2 | 22.5 | 25.2 | 46.9 | 95.6 | 134.4 | 179.8 | 213.7 | 249.9 | 278.0 | 297.7 | 238.3 | 39.1 |
| 12.0 | 11.4 | 23.7 | 35.2 | 45.5 | 57.7 | 55.8 | 105.8 | 143.0 | 188.7 | 222.3 | 255.7 | 280.2 | 297.4 | 236.6 | 38.4 |
| 16.0 | 6.8 | 40.0 | 60.7 | 77.7 | 95.4 | 80.8 | 122.4 | 168.3 | 208.4 | 236.9 | 260.4 | 279.4 | 295.5 | 235.0 | 39.9 |
| 20.0 | 3.2 | 53.0 | 72.4 | 76.0 | 88.2 | 79.1 | 127.6 | 166.2 | 202.3 | 229.8 | 254.1 | 272.7 | 288.5 | 231.0 | 41.1 |
| 25.0 | 1.0 | 59.4 | 85.0 | 69.6 | 60.6 | 77.8 | 128.0 | 161.3 | 190.2 | 219.5 | 247.7 | 266.1 | 281.9 | 225.8 | 43.0 |
| 30.0 | -0.1 | 65.1 | 87.0 | 56.0 | 23.4 | 58.3 | 114.7 | 159.6 | 180.9 | 209.0 | 238.0 | 258.0 | 277.6 | 221.5 | 44.6 |
| 35.0 | -1.2 | 67.3 | 79.6 | 42.7 | 20.3 | 56.5 | 106.6 | 146.7 | 167.7 | 195.9 | 224.0 | 238.9 | 268.7 | 211.1 | 46.7 |
| 40.0 | 8.2 | 68.2 | 69.3 | 5.4 | 18.7 | 56.7 | 100.0 | 135.4 | 157.4 | 185.5 | 213.6 | 230.2 | 263.4 | 196.5 | 52.9 |
| 45.0 | 16.0 | 48.1 | 32.5 | 2.1 | 14.3 | 43.8 | 92.8 | 126.0 | 150.4 | 175.2 | 200.0 | 218.3 | 255.0 | 187.2 | 53.0 |
| $\psi$ | 0.0 | 4.0 | 8.0 | 12.0 | 16.0 | 20.0 | 25.0 | 30.0 | 35.0 | 40.0 | 45.0 | 50.0 | 60.0 | 75.0 | 90.0 |

(b) Moment components.

Figure A3.- Concluded.

$\alpha$          $\Delta D/Q$

| $\alpha$ | 0.0 | 4.0 | 8.0 | 12.0 | 16.0 | 20.0 | 25.0 | 30.0 | 35.0 | 40.0 | 45.0 | 50.0 | 60.0 | 75.0 | 90.0 |
|---|---|---|---|---|---|---|---|---|---|---|---|---|---|---|---|
| 0.0 | 4.2 | 2.5 | 1.0 | 3.5 | 2.4 | 2.4 | 0.8 | 6.7 | 3.9 | 6.5 | 4.2 | 2.1 | 4.8 | 3.6 | 7.8 |
| 4.0 | 2.4 | 1.8 | 4.2 | 5.7 | 4.3 | 3.1 | 2.9 | 5.3 | 5.8 | 10.2 | 7.9 | 3.1 | 1.6 | -0.4 | 10.7 |
| 8.0 | 3.2 | 2.7 | 1.4 | 3.5 | 4.2 | 5.6 | 5.5 | 6.4 | 6.0 | 9.0 | 9.4 | 9.0 | 1.1 | 3.5 | 10.9 |
| 12.0 | 1.9 | 1.0 | 2.1 | 4.4 | 6.0 | 4.6 | 6.2 | 7.3 | 8.0 | 10.3 | 13.0 | 9.9 | 2.2 | -1.2 | 5.8 |
| 20.0 | 0.3 | 2.1 | 0.4 | 0.1 | 1.1 | 3.1 | 6.0 | 6.4 | 10.4 | 8.6 | 12.9 | 9.6 | 9.4 | -5.1 | 8.6 |

$\alpha$          $\Delta Y/Q$

| $\alpha$ | 0.0 | 4.0 | 8.0 | 12.0 | 16.0 | 20.0 | 25.0 | 30.0 | 35.0 | 40.0 | 45.0 | 50.0 | 60.0 | 75.0 | 90.0 |
|---|---|---|---|---|---|---|---|---|---|---|---|---|---|---|---|
| 0.0 | -2.0 | -0.1 | 1.5 | 4.4 | 2.8 | 2.5 | -1.6 | 12.2 | 10.1 | 11.6 | 7.6 | 3.4 | 2.5 | 4.7 | -4.6 |
| 4.0 | -1.3 | 1.4 | 3.0 | 3.7 | 2.0 | 4.7 | 3.3 | 4.2 | 6.8 | 9.0 | 7.6 | 4.7 | 1.5 | 5.5 | -2.0 |
| 8.0 | -1.9 | 1.9 | 2.5 | 3.1 | 3.5 | 4.2 | 1.9 | 1.1 | 2.4 | 3.0 | 4.5 | 5.8 | 2.3 | 8.7 | -2.2 |
| 12.0 | -1.7 | 0.7 | 2.3 | 4.3 | 5.8 | 3.3 | 5.1 | 3.7 | 3.1 | 3.9 | 4.7 | 3.7 | 3.4 | 7.4 | -2.0 |
| 20.0 | -0.6 | 1.5 | 1.5 | 1.3 | 1.4 | 3.0 | 2.9 | 4.9 | 3.3 | 3.3 | 3.5 | 4.1 | 2.4 | 11.7 | -3.8 |

$\alpha$          $\Delta L/Q$

| $\alpha$ | 0.0 | 4.0 | 8.0 | 12.0 | 16.0 | 20.0 | 25.0 | 30.0 | 35.0 | 40.0 | 45.0 | 50.0 | 60.0 | 75.0 | 90.0 |
|---|---|---|---|---|---|---|---|---|---|---|---|---|---|---|---|
| 0.0 | -1.2 | 1.5 | 3.8 | 5.3 | 4.7 | 3.0 | 10.0 | 11.4 | 11.7 | 10.8 | 3.7 | 13.1 | -5.1 | -14.8 | -12.0 |
| 4.0 | -0.3 | 0.3 | 0.7 | 1.9 | 4.3 | 4.7 | 7.1 | 5.9 | 5.9 | 12.6 | 11.6 | 10.0 | -7.0 | -20.3 | -8.2 |
| 8.0 | -2.1 | -0.5 | 0.3 | 2.9 | -0.7 | 2.2 | 3.7 | 5.3 | 9.3 | 12.8 | 11.5 | 8.5 | -5.2 | -20.5 | -13.2 |
| 12.0 | -2.1 | -2.8 | -3.1 | -2.6 | -0.2 | 0.2 | 1.7 | 4.0 | 8.9 | 11.9 | 10.9 | 11.4 | -5.5 | -18.7 | -8.8 |
| 20.0 | -0.6 | -3.9 | -4.2 | -4.4 | -3.3 | -4.6 | -3.4 | 0.0 | 3.0 | 6.9 | 7.1 | 8.2 | 6.6 | -26.0 | -9.7 |

$\alpha$          $\Delta RM/Q$

| $\alpha$ | 0.0 | 4.0 | 8.0 | 12.0 | 16.0 | 20.0 | 25.0 | 30.0 | 35.0 | 40.0 | 45.0 | 50.0 | 60.0 | 75.0 | 90.0 |
|---|---|---|---|---|---|---|---|---|---|---|---|---|---|---|---|
| 0.0 | -17.9 | -42.0 | 8.9 | 9.8 | 13.9 | -22.2 | -13.6 | 37.0 | -38.2 | 7.0 | 45.7 | 5.8 | 10.8 | 63.6 | -55.2 |
| 4.0 | 1.8 | -5.6 | 13.1 | -30.3 | -15.6 | 45.4 | -24.0 | -25.5 | -36.9 | -42.3 | -22.2 | -20.9 | -23.5 | 56.6 | 37.7 |
| 8.0 | 7.5 | -11.8 | -1.2 | 19.3 | 33.5 | 10.8 | -18.5 | -32.0 | -16.2 | 11.5 | -48.1 | 21.9 | -24.8 | 56.3 | -16.5 |
| 12.0 | 0.8 | -34.4 | -37.2 | 13.3 | 43.6 | 9.5 | -20.2 | -5.9 | -10.5 | -5.4 | -57.2 | -27.1 | -15.6 | -5.1 | 7.9 |
| 20.0 | 4.7 | -10.4 | 5.5 | -36.4 | -45.8 | 21.0 | -43.8 | 12.0 | -20.3 | -19.5 | 29.1 | 24.9 | -72.4 | 36.7 | -24.7 |

$\alpha$          $\Delta PM/Q$

| $\alpha$ | 0.0 | 4.0 | 8.0 | 12.0 | 16.0 | 20.0 | 25.0 | 30.0 | 35.0 | 40.0 | 45.0 | 50.0 | 60.0 | 75.0 | 90.0 |
|---|---|---|---|---|---|---|---|---|---|---|---|---|---|---|---|
| 0.0 | -30.7 | -2.8 | 4.1 | 52.9 | 39.4 | 56.0 | 82.5 | 90.5 | 11.8 | 33.6 | 33.0 | 5.3 | 0.8 | -6.2 | -76.4 |
| 4.0 | 26.3 | 17.9 | 74.1 | 94.6 | 92.0 | 94.9 | 90.0 | 110.5 | 68.6 | 52.2 | 32.4 | -20.9 | -22.7 | -47.2 | 19.2 |
| 8.0 | 49.7 | 47.3 | 65.7 | 94.5 | 95.4 | 72.4 | 84.3 | 102.5 | 72.8 | 61.8 | 16.9 | -20.1 | -53.2 | -1.3 | 38.8 |
| 12.0 | 53.0 | 65.8 | 90.5 | 125.5 | 88.4 | 95.7 | 88.9 | 98.6 | 92.5 | 38.4 | 27.7 | 5.0 | -34.4 | -15.9 | -19.6 |
| 20.0 | 78.3 | 105.0 | 107.1 | 92.6 | 101.1 | 138.6 | 94.8 | 107.4 | 97.0 | 96.3 | 47.7 | 42.2 | 26.5 | -128.2 | 78.1 |

$\alpha$          $\Delta YM/Q$

| $\alpha$ | 0.0 | 4.0 | 8.0 | 12.0 | 16.0 | 20.0 | 25.0 | 30.0 | 35.0 | 40.0 | 45.0 | 50.0 | 60.0 | 75.0 | 90.0 |
|---|---|---|---|---|---|---|---|---|---|---|---|---|---|---|---|
| 0.0 | 0.3 | 11.3 | 33.8 | 50.4 | 43.7 | 45.1 | 39.0 | 51.2 | 47.3 | 44.3 | 27.4 | 22.2 | 5.8 | 1.7 | -9.6 |
| 4.0 | 1.8 | 15.6 | 31.7 | 29.1 | 28.6 | 33.0 | 30.4 | 24.5 | 31.6 | 42.3 | 27.1 | 12.6 | 7.7 | 2.7 | -10.8 |
| 8.0 | -2.0 | 15.7 | 18.0 | 14.7 | 21.4 | 27.3 | 12.8 | 4.9 | -10.1 | -11.2 | -8.7 | -1.1 | 17.7 | 8.9 | -10.4 |
| 12.0 | -4.5 | 6.1 | 16.3 | 23.0 | 25.1 | 20.8 | 22.6 | 9.4 | 6.3 | 3.6 | 0.1 | 0.5 | 6.7 | -1.8 | -7.6 |
| 20.0 | -4.5 | 6.1 | 10.9 | 7.4 | 28.5 | 22.6 | 18.0 | 14.3 | 11.2 | 12.1 | 8.9 | 7.2 | 6.3 | 0.3 | -8.8 |
| $\psi$ | 0.0 | 4.0 | 8.0 | 12.0 | 16.0 | 20.0 | 25.0 | 30.0 | 35.0 | 40.0 | 45.0 | 50.0 | 60.0 | 75.0 | 90.0 |

(a) Yaw-sweep data.

Figure A4.- Interference tares.

| $\alpha$ | $\Delta D/Q$ | | | | $\Delta RM/Q$ | | | |
|---|---|---|---|---|---|---|---|---|
| 0.0 | 3.2 | 2.0 | 2.7 | 8.4 | -34.3 | 5.2 | -44.8 | 61.0 |
| 4.0 | 3.2 | 1.7 | 4.5 | 6.5 | -7.7 | 31.1 | 24.3 | 13.5 |
| 8.0 | 4.4 | 1.7 | 3.7 | 6.5 | 16.0 | -9.8 | -24.6 | -32.9 |
| 12.0 | 2.6 | 2.3 | 3.7 | 7.0 | -44.7 | -2.5 | -21.5 | -32.6 |
| 16.0 | 0.6 | 2.1 | 5.2 | 8.9 | -38.7 | 54.7 | 11.5 | -27.0 |
| 20.0 | 1.7 | 1.1 | 4.4 | 9. | -28.1 | 21.8 | 60.0 | 19.3 |
| 25.0 | 0.7 | -0.8 | 5.5 | 5.5 | 19.7 | -3.1 | -29.0 | -25.1 |
| 30.0 | 0.3 | -3.8 | 1.5 | 1.5 | -8.4 | -16.0 | -62.6 | 16.6 |
| 35.0 | -1.1 | -6.7 | -0.4 | 5.8 | -4.2 | -41.2 | -65.7 | -13.9 |
| 40.0 | -4.3 | -8.5 | -7.4 | 0.0 | 29.3 | -56.3 | -44.9 | -38.8 |
| 45.0 | -2.2 | -3.4 | -6.1 | -2.6 | 10.9 | -95.9 | -4.8 | -35.5 |

| $\alpha$ | $\Delta Y/Q$ | | | | $\Delta PM/Q$ | | | |
|---|---|---|---|---|---|---|---|---|
| 0.0 | -2.1 | 4.1 | 8.4 | 11.1 | -5.3 | 35.2 | 75.8 | 43.6 |
| 4.0 | -0.8 | 1.9 | 6.8 | 7.7 | 22.4 | 53.4 | 93.3 | 41.1 |
| 8.0 | -1.9 | 0.7 | 1.2 | 2.7 | 45.9 | 89.0 | 70.4 | 29.8 |
| 12.0 | -2.6 | 3.4 | 2.3 | 4.4 | 61.9 | 55.5 | 67.8 | 75.0 |
| 16.0 | -0.9 | 4.9 | 3.9 | 3.8 | 57.1 | 67.5 | 74.7 | 60.1 |
| 20.0 | -2.1 | 5.1 | 3.6 | 4.7 | 70.6 | 73.5 | 59.7 | 80.4 |
| 25.0 | -1.1 | 1.7 | 1.8 | 3.1 | 67.7 | 78.0 | 115.9 | 40.7 |
| 30.0 | -1.7 | -2.3 | 0.0 | 0.6 | 82.1 | 62.1 | 118.2 | 51.3 |
| 35.0 | -1.5 | -14.0 | 2.6 | 2.5 | 89.3 | 89.6 | 72.5 | 11.9 |
| 40.0 | 1.7 | -14.3 | -1.7 | 5.1 | 43.0 | -12.0 | 39.3 | 34.8 |
| 45.0 | 1.0 | -9.2 | -0.6 | 3.7 | 75.1 | 80.8 | 49.6 | 90.5 |

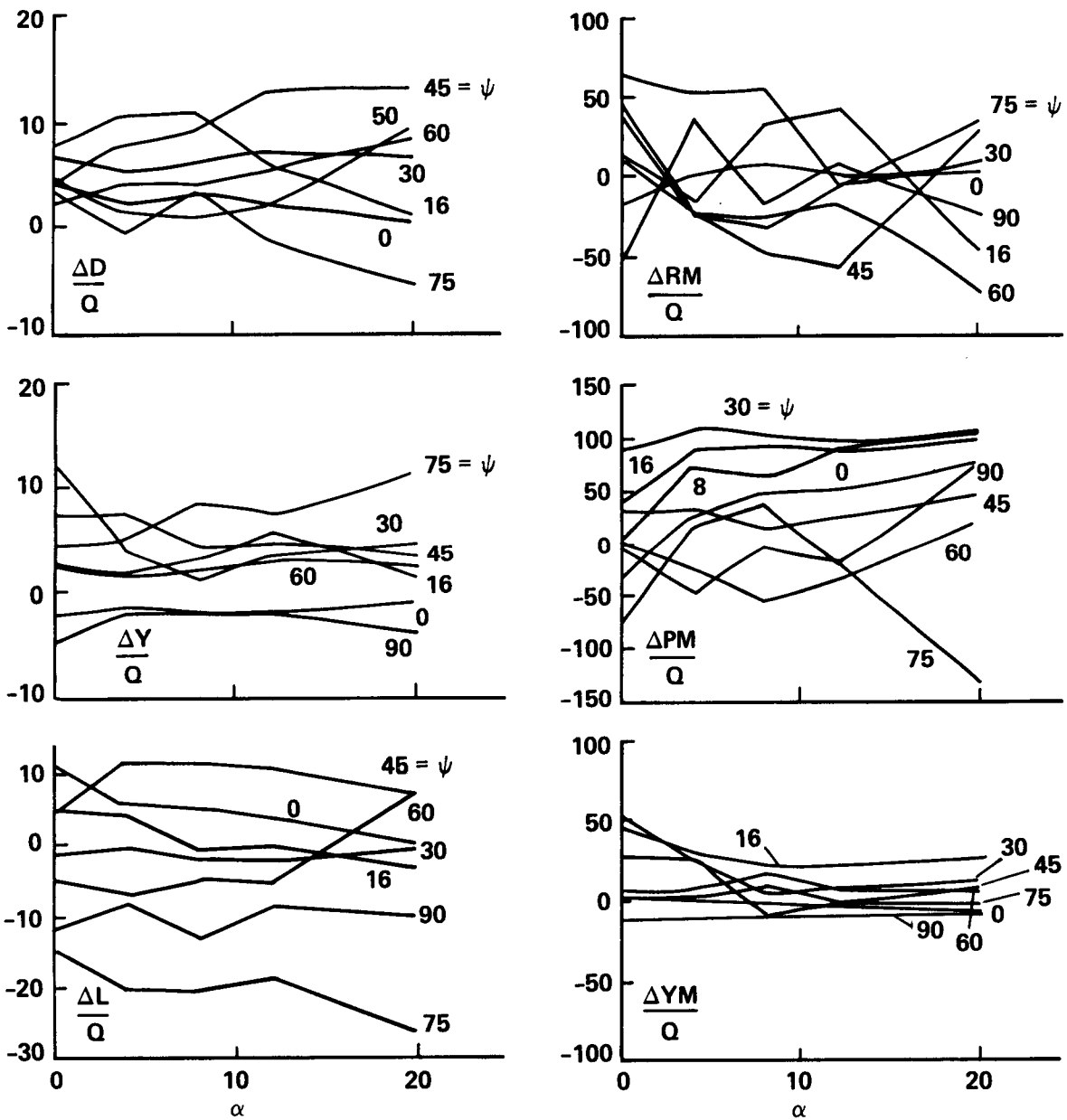| $\alpha$ | $\Delta L/Q$ | | | | $\Delta YM/Q$ | | | |
|---|---|---|---|---|---|---|---|---|
| 0.0 | 0.6 | 2.5 | 8.8 | 6.4 | 4.1 | 40.0 | 40.3 | 27.2 |
| 4.0 | -0.2 | 2.9 | 2.8 | 6.8 | 0.3 | 19.0 | 28.2 | 28.4 |
| 8.0 | -1.1 | 1.2 | 5.4 | 8.6 | 1.6 | 1.5 | 3.3 | -9.5 |
| 12.0 | -3.2 | -2.7 | 0.4 | 5.2 | 0.4 | 27.2 | 11.0 | 1.4 |
| 16.0 | -1.4 | -3.5 | -1.6 | 2.5 | -2.6 | 26.5 | 11.9 | 13.9 |
| 20.0 | -2.0 | -3.7 | -2.3 | 2.3 | -2.5 | 28.7 | 11.3 | 10.6 |
| 25.0 | -4.9 | -8.0 | -1.9 | 2.4 | -2.1 | -4.0 | 7.1 | 2.8 |
| 30.0 | -4.4 | -6.1 | -6.0 | 1.3 | 0.2 | -14.8 | 1.6 | -2.5 |
| 35.0 | -5.1 | -1.0 | -3.4 | 0.5 | -1.6 | -29.1 | 10.0 | -2.2 |
| 40.0 | -5.5 | -4.5 | -3.6 | 2.2 | 0.7 | -20.0 | 1.1 | -6.0 |
| 45.0 | -1.9 | -0.1 | -4.5 | -3.2 | -1.7 | -5.1 | 1.9 | -8.1 |
| $\psi$ | 0.0 | 16.0 | 30.0 | 45.0 | 0.0 | 16.0 | 30.0 | 45.0 |

(b) Pitch-sweep data.

Figure A4.- Concluded.
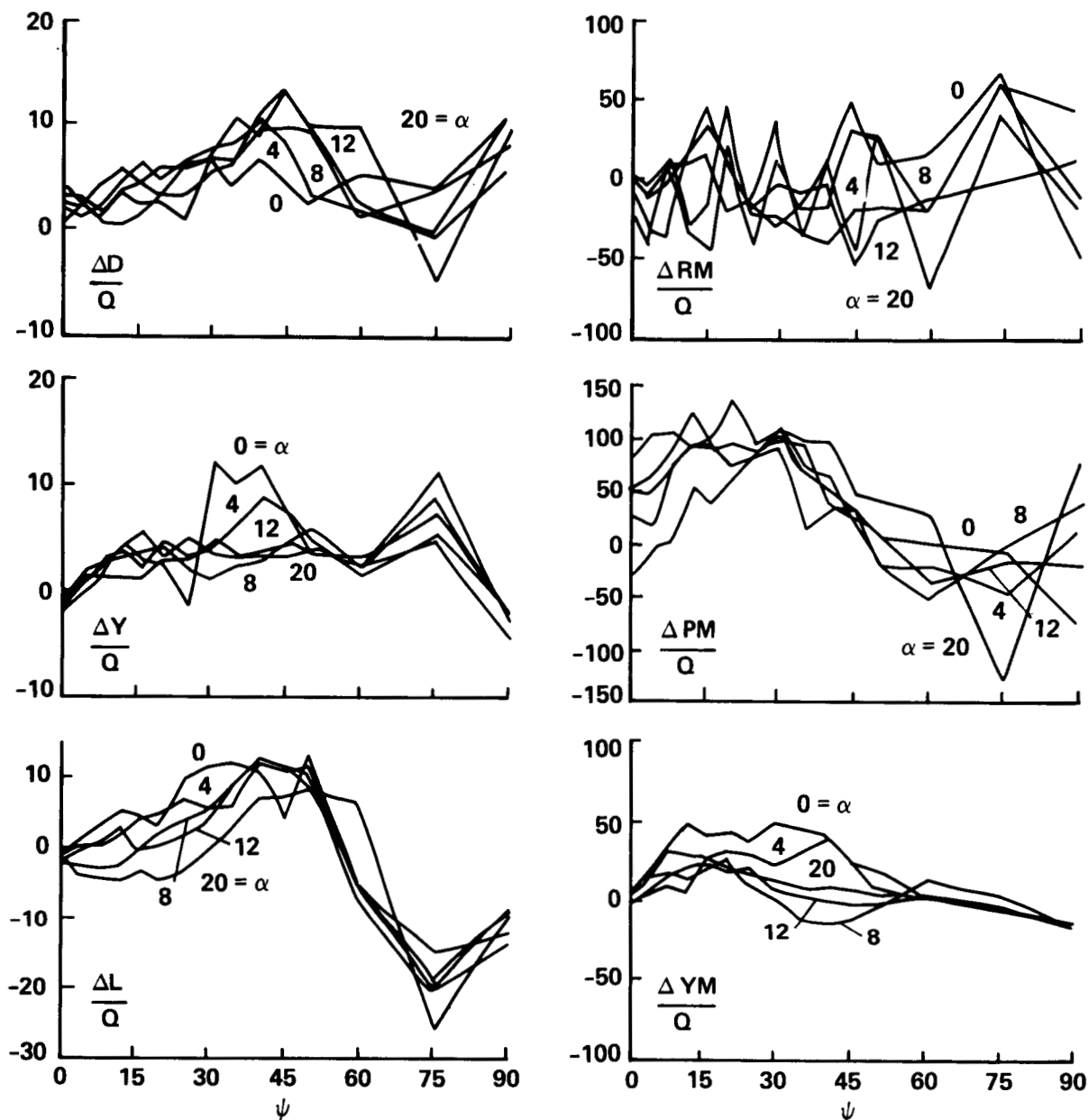
(a) DATA VS YAW ANGLE

Figure A5.- Interference tares: yaw-sweep data.

(b)  DATA VS ANGLE OF ATTACK

Figure A5.- Concluded.

|  | ψ | 0.0 | 4.0 | 8.0 | 12.0 | 16.0 | 20.0 | 25.0 | 30.0 | 35.0 | 40.0 | 45.0 | 50.0 | 60.0 | 75.0 | 90.0 | ERROR STATISTICS | | | |
|---|---|---|---|---|---|---|---|---|---|---|---|---|---|---|---|---|---|---|---|---|
|  |  |  |  |  |  |  |  |  |  |  |  |  |  |  |  |  | Min | Max | Mean | Std |
| $\Delta D/Q$ | | 2.4 | 2.0 | 1.8 | 3.4 | 3.6 | 3.8 | 4.3 | 6.4 | 6.8 | 8.9 | 9.5 | 6.7 | 3.8 | 0.1 | 8.8 | -5.3 | 5.6 | 0.0 | 2.1 |
| $\Delta Y/Q$ | | -1.5 | 1.1 | 2.2 | 3.4 | 3.1 | 3.5 | 4.0 | 5.2 | 5.1 | 6.2 | 5.6 | 4.3 | 2.4 | 7.6 | -2.9 | -5.6 | 7.0 | -0.1 | 2.0 |
| $\Delta L/Q$ | | -1.3 | -1.1 | -0.5 | 0.6 | 1.0 | 1.1 | 3.8 | 5.3 | 7.8 | 10.0 | 10.6 | 9.0 | -3.2 | -20.1 | -10.1 | -7.2 | 9.8 | 0.0 | 3.2 |
| $\Delta RM/Q$ | | -6.0 | -6.0 | -6.0 | -6.0 | -6.0 | -6.0 | -6.0 | -6.0 | -6.0 | -6.0 | -6.0 | -6.0 | -6.0 | -6.0 | -6.0 | -66.4 | 69.6 | 1.1 | 29.0 |

$\Delta PM/Q$ :

| α | 0.0 | 4.0 | 8.0 | 12.0 | 16.0 | 20.0 | 25.0 | 30.0 | 35.0 | 40.0 | 45.0 | 50.0 | 60.0 | 75.0 | 90.0 | Min | Max | Mean | Std |
|---|---|---|---|---|---|---|---|---|---|---|---|---|---|---|---|---|---|---|---|
| 0.0 | -25.0 | -5.0 | 13.0 | 32.0 | 50.0 | 67.0 | 86.0 | 79.0 | 52.0 | 28.0 | 18.0 | 5.0 | 1.0 | -20.0 | -38.0 | | | | |
| 4.0 | 18.0 | 45.0 | 70.0 | 90.0 | 102.0 | 107.0 | 102.0 | 97.0 | 73.0 | 52.0 | 32.0 | -8.0 | -23.0 | -19.0 | -11.0 | | | | |
| 8.0 | 40.0 | 57.0 | 73.0 | 85.0 | 90.0 | 93.0 | 93.0 | 90.0 | 82.0 | 62.0 | 17.0 | -20.0 | -53.0 | -17.0 | 15.0 | | | | |
| 12.0 | 50.0 | 75.0 | 95.0 | 107.0 | 107.0 | 107.0 | 105.0 | 100.0 | 80.0 | 47.0 | 25.0 | 5.0 | -34.0 | -15.0 | 41.0 | | | | |
| 20.0 | 90.0 | 103.0 | 108.0 | 111.0 | 112.0 | 114.0 | 112.0 | 107.0 | 102.0 | 96.0 | 48.0 | 42.0 | 27.0 | -12.0 | 94.0 | | | | |
| 45.0 | 90.0 | 103.0 | 108.0 | 111.0 | 112.0 | 114.0 | 112.0 | 107.0 | 102.0 | 96.0 | 48.0 | 42.0 | 27.0 | -12.0 | 94.0 | -116.2 | 30.2 | -4.5 | 19.5 |
| $\Delta YM/Q$ -1.8 | 11.0 | 22.1 | 24.9 | 29.5 | 29.8 | 24.6 | 20.9 | 17.3 | 18.2 | 11.0 | 8.3 | 8.8 | 2.4 | -9.4 | | -29.4 | 30.3 | 0.0 | 11.6 |

Figure A6. Estimated interference tares.

# APPENDIX B.-UNIVERSITY OF MARYLAND WIND TUNNEL DATA

The measurements made at the University of Maryland (UOM) 8- by 11-ft wind tunnel are given in reference 6 for a smooth-surfaced 8- by 8- by 20-ft container, along with additional measurements over a smaller grid to test the effects of variations in box details (rounded ends and corrugated sides) and box size.

Data from reference 6 for the smooth box are quoted in figure B1. These include corrections for interference tares; the tares were measured only sparsely and at $\alpha \le 25°$, and, as in the ARC test, were reported to be erratic. The measurement grid in figure B1 is dense at low sideslip angle but empty in the interval $50° < \beta < 90°$. This provides good function definition at low headings in the vicinity of the trim attitude for the container carried with a two point suspension, but poor definition in the region where the side force and yaw moment have extreme magnitudes and strong nonlinearities, and in the vicinity of its broadside trim attitude when carried with a single-point suspension. In general, grid point density is a factor in the accuracy of estimating a nonlinear function from measurements.

The following discussion considers; 1) the agreement of these data with the zero lines and mutual relationships given in section 3 from the symmetry of the box, and 2) the agreement of these data with the estimated static aerodynamics derived in section 4 from the Ames data.

Note that the UOM data is taken at positive sideslip (negative $\psi$). Therefore, equations 3.10 and 3.12 of the text are combined to give a relation analogous to equation 3.12 for positive sideslip:

$$\begin{pmatrix} D \\ Y \\ L \\ RM \\ PM \\ YM \end{pmatrix}_{(\beta,\alpha)} = \begin{pmatrix} D \\ -\cos\phi_w Y - \sin\phi_w L \\ -\sin\phi_w Y + \cos\phi_w L \\ -RM \\ \cos\phi_w PM - \sin\phi_w YM \\ -\sin\phi_w PM - \cos\phi_w YM \end{pmatrix}_{(\beta_1,\alpha_1)} \qquad (B1)$$

where

$$\tan\alpha_1 = \tan\beta / \cos\alpha$$

$$\sin\beta_1 = \sin\alpha\cos\beta$$

$$\cot\phi_w = \tan\alpha\sin\beta = \tan\alpha_1\sin\beta_1$$

Further, throughout this appendix, $S_1, S_2, ..., S_6$, are understood to denote regions of $\mathcal{D}_1$ which are defined by changing $\psi$ to $\beta$ in figure 3.3, and the Ames data at $(\beta, \alpha)$ are understood to be obtained from the data given at $(-\beta, \alpha)$ in figure 4.5 using the symmetry properties in equation 3.10.

## B1. Drag

First, the drag data are tested for the agreement of values at equivalent points in the regions $S_1$ and $S_2$ in accordance with equation (B1) by calculating the discrepancy:

$$\delta D(\beta,\alpha) = DU(\beta,\alpha) - DU(\beta_1,\alpha_1) \qquad (\beta,\alpha) \in S_1 \text{ or } S_2 \qquad (B2)$$

The letter "U" is appended in the nomenclature $(DU, LU, ... YMU)$ throughout this section to indicate the UOM data in figure B1. The results, (fig. B3) show good agreement with discrepancies below $10Q$ lb throughout $S_1$ and $S_2$.

Second, these differences are eliminated by averaging the data at related points in $S_1$ and $S_2$. The resulting revised drag table (omitted for brevity) can be compared with the Ames data by calculating the difference

$$\Delta D = \widehat{D} - \widehat{DU} \qquad (B3)$$

where $\widehat{D}, \widehat{DU}$ refer to the revised Ames data (fig. 4.5) and the revised UOM data, respectively. The superscript $\widehat{(\,)}$ refers to revised data throughout this section. This comparison is included in figure B3 and shows small differences below 5% of the drag at all points in the UOM measurement grid.

### B2. Side Force and Lift

The side-force data of figure B1 show good numerical agreement with its theoretical zero values at $\beta = 0, 90°$; the discrepancies have the same sign at both extremes of $\beta$ and this suggests a small tunnel bias in measuring side force. The lift data in figure B1 show good agreement with the expected zero value along the boundary $\alpha = 0$ (unlike the Ames data) as well as at $\beta = 90°$. Only small revisions, using equations 4.9, 4.10 from the text, are needed to null these data tables along the expected zero-force lines.

The revised data are omitted for brevity. Their agreement with equation B1 was tested by calculating the discrepancy from lift predicted from measurements at the equivalent point;

$$\delta L(\beta, \alpha) = \widehat{LU}(\beta, \alpha) + \sin \phi_w \widehat{YU}(\beta_1, \alpha_1) - \cos \phi_w \widehat{LU}(\beta_1, \alpha_1) \qquad (\beta, \alpha) \in S_1 \text{ or } S_2 \qquad (B4)$$

The results are tabulated and plotted in figure B4; discrepancies are below $10Q$ lb over about half the region of comparison, but larger discrepancies, reaching $25Q$ lb, occur otherwise. The two estimates of lift in equation B4 are compared in the plot and this shows good to fair agreement in curve shapes. Further, $\delta L \geq 0$ at all gridpoints; that is, the lift data is greater than lift predicted from measurements at the equivalent point. Lift can also be compared with its value predicted from the Y measurements alone;

$$\delta L'(\beta, \alpha) = \widehat{LU}(\beta, \alpha) + (\widehat{YU}(\beta, \alpha) \cot \phi_w + \widehat{YU}(\beta_1, \alpha_1) \csc \phi_w) \qquad (\beta, \alpha) \in S_1 \text{ or } S_2 \qquad (B5)$$

The results (not shown) were similar to those for $\delta L$; that is, $\delta L'$ exceeds $10Q$ lb over the same region as $\delta L$ above, and $\widehat{LU}$ is greater than predicted from the side force data at all grid points in $S_1$ and $S_2$. These differences are assumed to be due to errors in measuring lift and side force and these errors are at least as large as the discrepancies.

A comparison with the estimate from the Ames data (fig. 4.5) is included in figure B4, where;

$$\left. \begin{array}{l} \Delta Y = \widehat{Y} - \widehat{YU} \\ \Delta L = \widehat{L} - \widehat{LU} \end{array} \right\} \qquad (B6)$$

These differences contain the estimation errors and the small effects of differences in wind tunnel model surfaces. The side-force differences exceed $10Q$ *lbs* at only a few points and are otherwise

small, and plots of $\widehat{Y}$ and $\widehat{YU}$ in figure B4 demonstrate this good agreement graphically. The lift results show significant differences in the range of 10 to $30Q$ $lb$ over a large part of $\mathcal{R}_0$. This result for $\Delta L$ is close to the results for $\delta L$ and $\delta L'$ just given above, both in magnitude of the difference and the region of significant differences. Further, $\Delta L$ is negative at all grid points so that $\widehat{LU}$ exceeds the estimate from the Ames data throughout $\mathcal{R}_0$. Collectively, these comparisons suggest that the UOM lift data is less accurate than the side-force measurements in the region of largest differences, with these differences indicating the probable size of the lift measurement errors.

## B3. Roll Moment

A comparison of figures B2 and 2.3 shows a considerable difference from the Ames roll moment measurements. $RM$ was assumed an antisymmetric function in section 3 on the basis of the UOM data. An antisymmetric function will satisfy

$$\left.\begin{array}{l} RM(\beta,\alpha) = -RM(\beta_1,\alpha_1) \\ RM = 0° \quad \text{at} \quad \beta = 0°, \quad \text{or} \quad \beta = 90° , \quad \text{or} \quad \alpha = 0° \quad \text{or} \quad \tan\beta = \sin\alpha \end{array}\right\} \quad (B7)$$

The data (fig. B1) reach table extremes of $-125Q$ ft-lb, $77Q$ ft-lb. Although their magnitudes differ significantly, these extremes have opposite signs and occur at nearly equivalent points, consistent with equation B7. A symmetric function would have the same sign at equivalent points. In addition, the UOM data show small to moderate values along the boundaries where zero is predicted for an antisymmetric function in equation B7. These values are within the range of the discrepancies from the expected zero lines seen in the $PM$ and $YM$ data discussed next, and are assumed here to be measurement errors. The evidence does not rigorously exclude a small symmetric aerodynamic effect superposed with a dominant antisymmetric effect, but does indicate that such an effect, if present, is smaller than the measurement errors and would be negligible in its effects on load dynamics.

As was done in section 4 , the data are separated into symmetric and antisymmetric components over the regions $S_1$ and $S_2$ in accordance with equation B1, using:

$$\left.\begin{array}{l} RMUS(\beta,\alpha) = 0.5(RMU(\beta,\alpha) + RMU(\beta_1,\alpha_1)) \\ RMUA(\beta,\alpha) = 0.5(RMU(\beta,\alpha) - RMU(\beta_1,\alpha_1)) \end{array}\right\} \quad (B8)$$

Assuming roll is antisymmetric, then $RMUS$ is the average measurement error and $RMUA$ is the roll moment plus the antisymmetric component of the measurement errors. In the results (fig. B5), RMUA shows good agreement with the theoretical null lines. The average error, $RMUS$, exceeds $RMUA$ in magnitude over much of $S_1$ and $S_2$; this occurs in the region where both $RMUS$ and $RMUA$ have small magnitudes (below $25Q$ ft-lb) and for this region $RMUA$ is a very uncertain estimate of a small roll moment. Elsewhere, $RMUS$ reaches $36Q$ ft-lb, but this is only a moderate fraction of $RMUA$ in this region (50 to $90Q$ ft-lb). The data can be revised to agree with the theoretical zero lines and equation B1. This revision provides an estimate of the roll moment which can be used in place of the null value adopted in the text. A plot of this estimate is included in figure B5. However, the estimated roll moment is small, below $50Q$ ft-lb at nearly all grid points and would have little effect on the static or dynamic behavior of the load compared

to the restoring torques applied by a suspension. Consequently, the approximation, $\widehat{RM} = 0$, is expected to be adequate for a realistic simulation of the suspended load.

## B4. Yaw and Pitching Moment

The yaw-moment data in figures B1 and B2 show small to moderate nonzero values along the expected zero-yaw moment lines at $\beta = 0, 90°$. A comparison of figure B2 and 2.3 shows good qualitative agreement of curve shapes with the Ames data (after accounting for the sign reversal for yaw moment). The pitching-moment data also shows small to moderate nonzero values along its expected zero-moment lines at $\alpha = 0, \beta = 90°$. A comparison with figure 2.3 shows a considerable difference from the Ames data both qualitatively for $\beta$ above 30° and quantitatively everywhere.

The data can be revised to null the tables at the theoretical zero-moment lines using equations 4.9, 4.10 (and replacing $YC$ and $LC$ in those equations with $YMU, PMU$, respectively), and then the discrepancies from values computed from data at the equivalent point are

$$\left.\begin{array}{l} \delta PM = \widehat{PMU} - PMU_1 \\ PMU_1(\beta, \alpha) = \cos\phi_w \widehat{PMU}(\beta_1, \alpha_1) - \sin\phi_w \widehat{YMU}(\beta_1, \alpha_1) \end{array}\right\} \qquad (B9)$$

The results for $\delta PM$ (fig. B6) show moderate discrepancies (up to $50Q$ ft-lb) over most of $S_1$ and $S_2$ with a small region of larger discrepancies. The pitching moment functions compared in equation B9 are also plotted separately in figure B6 and this comparison shows good agreement of curve shapes.

The revised UOM and Ames data (fig. 4.5) are compared in figure B7;

$$\left.\begin{array}{l} \Delta PM = \widehat{PM} - \widehat{PMU} \\ \Delta YM = \widehat{YM} - \widehat{YMU} \end{array}\right\} \qquad (B10)$$

The numerical results show the same level of agreement for both components, with differences below $100Q$ ft-lb at nearly all grid points, and below $50Q$ ft-lb over most of $\mathcal{R}_0$. Plots are included and show good agreement of curve shapes for the two sources of data.

## Conclusions

The UOM data show good agreement with all zero-force and zero-moment lines predicted by the analysis of section 3, and are consistent with the estimate of the aerodynamics given in section 4, particularly with the rejection of the Ames $RM$ and $PM$ data as being dominated by errors, and with the estimate of PM from the Ames yaw-moment data.

Agreement with equation B1 can be tested in the regions $S_1$ and $S_2$. Agreement is good in the case of the drag data. The lift and side-force data, and the pitch- and yaw-moment data show good agreement of curve shapes, but moderate to significant numerical discrepancies from equation B1.

The roll-moment data are consistent with an antisymmetric function, but the data indicates that roll is a small moment which can be neglected and that an estimate of $RM$ from the data would have uncertainties of the size of the roll moment itself over most of the region $\mathcal{R}_0$.

Comparisons in the region $\mathcal{R}_0$ with the estimates derived from the Ames data show small differences in drag and side force, while lift, pitch, and yaw moments show good agreement in curve shapes, but moderate to significant numerical differences in some regions.

63

The UOM data lacks measurements in the interval $50° < \beta < 90°$ so that nonlinear aerodynamics are poorly defined in this region and an extrapolation of this data to the region $S_4$ using equation B1 would be similarly affected.

$DU/Q$

| α | | | | | | | | | | | | | | | |
|---|---|---|---|---|---|---|---|---|---|---|---|---|---|---|---|
| 0.0 | 55.0 | 57.6 | 59.7 | 62.7 | 65.4 | 68.0 | 72.1 | 76.3 | 79.6 | 88.7 | 100.2 | 113.2 | 137.6 | 163.3 | 225.8 |
| 2.0 | 57.0 | 58.4 | 60.0 | 63.3 | 65.9 | 68.7 | 72.4 | 76.9 | 80.5 | 89.1 | 102.2 | 114.4 | 137.7 | 163.3 | 225.4 |
| 4.0 | 59.8 | 60.8 | 62.5 | 65.7 | 68.1 | 70.4 | 74.2 | 78.3 | 81.8 | 91.5 | 105.5 | 117.4 | 139.3 | 164.6 | 224.7 |
| 6.0 | 62.2 | 63.6 | 65.4 | 68.8 | 71.3 | 73.4 | 77.0 | 81.0 | 85.1 | 97.2 | 109.6 | 120.0 | 141.1 | 166.0 | 224.8 |
| 8.0 | 64.8 | 66.2 | 68.4 | 72.2 | 75.1 | 77.2 | 80.9 | 84.8 | 88.8 | 101.6 | 114.0 | 124.7 | 143.3 | 168.1 | 225.7 |
| 10.0 | 68.2 | 69.4 | 71.0 | 75.0 | 78.6 | 81.8 | 85.5 | 89.0 | 94.3 | 106.7 | 118.9 | 129.0 | 146.1 | 172.5 | 225.7 |
| 12.0 | 71.4 | 72.6 | 74.1 | 78.4 | 81.9 | 85.1 | 89.1 | 93.9 | 98.1 | 110.0 | 123.6 | 133.8 | 150.6 | 174.7 | 225.5 |
| 14.0 | 75.5 | 76.5 | 78.3 | 82.3 | 85.4 | 89.4 | 94.1 | 98.5 | 103.4 | 115.9 | 128.8 | 136.5 | 156.6 | 177.1 | 226.7 |
| 16.0 | 79.9 | 81.2 | 82.9 | 86.2 | 90.1 | 94.1 | 98.5 | 104.2 | 109.3 | 121.6 | 133.2 | 141.8 | 161.8 | 178.3 | 226.1 |
| 20.0 | 88.4 | 90.3 | 93.1 | 97.4 | 102.5 | 105.9 | 110.6 | 117.9 | 122.8 | 134.1 | 143.8 | 151.9 | 166.6 | 181.7 | 225.7 |
| 25.0 | 99.9 | 103.2 | 106.2 | 111.7 | 117.1 | 121.7 | 128.1 | 133.7 | 138.5 | 148.0 | 154.4 | 161.7 | 175.9 | 186.6 | 226.0 |
| 30.0 | 111.9 | 114.9 | 118.3 | 124.0 | 130.0 | 133.0 | 139.5 | 143.8 | 148.9 | 156.8 | 164.6 | 171.5 | 185.1 | 193.4 | 227.4 |
| 40.0 | 139.8 | 141.0 | 144.7 | 147.3 | 151.0 | 157.9 | 161.9 | 164.6 | 168.1 | 177.0 | 186.5 | 194.8 | 207.9 | 206.9 | 226.6 |
| 45.0 | 159.3 | 157.5 | 159.6 | 162.4 | 168.6 | 172.5 | 174.7 | 176.0 | 179.5 | 188.5 | 197.6 | 207.1 | 217.9 | 217.0 | 227.2 |

$YU/Q$

| α | | | | | | | | | | | | | | | |
|---|---|---|---|---|---|---|---|---|---|---|---|---|---|---|---|
| 0.0 | -2.3 | -7.8 | -10.7 | -15.1 | -18.5 | -20.9 | -23.8 | -27.0 | -30.0 | -37.7 | -50.0 | -58.8 | -73.3 | -77.7 | 0.3 |
| 2.0 | -1.8 | -7.3 | -10.5 | -14.3 | -18.0 | -21.0 | -24.5 | -27.7 | -31.0 | -38.7 | -49.3 | -58.7 | -72.1 | -76.3 | -0.6 |
| 4.0 | -1.6 | -7.7 | -11.2 | -14.7 | -18.2 | -21.5 | -25.6 | -29.4 | -32.2 | -40.3 | -50.0 | -58.4 | -70.7 | -76.4 | 0.1 |
| 6.0 | -1.8 | -8.1 | -12.5 | -16.8 | -19.7 | -22.9 | -27.0 | -31.3 | -35.1 | -41.8 | -50.9 | -58.4 | -69.6 | -75.9 | 0.0 |
| 8.0 | -2.0 | -9.0 | -14.3 | -19.9 | -22.7 | -25.6 | -29.7 | -33.6 | -37.5 | -44.5 | -51.7 | -58.1 | -67.5 | -76.5 | -0.4 |
| 10.0 | -1.9 | -10.0 | -16.0 | -23.2 | -27.6 | -30.6 | -35.2 | -39.1 | -42.7 | -48.6 | -53.2 | -59.0 | -65.5 | -75.9 | -1.2 |
| 12.0 | -1.9 | -10.9 | -18.0 | -26.0 | -32.1 | -36.5 | -40.5 | -44.7 | -47.2 | -52.4 | -58.4 | -62.2 | -63.6 | -75.4 | -0.7 |
| 14.0 | -2.7 | -12.2 | -20.0 | -29.2 | -35.8 | -40.5 | -45.1 | -48.9 | -49.4 | -54.0 | -60.3 | -61.9 | -65.5 | -74.7 | -1.1 |
| 16.0 | -3.2 | -13.2 | -22.6 | -31.7 | -39.4 | -43.5 | -47.9 | -50.9 | -52.6 | -55.4 | -56.7 | -58.8 | -64.5 | -74.0 | -2.4 |
| 20.0 | -4.0 | -16.7 | -29.1 | -40.0 | -47.7 | -50.8 | -54.0 | -59.2 | -62.0 | -61.4 | -52.1 | -53.9 | -63.0 | -71.0 | -3.3 |
| 25.0 | -5.5 | -21.6 | -34.0 | -47.8 | -56.2 | -59.8 | -59.7 | -64.2 | -68.0 | -64.3 | -47.0 | -48.8 | -58.2 | -67.2 | -2.8 |
| 30.0 | -3.9 | -22.1 | -36.0 | -49.1 | -58.1 | -43.1 | -51.2 | -55.4 | -58.1 | -59.4 | -44.0 | -44.2 | -53.2 | -61.4 | -1.8 |
| 40.0 | -5.3 | -11.2 | -9.7 | -17.7 | -22.3 | -20.9 | -22.0 | -24.5 | -27.1 | -31.9 | -37.3 | -38.6 | -42.0 | -47.4 | 0.2 |
| 45.0 | -5.7 | -5.8 | -5.7 | -5.6 | -8.0 | -11.0 | -10.2 | -10.3 | -12.7 | -17.3 | -25.9 | -30.7 | -34.0 | -38.5 | -1.7 |

$LU/Q$

| α | | | | | | | | | | | | | | | |
|---|---|---|---|---|---|---|---|---|---|---|---|---|---|---|---|
| 0.0 | 0.2 | 0.6 | 0.0 | 0.6 | 0.1 | 0.1 | 0.2 | 0.4 | 0.2 | -2.3 | -3.1 | 7.9 | 6.6 | -1.7 | 2.2 |
| 2.0 | 6.8 | 6.3 | 6.6 | 7.2 | 7.6 | 8.1 | 8.7 | 10.1 | 10.9 | 9.7 | 20.7 | 22.6 | 20.0 | 1.0 | -2.2 |
| 4.0 | 11.5 | 11.7 | 12.0 | 13.4 | 15.2 | 16.0 | 18.2 | 19.2 | 20.4 | 23.3 | 34.8 | 37.5 | 33.6 | 6.0 | -3.1 |
| 6.0 | 16.1 | 16.1 | 15.8 | 18.3 | 21.4 | 23.2 | 26.6 | 28.9 | 30.6 | 41.8 | 49.2 | 51.2 | 44.1 | 10.1 | -1.2 |
| 8.0 | 19.5 | 19.6 | 20.5 | 21.9 | 25.3 | 28.1 | 32.6 | 36.3 | 38.9 | 51.6 | 60.3 | 64.2 | 51.3 | 13.8 | 0.6 |
| 10.0 | 24.1 | 24.3 | 24.3 | 25.5 | 28.0 | 31.6 | 36.6 | 39.1 | 44.0 | 56.1 | 69.8 | 74.0 | 57.1 | 20.7 | 0.8 |
| 12.0 | 27.0 | 28.1 | 28.4 | 30.2 | 32.3 | 35.9 | 40.0 | 44.6 | 49.8 | 61.0 | 73.0 | 77.6 | 60.8 | 26.4 | 0.7 |
| 14.0 | 30.9 | 32.0 | 32.6 | 34.3 | 36.9 | 40.6 | 45.4 | 50.5 | 56.2 | 67.2 | 73.3 | 71.9 | 54.2 | 29.7 | 3.1 |
| 16.0 | 35.3 | 36.4 | 36.9 | 38.4 | 41.8 | 45.2 | 50.6 | 55.3 | 61.0 | 73.6 | 80.3 | 72.9 | 60.1 | 32.8 | 3.1 |
| 20.0 | 44.8 | 45.3 | 45.8 | 48.5 | 52.4 | 56.4 | 62.2 | 66.5 | 69.7 | 79.7 | 87.5 | 80.7 | 58.9 | 36.2 | 4.2 |
| 25.0 | 56.2 | 56.1 | 57.0 | 59.1 | 63.1 | 68.6 | 74.9 | 77.1 | 79.0 | 84.9 | 91.0 | 85.7 | 66.8 | 42.1 | 5.0 |
| 30.0 | 65.1 | 65.5 | 67.6 | 70.0 | 73.8 | 78.8 | 81.0 | 79.9 | 80.2 | 81.5 | 90.7 | 89.2 | 71.7 | 47.1 | 8.0 |
| 40.0 | 81.1 | 81.2 | 83.3 | 83.4 | 84.3 | 88.0 | 86.8 | 86.3 | 89.2 | 89.2 | 90.2 | 89.8 | 77.5 | 52.7 | 8.1 |
| 45.0 | 87.1 | 84.7 | 85.6 | 88.1 | 91.0 | 91.5 | 91.1 | 90.4 | 91.4 | 92.2 | 92.0 | 88.8 | 76.6 | 54.3 | 7.3 |
| β | 0.0 | 2.0 | 4.0 | 6.0 | 8.0 | 10.0 | 12.0 | 14.0 | 16.0 | 20.0 | 25.0 | 30.0 | 40.0 | 50.0 | 90.0 |

(a) Force components.

Figure B1.- Wind tunnel data for a smooth-surfaced 8- by 8- by 20-ft container;
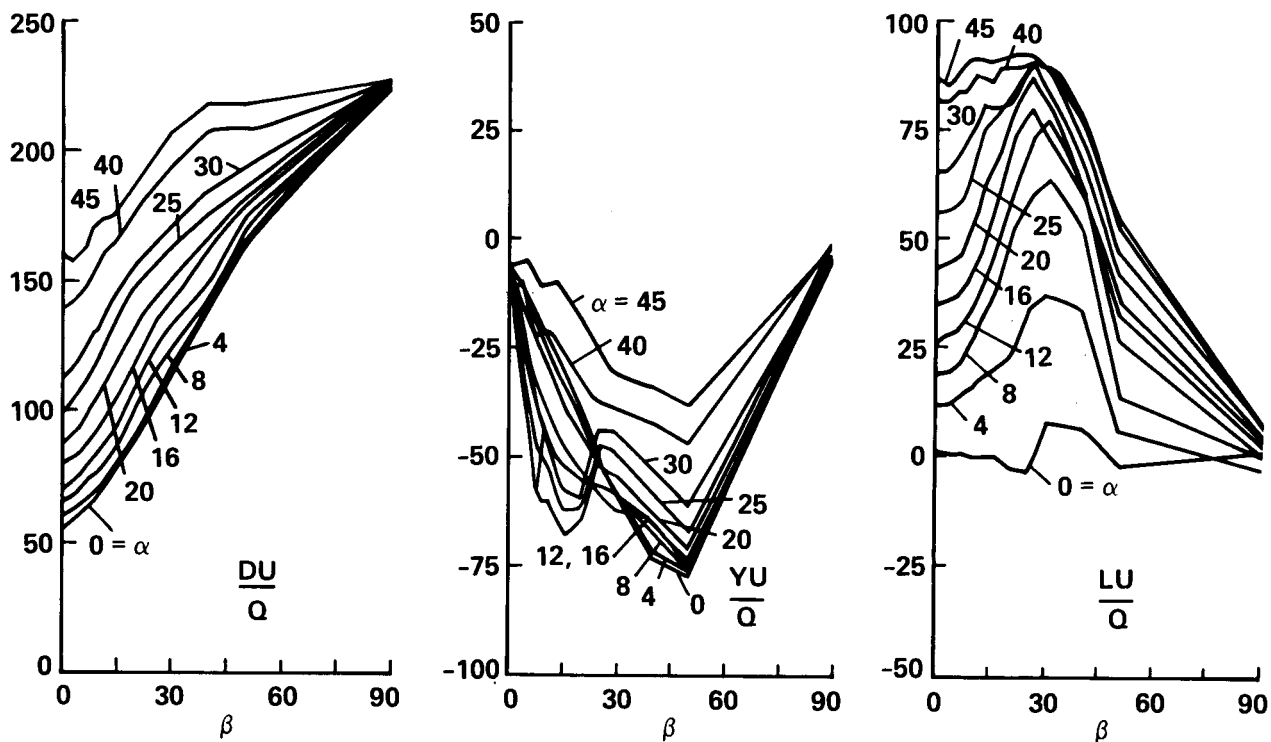University of Maryland (ref. 6).

$\alpha$           *RMU/Q*

| $\alpha$ | | | | | | | | | | | | | | | |
|---|---|---|---|---|---|---|---|---|---|---|---|---|---|---|
| 0.0 | 1.1 | -1.0 | -0.6 | -7.6 | -9.5 | -6.4 | -4.5 | -12.4 | -3.4 | -1.0 | 3.6 | -28.0 | -23.4 | -17.3 | -2.9 |
| 2.0 | 1.1 | -3.1 | -1.8 | -7.5 | -8.9 | -4.6 | -4.9 | -12.7 | -4.5 | -3.0 | -26.6 | -31.5 | -13.4 | 14.0 | -3.6 |
| 4.0 | 0.9 | -4.5 | -6.0 | -7.9 | -8.1 | -4.9 | -5.6 | -14.6 | -6.0 | -7.3 | -34.4 | -33.4 | -3.3 | 45.5 | -1.4 |
| 6.0 | 1.3 | -5.0 | -6.9 | -12.4 | -10.6 | -6.8 | -6.8 | -15.5 | -8.5 | -34.5 | -41.2 | -36.1 | 13.9 | 60.2 | 0.0 |
| 8.0 | 1.1 | -6.4 | -7.0 | -13.3 | -12.4 | -7.8 | -6.3 | -16.3 | -11.2 | -47.0 | -48.5 | -38.6 | 38.5 | 70.2 | -0.2 |
| 10.0 | 0.2 | -5.3 | -5.8 | -9.7 | -10.5 | -7.4 | -8.4 | -19.3 | -14.5 | -45.7 | -53.7 | -37.1 | 56.7 | 62.0 | 3.4 |
| 12.0 | -0.9 | -2.6 | -2.2 | -8.5 | -7.8 | -6.7 | -7.1 | -18.7 | -11.5 | -30.4 | -46.8 | -21.0 | 77.3 | 44.9 | -0.2 |
| 14.0 | -1.1 | -1.9 | 0.3 | -2.0 | -2.0 | 2.7 | -1.3 | -14.8 | -7.3 | -20.8 | -27.5 | 10.5 | 70.9 | 34.6 | -1.3 |
| 16.0 | -2.1 | -1.6 | 3.3 | -1.0 | 3.6 | 9.5 | 5.3 | -10.9 | -4.6 | -16.4 | -27.3 | -16.9 | 25.1 | 30.2 | 2.0 |
| 20.0 | -0.1 | 4.8 | 14.0 | 19.0 | 23.4 | 24.5 | 12.6 | -1.4 | 3.8 | -13.5 | -33.9 | -38.4 | -20.1 | 26.3 | 3.5 |
| 25.0 | 0.8 | 11.7 | 24.9 | 30.5 | 39.1 | 37.5 | 13.9 | 5.6 | 13.5 | 0.6 | -34.3 | -44.5 | -26.7 | 22.9 | 4.7 |
| 30.0 | -3.1 | 9.8 | 16.6 | 18.3 | 14.0 | -26.3 | 0.8 | 13.7 | 25.3 | 14.3 | -20.9 | -35.9 | -24.8 | 17.8 | 9.6 |
| 40.0 | -11.8 | -33.9 | -63.7 | -84.7 | -108.5 | -91.0 | -16.2 | -12.0 | -1.2 | -8.6 | -10.7 | -23.3 | -19.6 | -1.9 | -27.3 |
| 45.0 | -18.1 | -53.2 | -88.3 | -125.3 | -120.7 | -33.2 | -24.9 | -33.2 | -26.0 | -31.2 | -24.6 | -27.5 | -22.6 | -11.0 | -40.1 |

$\alpha$           *PMU/Q*

| $\alpha$ | | | | | | | | | | | | | | | |
|---|---|---|---|---|---|---|---|---|---|---|---|---|---|---|
| 0.0 | 18.5 | 20.7 | 28.1 | 27.1 | 25.2 | 18.8 | 17.5 | 16.7 | 8.5 | -3.1 | -9.4 | 10.6 | 10.3 | -9.3 | 9.1 |
| 2.0 | -28.8 | -29.6 | -11.2 | 2.2 | 12.1 | 13.6 | 18.5 | 24.5 | 21.4 | 22.4 | 38.5 | 47.3 | 44.9 | 14.7 | 8.6 |
| 4.0 | -66.2 | -68.5 | -55.8 | -21.7 | 1.7 | 11.2 | 21.9 | 28.4 | 32.2 | 49.5 | 65.8 | 78.1 | 76.4 | 30.0 | 6.7 |
| 6.0 | -90.0 | -87.0 | -80.6 | -45.0 | -13.6 | 10.1 | 26.5 | 40.3 | 48.1 | 64.1 | 86.4 | 98.1 | 107.0 | 34.1 | 6.2 |
| 8.0 | -96.7 | -93.3 | -90.7 | -57.9 | -23.6 | 0.2 | 26.7 | 46.9 | 54.5 | 57.3 | 84.6 | 111.2 | 130.9 | 29.4 | 2.8 |
| 10.0 | -87.0 | -85.9 | -81.9 | -60.8 | -36.9 | -8.9 | 9.1 | 27.6 | 37.3 | 41.1 | 76.1 | 110.2 | 150.9 | 4.0 | 3.7 |
| 12.0 | -70.5 | -68.3 | -63.2 | -47.2 | -34.7 | -21.1 | -1.8 | 21.5 | 36.7 | 48.2 | 73.9 | 114.4 | 166.6 | -23.1 | 3.7 |
| 14.0 | -49.8 | -46.1 | -41.6 | -27.6 | -15.5 | -9.1 | 7.3 | 28.7 | 47.2 | 71.7 | 79.4 | 116.6 | 114.6 | -25.7 | 1.3 |
| 16.0 | -22.2 | -21.6 | -14.3 | -5.5 | 4.3 | 17.9 | 36.9 | 51.5 | 55.3 | 80.6 | 62.6 | 47.8 | 52.7 | -21.9 | 2.8 |
| 20.0 | 34.9 | 33.5 | 33.0 | 34.1 | 39.6 | 53.7 | 71.7 | 80.9 | 77.4 | 83.8 | 58.5 | 21.6 | 4.1 | -8.9 | 1.8 |
| 25.0 | 98.5 | 94.2 | 84.5 | 79.8 | 77.0 | 79.2 | 117.1 | 124.8 | 116.1 | 106.4 | 62.3 | 38.9 | 29.4 | 12.7 | 0.8 |
| 30.0 | 139.5 | 132.2 | 117.4 | 106.1 | 102.4 | 121.0 | 136.0 | 137.1 | 134.5 | 136.8 | 103.9 | 78.7 | 60.1 | 36.1 | -8.0 |
| 40.0 | 166.5 | 155.6 | 159.5 | 159.7 | 164.7 | 167.5 | 158.8 | 162.1 | 160.7 | 160.1 | 144.4 | 126.3 | 101.2 | 67.6 | 5.7 |
| 45.0 | 165.8 | 156.0 | 159.3 | 163.6 | 171.6 | 168.8 | 167.7 | 171.6 | 172.3 | 167.2 | 149.4 | 135.5 | 108.2 | 77.1 | 1.8 |

$\alpha$           *YMU/Q*

| $\alpha$ | | | | | | | | | | | | | | | |
|---|---|---|---|---|---|---|---|---|---|---|---|---|---|---|
| 0.0 | 9.2 | 42.7 | 64.8 | 88.3 | 93.6 | 84.9 | 62.7 | 33.9 | 4.3 | -62.8 | -132.1 | -179.8 | -232.9 | -259.2 | -3.1 |
| 2.0 | 5.6 | 33.2 | 62.4 | 82.8 | 92.5 | 84.4 | 62.4 | 34.0 | 6.0 | -63.7 | -120.2 | -162.7 | -215.6 | -249.1 | -5.1 |
| 4.0 | 1.2 | 18.6 | 42.4 | 62.9 | 76.7 | 69.4 | 49.9 | 24.2 | -7.2 | -66.0 | -106.4 | -141.0 | -202.3 | -234.8 | -4.1 |
| 6.0 | 0.0 | 5.0 | 17.4 | 35.9 | 45.1 | 47.9 | 33.6 | 5.1 | -24.8 | -45.0 | -92.9 | -123.1 | -186.0 | -225.7 | -6.0 |
| 8.0 | -2.9 | -3.1 | -5.2 | 1.4 | 8.1 | 11.0 | 1.3 | -12.4 | -37.7 | -35.9 | -76.2 | -109.3 | -176.7 | -227.3 | -6.0 |
| 10.0 | -4.9 | -12.4 | -19.3 | -26.8 | -26.3 | -31.4 | -50.9 | -68.8 | -72.2 | -50.5 | -73.5 | -101.7 | -169.2 | -237.3 | -7.5 |
| 12.0 | -6.8 | -19.7 | -26.8 | -47.8 | -60.5 | -65.0 | -78.1 | -83.7 | -89.0 | -92.1 | -89.9 | -108.8 | -166.3 | -245.8 | -5.1 |
| 14.0 | -10.5 | -29.2 | -42.0 | -61.7 | -75.9 | -82.6 | -88.7 | -95.7 | -92.7 | -109.3 | -111.5 | -127.1 | -186.6 | -250.6 | -0.7 |
| 16.0 | -10.7 | -35.6 | -55.6 | -77.8 | -89.7 | -89.3 | -95.2 | -104.2 | -101.6 | -112.6 | -127.6 | -146.8 | -190.1 | -253.2 | -5.5 |
| 20.0 | -12.2 | -43.5 | -74.0 | -100.7 | -100.0 | -98.7 | -99.8 | -117.3 | -124.1 | -123.8 | -138.1 | -158.9 | -206.5 | -246.6 | -1.1 |
| 25.0 | -16.7 | -55.9 | -86.6 | -120.1 | -131.5 | -132.0 | -116.3 | -121.8 | -124.7 | -114.9 | -132.2 | -152.5 | -191.7 | -230.1 | -5.5 |
| 30.0 | -15.9 | -66.2 | -99.5 | -135.1 | -151.0 | -157.6 | -84.5 | -54.5 | -45.0 | -60.8 | -115.2 | -139.7 | -170.5 | -214.6 | -9.5 |
| 40.0 | -25.6 | -62.1 | -74.1 | -118.7 | -147.8 | -108.1 | -1.3 | 8.1 | -0.9 | -29.9 | -68.9 | -98.5 | -126.4 | -173.1 | -14.8 |
| 45.0 | -36.1 | -60.4 | -78.4 | -99.8 | -85.3 | 37.5 | 31.8 | 20.8 | 8.7 | -20.6 | -54.3 | -75.5 | -105.0 | -151.4 | -7.5 |

| $\beta$ | 0.0 | 2.0 | 4.0 | 6.0 | 8.0 | 10.0 | 12.0 | 14.0 | 16.0 | 20.0 | 25.0 | 30.0 | 40.0 | 50.0 | 90.0 |
|---|---|---|---|---|---|---|---|---|---|---|---|---|---|---|---|

(b) Moment components.

Figure B1.- Concluded.

(a) FORCE COMPONENTS (ft$^2$)
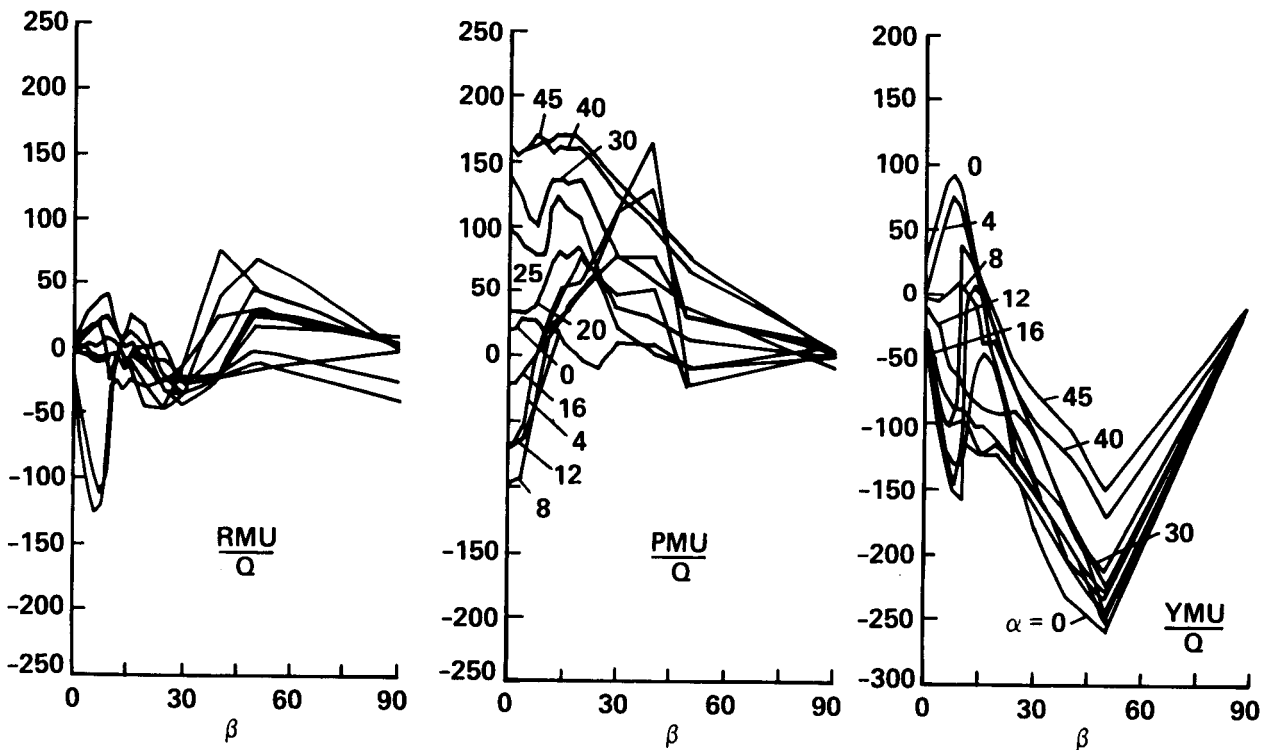
(b) MOMENT COMPONENTS, ft$^3$

Figure B2.- University of Maryland wind tunnel data.

α

| α | 0.0 | 2.0 | 4.0 | 6.0 | 8.0 | 10.0 | 12.0 | 14.0 | 16.0 | 20.0 | 25.0 | 30.0 | 40.0 |
|---|---|---|---|---|---|---|---|---|---|---|---|---|---|
| 0.0 | 0.0 | 0.6 | -0.1 | 0.5 | 0.6 | -0.2 | 0.7 | 0.8 | -0.3 | 0.3 | 0.3 | 1.3 | -2.2 |
| 2.0 | -0.6 | 0.0 | -0.8 | -0.3 | -0.3 | -0.7 | -0.2 | 0.4 | -0.7 | -1.1 | -0.7 | -0.1 | -3.1 |
| 4.0 | 0.1 | 0.8 | 0.0 | 0.3 | -0.3 | -0.6 | 0.1 | 0.0 | -1.1 | -1.4 | -0.3 | -0.1 | -3.9 |
| 6.0 | -0.5 | 0.3 | -0.3 | 0.0 | -0.8 | -1.5 | -1.2 | -1.1 | -0.9 | 0.3 | -0.8 | -2.0 | -4.8 |
| 8.0 | -0.6 | 0.3 | 0.3 | 0.8 | 0.0 | -1.3 | -0.9 | -0.5 | -1.1 | -0.2 | -1.6 | -2.6 | -5.1 |
| 10.0 | 0.2 | 0.7 | 0.5 | 1.5 | 1.2 | 0.0 | 0.4 | -0.3 | 0.3 | 1.0 | -1.4 | -2.8 | -5.7 |
| 12.0 | -0.7 | 0.2 | -0.2 | 1.3 | 0.8 | -0.4 | -0.1 | 0.0 | -0.4 | -0.3 | -2.0 | -1.8 | -6.4 |
| 14.0 | -0.8 | -0.4 | -0.1 | 1.1 | 0.4 | 0.1 | 0.1 | -0.2 | -0.8 | -0.7 | -2.6 | -4.9 | -5.0 |
| 16.0 | 0.3 | 0.7 | 0.9 | 0.8 | 0.8 | -0.3 | -0.1 | 0.4 | -0.4 | -1.1 | -3.4 | -3.7 | -3.2 |
| 20.0 | -0.3 | 1.1 | 1.0 | -0.3 | 0.3 | -0.9 | -0.2 | 1.5 | 0.6 | 0.1 | -2.3 | -2.5 | -4.1 |
| 25.0 | -0.3 | 0.7 | 0.0 | 1.1 | 1.7 | 1.5 | 2.9 | 3.8 | 3.4 | 2.9 | -1.1 | -2.6 | -5.0 |
| 30.0 | -1.3 | 0.1 | 0.3 | 2.2 | 3.3 | 1.4 | 4.4 | 3.5 | 3.4 | 2.4 | 0.7 | -2.2 | -5.9 |
| 40.0 | 2.2 | 2.9 | 4.6 | 4.7 | 4.8 | 5.7 | 3.5 | 2.8 | 3.2 | 4.4 | 4.3 | 1.9 | |
| 45.0 | 8.8 | 6.5 | 6.7 | 6.7 | 8.6 | 7.4 | 5.9 | 5.0 | 5.3 | 6.9 | 4.9 | 3.9 | |

(a) $\delta D/Q$: Difference between drag measurements at equivalent points.

α

| α | | | | | | | | | | | | | | | |
|---|---|---|---|---|---|---|---|---|---|---|---|---|---|---|---|
| 0.0 | 2.9 | 2.7 | 2.3 | 3.3 | 4.2 | 5.5 | 6.1 | 6.5 | 7.3 | 7.1 | 8.3 | 7.7 | 2.7 | 2.2 | -9.3 |
| 2.0 | 2.7 | 3.5 | 3.4 | 3.9 | 5.0 | 5.9 | 6.4 | 6.7 | 7.0 | 7.4 | 7.1 | 7.0 | 3.5 | 4.4 | -8.9 |
| 4.0 | 2.3 | 3.7 | 3.6 | 4.1 | 5.1 | 6.0 | 5.8 | 6.2 | 6.7 | 6.9 | 5.4 | 5.4 | 2.7 | 5.7 | -8.2 |
| 6.0 | 3.1 | 4.2 | 4.2 | 4.5 | 5.2 | 6.0 | 5.7 | 6.0 | 6.2 | 4.6 | 4.2 | 4.1 | 2.2 | 7.4 | -8.3 |
| 8.0 | 4.2 | 5.3 | 5.0 | 5.1 | 5.2 | 5.8 | 5.7 | 5.9 | 5.6 | 3.0 | 2.6 | 2.0 | 2.9 | 9.5 | -9.2 |
| 10.0 | 5.5 | 6.0 | 5.9 | 5.9 | 5.8 | 5.4 | 5.4 | 5.8 | 5.0 | 2.6 | 2.0 | 1.2 | 3.1 | 7.7 | -9.2 |
| 12.0 | 6.1 | 6.4 | 5.9 | 5.8 | 5.6 | 5.4 | 5.2 | 5.0 | 5.1 | 3.3 | 1.4 | 1.1 | 1.4 | 7.4 | -9.0 |
| 14.0 | 6.5 | 6.8 | 6.2 | 6.1 | 6.0 | 5.7 | 4.9 | 4.7 | 4.0 | 2.0 | 0.5 | 0.9 | -1.4 | 6.4 | -10.2 |
| 16.0 | 7.3 | 7.2 | 6.6 | 6.4 | 5.5 | 5.1 | 4.9 | 3.8 | 2.6 | 0.9 | 0.4 | 0.2 | -3.1 | 6.5 | -9.6 |
| 20.0 | 7.1 | 7.7 | 6.6 | 4.7 | 2.9 | 3.2 | 3.0 | 1.4 | 0.9 | -0.9 | -1.1 | -3.1 | -3.4 | 5.6 | -9.2 |
| 25.0 | 8.3 | 7.0 | 5.1 | 3.8 | 2.3 | 1.9 | 0.6 | -0.1 | -0.6 | -1.4 | -0.6 | -2.4 | -4.9 | 5.8 | -9.5 |
| 30.0 | 7.7 | 6.8 | 5.0 | 3.4 | 1.1 | 1.7 | 1.2 | -0.1 | -1.9 | -1.8 | -1.6 | -2.4 | -5.0 | 3.8 | -10.9 |
| 40.0 | 2.7 | 3.4 | 2.1 | 3.2 | 3.2 | -0.2 | -2.2 | -2.4 | -2.8 | -4.3 | -3.2 | -3.2 | -5.5 | 1.7 | -10.1 |
| 45.0 | -0.9 | 1.6 | 1.4 | 2.2 | 0.5 | -2.6 | -4.1 | -3.9 | -5.3 | -5.3 | -5.4 | -6.8 | -7.7 | -2.3 | -10.7 |
| $\beta$ | 0.0 | 2.0 | 4.0 | 6.0 | 8.0 | 10.0 | 12.0 | 14.0 | 16.0 | 20.0 | 25.0 | 30.0 | 40.0 | 50.0 | 90.0 |

(b) $\Delta D/Q$: Difference from revised Ames data.

Figure B3.- Drag comparisons.  Notes: $\delta D(\beta, \alpha) = DU(\beta, \alpha) - DU(\beta_1, \alpha_1)$; $\beta_1(\beta, \alpha)$, $\alpha_1(\beta, \alpha)$ from equation B1; and $\Delta D = \widehat{D} - \widehat{DU}$.

**α**

| α | 0.0 | 2.0 | 4.0 | 6.0 | 8.0 | 10.0 | 12.0 | 14.0 | 16.0 | 20.0 | 25.0 | 30.0 | 40.0 |
|---|---|---|---|---|---|---|---|---|---|---|---|---|---|
| 0.0 | 0.0 | 0.0 | 0.0 | 0.0 | 0.0 | 0.0 | 0.0 | 0.0 | 0.0 | 0.0 | 0.0 | 0.0 | 0.0 |
| 2.0 | 1.1 | 0.3 | 0.6 | 0.5 | 0.8 | 0.3 | 0.1 | 0.9 | 1.5 | 0.4 | 9.4 | -0.4 | 9.2 |
| 4.0 | 2.8 | 2.5 | 2.5 | 2.3 | 3.1 | 2.2 | 2.4 | 2.1 | 1.7 | 1.8 | 11.1 | 1.4 | 21.0 |
| 6.0 | 3.0 | 3.0 | 2.6 | 2.7 | 3.4 | 1.9 | 2.5 | 2.3 | 2.2 | 8.6 | 11.6 | 2.2 | 27.3 |
| 8.0 | 2.9 | 2.8 | 3.7 | 3.1 | 3.9 | 1.8 | 1.7 | 2.3 | 2.0 | 9.2 | 11.7 | 4.6 | 26.6 |
| 10.0 | 5.1 | 4.5 | 4.1 | 3.3 | 3.4 | 1.7 | 0.7 | -0.3 | 1.9 | 8.5 | 15.2 | 13.5 | 27.6 |
| 12.0 | 5.0 | 4.7 | 3.9 | 3.8 | 3.2 | 1.0 | -0.5 | 0.1 | 2.7 | 9.2 | 15.9 | 24.4 | 29.6 |
| 14.0 | 5.7 | 5.3 | 4.1 | 3.2 | 3.2 | 1.0 | -0.2 | 1.1 | 4.3 | 9.5 | 12.3 | 10.8 | 20.6 |
| 16.0 | 7.0 | 6.4 | 5.3 | 3.3 | 3.7 | 1.4 | 1.8 | 3.6 | 5.7 | 10.9 | 14.3 | 8.2 | 24.8 |
| 20.0 | 8.7 | 7.5 | 5.8 | 5.6 | 5.9 | 4.8 | 6.5 | 8.6 | 8.8 | 12.7 | 17.2 | 11.5 | 18.0 |
| 25.0 | 7.7 | 7.4 | 6.6 | 6.4 | 8.1 | 8.6 | 10.6 | 13.2 | 15.9 | 22.0 | 25.8 | 16.9 | 19.3 |
| 30.0 | 7.7 | 7.5 | 8.7 | 9.6 | 11.5 | 11.7 | 12.7 | 14.1 | 15.6 | 19.4 | 28.6 | 22.9 | 16.8 |
| 40.0 | 8.9 | 9.9 | 12.0 | 12.9 | 14.4 | 17.3 | 15.6 | 15.5 | 19.0 | 20.1 | 20.9 | 19.3 | |
| 45.0 | 12.6 | 11.2 | 11.7 | 14.4 | 17.3 | 17.3 | 17.2 | 17.4 | 19.0 | 20.2 | 20.5 | 17.6 | |

(a) $\delta L/Q$: Lift difference from lift derived from measurements at equivalent points.

**α**

| α | 0.0 | 2.0 | 4.0 | 6.0 | 8.0 | 10.0 | 12.0 | 14.0 | 16.0 | 20.0 | 25.0 | 30.0 | 40.0 | 50.0 | 90.0 |
|---|---|---|---|---|---|---|---|---|---|---|---|---|---|---|---|
| 0.0 | 0.0 | 0.3 | -1.9 | -1.1 | -1.3 | -1.5 | -1.1 | 0.0 | 0.9 | 0.2 | 0.5 | 0.1 | 5.6 | -1.0 | 0.0 |
| 2.0 | 0.0 | 0.2 | -1.8 | -1.5 | -1.3 | -0.5 | 0.7 | 1.7 | 2.8 | 2.3 | 1.2 | 2.5 | 6.6 | 0.1 | 0.0 |
| 4.0 | 0.0 | 0.9 | -0.9 | -0.8 | -0.7 | -0.4 | 0.6 | 3.0 | 4.4 | 4.6 | 3.6 | 4.1 | 7.7 | 3.5 | 0.0 |
| 6.0 | 0.0 | 0.4 | -1.2 | -0.5 | -1.2 | -0.5 | 1.1 | 3.4 | 5.2 | 4.1 | 4.5 | 4.8 | 6.9 | 0.7 | 0.0 |
| 8.0 | 0.0 | 0.4 | -0.9 | 1.0 | 0.1 | 0.6 | 2.4 | 4.1 | 5.8 | 5.2 | 4.6 | 5.0 | 4.5 | -0.2 | 0.0 |
| 10.0 | 0.0 | 1.1 | 0.1 | 2.5 | 2.0 | 2.9 | 5.4 | 6.6 | 7.5 | 6.6 | 4.8 | 5.3 | 2.1 | -1.2 | 0.0 |
| 12.0 | 0.0 | 1.3 | 0.7 | 3.2 | 3.7 | 6.1 | 8.1 | 9.3 | 8.8 | 8.0 | 8.7 | 7.9 | -0.4 | -2.2 | 0.0 |
| 14.0 | 0.0 | 1.2 | 0.7 | 3.7 | 4.0 | 6.0 | 7.8 | 8.6 | 6.0 | 6.4 | 10.0 | 7.2 | 1.0 | -2.8 | 0.0 |
| 16.0 | 0.0 | 1.1 | 1.6 | 3.7 | 4.4 | 4.9 | 5.8 | 5.7 | 4.4 | 4.7 | 5.8 | 3.6 | -0.7 | -3.8 | 0.0 |
| 20.0 | 0.0 | 2.3 | 4.2 | 8.1 | 8.8 | 7.3 | 5.9 | 7.3 | 6.3 | 5.3 | -0.9 | -1.5 | -1.7 | -6.7 | 0.0 |
| 25.0 | 0.0 | 5.3 | 6.9 | 13.4 | 14.5 | 13.1 | 8.0 | 8.4 | 8.1 | 3.9 | -9.3 | -5.6 | -4.0 | -6.5 | 0.0 |
| 30.0 | 0.0 | 7.4 | 10.6 | 17.1 | 19.6 | 0.9 | 5.4 | 6.5 | 6.1 | 4.4 | -10.2 | -7.9 | -4.6 | -6.8 | 0.0 |
| 40.0 | 0.0 | 0.3 | -6.8 | -2.1 | -0.8 | -1.9 | -0.4 | -0.5 | -0.5 | -2.9 | -2.7 | -4.6 | -4.0 | -6.9 | 0.0 |
| 45.0 | 0.0 | -1.6 | -3.4 | -5.0 | -4.1 | -1.1 | -1.9 | -4.6 | -5.1 | -7.4 | -7.0 | -6.1 | -5.5 | -10.6 | 0.0 |

(b) $\Delta Y/Q$: Difference from revised Ames data.

| α | 0.0 | 2.0 | 4.0 | 6.0 | 8.0 | 10.0 | 12.0 | 14.0 | 16.0 | 20.0 | 25.0 | 30.0 | 40.0 | 50.0 | 90.0 |
|---|---|---|---|---|---|---|---|---|---|---|---|---|---|---|---|
| 0.0 | 0.0 | 0.0 | 0.0 | 0.0 | 0.0 | 0.0 | 0.0 | 0.0 | 0.0 | 0.0 | 0.0 | 0.0 | 0.0 | 0.0 | 0.0 |
| 2.0 | -1.1 | -0.3 | -1.2 | -1.0 | -1.7 | -1.5 | -1.3 | -2.1 | -2.7 | -2.7 | -14.3 | -6.1 | -9.3 | -2.7 | 0.0 |
| 4.0 | -0.9 | -0.7 | -1.6 | -1.2 | -2.2 | -2.1 | -3.2 | -3.0 | -3.3 | -5.9 | -18.0 | -11.2 | -17.2 | -5.3 | 0.0 |
| 6.0 | -1.8 | -1.5 | -1.8 | -2.1 | -4.0 | -3.9 | -5.3 | -5.5 | -5.5 | -16.1 | -22.8 | -16.6 | -23.0 | -6.7 | 0.0 |
| 8.0 | -1.6 | -1.5 | -3.0 | -2.2 | -4.3 | -4.1 | -5.5 | -6.5 | -6.6 | -18.6 | -26.1 | -22.1 | -25.3 | -8.2 | 0.0 |
| 10.0 | -4.1 | -3.6 | -3.7 | -2.8 | -4.1 | -4.9 | -6.9 | -5.8 | -7.5 | -17.3 | -29.9 | -27.9 | -28.2 | -12.4 | 0.0 |
| 12.0 | -3.9 | -4.3 | -4.7 | -4.8 | -6.0 | -6.7 | -7.9 | -8.0 | -9.0 | -16.7 | -27.9 | -27.9 | -31.3 | -14.9 | 0.0 |
| 14.0 | -5.7 | -6.3 | -7.2 | -6.6 | -7.7 | -8.0 | -9.2 | -9.6 | -11.0 | -17.4 | -21.5 | -18.6 | -22.9 | -14.6 | 0.0 |
| 16.0 | -7.9 | -8.9 | -9.9 | -8.6 | -10.0 | -9.4 | -10.7 | -10.6 | -11.7 | -18.8 | -22.4 | -16.9 | -28.1 | -15.5 | 0.0 |
| 20.0 | -8.9 | -9.5 | -10.6 | -10.6 | -12.4 | -12.9 | -15.1 | -15.6 | -15.2 | -19.5 | -24.7 | -19.6 | -21.3 | -14.2 | 0.0 |
| 25.0 | -8.2 | -8.9 | -11.1 | -11.7 | -14.8 | -17.9 | -21.8 | -22.1 | -22.3 | -24.7 | -27.4 | -20.2 | -21.1 | -12.7 | 0.0 |
| 30.0 | -7.8 | -9.7 | -13.7 | -15.4 | -19.0 | -22.0 | -22.2 | -20.1 | -19.6 | -19.3 | -27.2 | -21.5 | -18.4 | -10.0 | 0.0 |
| 40.0 | -14.5 | -16.5 | -20.6 | -19.6 | -19.5 | -22.2 | -20.0 | -19.0 | -21.3 | -20.8 | -20.7 | -21.0 | -18.2 | -7.6 | 0.0 |
| 45.0 | -18.1 | -17.0 | -19.2 | -20.7 | -22.6 | -22.7 | -21.8 | -21.3 | -22.5 | -22.4 | -22.6 | -21.3 | -16.5 | -7.1 | 0.0 |
| $\beta$ | 0.0 | 2.0 | 4.0 | 6.0 | 8.0 | 10.0 | 12.0 | 14.0 | 16.0 | 20.0 | 25.0 | 30.0 | 40.0 | 50.0 | 90.0 |

(c) $\Delta L/Q$: difference from revised Ames data.

Figure B4.-Lift and side force comparisons. Notes: $\delta L = \widehat{LU} - LU1_1$;
$LU_1(\beta, \alpha) = -\sin \phi_w \widehat{YU}(\beta_1, \alpha_1) + \cos \phi_w \widehat{LU}(\beta_1, \alpha_1)$; and $\beta_1(\beta, \alpha), \alpha_1(\beta, \alpha)$ from equation B1.
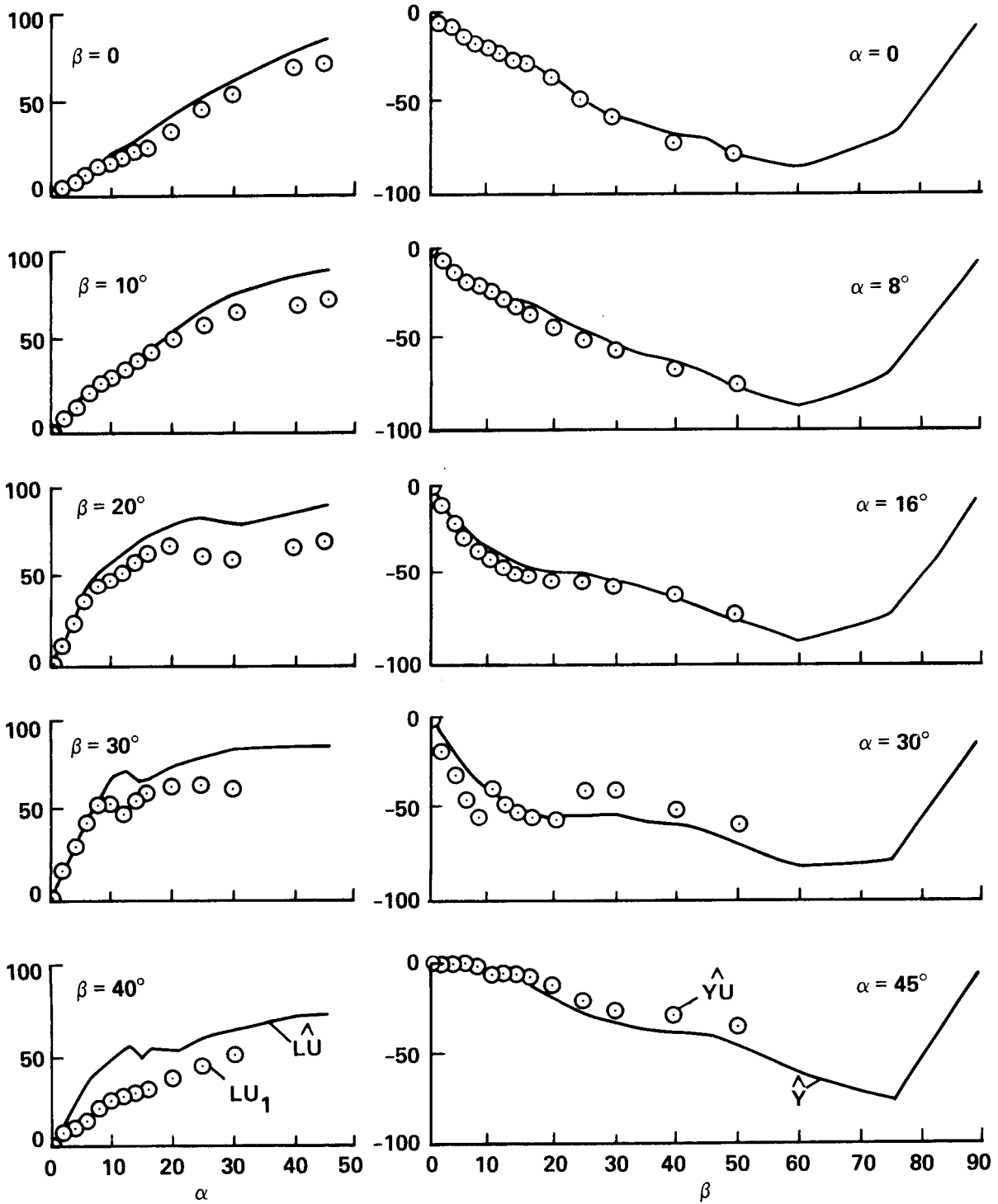
(d) COMPARISON OF LIFT FROM
    DATA AT EQUIVALENT POINTS

(e) SIDE FORCE; COMPARISON WITH
    REVISED AMES DATA

Figure B4.- Concluded.

70

α

| α | 0.0 | 2.0 | 4.0 | 6.0 | 8.0 | 10.0 | 12.0 | 14.0 | 16.0 | 20.0 | 25.0 | 30.0 | 40.0 |
|---|---|---|---|---|---|---|---|---|---|---|---|---|---|
| 0.0 | 1.1 | 0.1 | 0.2 | -3.2 | -4.2 | -3.1 | -2.7 | -6.8 | -2.8 | -0.6 | 2.2 | -15.6 | -17.6 |
| 2.0 | 0.1 | -3.1 | -3.1 | -6.2 | -7.6 | -4.9 | -3.7 | -7.3 | -3.1 | 0.8 | -8.0 | -11.7 | -21.1 |
| 4.0 | 0.1 | -3.2 | -6.0 | -7.4 | -7.5 | -5.3 | -3.9 | -7.2 | -1.5 | 2.8 | -6.0 | -9.5 | -26.7 |
| 6.0 | -3.2 | -6.2 | -7.4 | -12.4 | -11.8 | -8.1 | -7.3 | -8.6 | -4.3 | -8.1 | -6.3 | -9.9 | -28.5 |
| 8.0 | -4.2 | -7.6 | -7.6 | -12.0 | -12.4 | -9.1 | -6.9 | -9.0 | -3.8 | -12.1 | -6.8 | -12.5 | -24.9 |
| 10.0 | -3.1 | -5.0 | -5.4 | -8.3 | -9.2 | -7.5 | -7.2 | -8.3 | -2.6 | -10.4 | -9.3 | -20.1 | -24.5 |
| 12.0 | -2.7 | -3.8 | -3.9 | -7.6 | -7.2 | -7.4 | -6.7 | -9.1 | -2.2 | -6.5 | -11.8 | -22.7 | -8.7 |
| 14.0 | -6.8 | -7.3 | -7.1 | -8.6 | -9.0 | -7.7 | -8.7 | -12.9 | -6.3 | -7.8 | -8.6 | 5.3 | 5.7 |
| 16.0 | -2.8 | -3.1 | -1.5 | -5.1 | -4.3 | -2.5 | -3.3 | -9.6 | -4.9 | -7.0 | -9.1 | -3.4 | 3.5 |
| 20.0 | -0.6 | 0.8 | 1.6 | -8.5 | -10.8 | -7.1 | -6.1 | -9.2 | -4.6 | -9.3 | -11.7 | -10.2 | -17.0 |
| 25.0 | 2.2 | -7.8 | -5.3 | -6.4 | -5.7 | -5.9 | -10.0 | -10.1 | -6.7 | -12.6 | -22.6 | -21.9 | -23.1 |
| 30.0 | -15.6 | -11.0 | -8.8 | -9.6 | -12.3 | -26.8 | 1.4 | -2.8 | -2.3 | -12.2 | -25.8 | -27.4 | -24.7 |
| 40.0 | -17.6 | -22.1 | -28.5 | -25.2 | -26.1 | -11.3 | 7.7 | -7.0 | -12.7 | -20.0 | -19.6 | -24.1 | |
| 45.0 | -19.2 | -22.2 | -27.4 | -35.3 | -29.6 | 11.3 | -1.7 | -16.7 | -17.7 | -24.7 | -23.9 | -24.2 | |

(a) RMS/Q: Symmetric component of roll moment data.

α

| α | | | | | | | | | | | | | |
|---|---|---|---|---|---|---|---|---|---|---|---|---|---|
| 0.0 | 0.0 | -1.1 | -0.8 | -4.4 | -5.3 | -3.3 | -1.8 | -5.6 | -0.7 | -0.4 | 1.4 | -12.4 | -5.8 |
| 2.0 | 1.0 | 0.0 | 1.3 | -1.3 | -1.3 | 0.3 | -1.2 | -5.4 | -1.4 | -3.8 | -18.6 | -19.8 | 7.7 |
| 4.0 | 0.8 | -1.3 | 0.0 | -0.5 | -0.6 | 0.4 | -1.7 | -7.4 | -4.5 | -10.1 | -28.4 | -23.9 | 23.4 |
| 6.0 | 4.4 | 1.2 | 0.5 | 0.0 | 1.2 | 1.3 | 0.5 | -6.9 | -4.2 | -26.4 | -34.9 | -26.2 | 42.4 |
| 8.0 | 5.3 | 1.2 | 0.6 | -1.3 | 0.0 | 1.3 | 0.6 | -7.3 | -7.4 | -34.9 | -41.7 | -26.1 | 63.4 |
| 10.0 | 3.3 | -0.3 | -0.4 | -1.4 | -1.3 | 0.1 | -1.2 | -11.0 | -11.9 | -35.3 | -44.4 | -17.0 | 81.2 |
| 12.0 | 1.8 | 1.2 | 1.7 | -0.9 | -0.6 | 0.7 | -0.4 | -9.6 | -9.3 | -23.9 | -35.0 | 1.7 | 86.0 |
| 14.0 | 5.6 | 5.4 | 7.4 | 6.6 | 7.0 | 10.4 | 7.4 | -1.9 | -1.0 | -13.0 | -18.9 | 5.2 | 65.2 |
| 16.0 | 0.7 | 1.5 | 4.8 | 4.1 | 7.9 | 12.0 | 8.6 | -1.3 | 0.3 | -9.4 | -18.2 | -13.5 | 21.6 |
| 20.0 | 0.4 | 4.0 | 12.4 | 27.5 | 34.2 | 31.6 | 18.7 | 7.8 | 8.4 | -4.2 | -22.2 | -28.2 | -3.1 |
| 25.0 | -1.4 | 19.5 | 30.2 | 36.9 | 44.8 | 43.4 | 23.9 | 15.7 | 20.2 | 13.2 | -11.7 | -22.6 | -3.6 |
| 30.0 | 12.4 | 20.8 | 25.4 | 27.9 | 26.3 | 0.5 | -0.6 | 16.5 | 27.6 | 26.5 | 4.9 | -8.5 | -0.1 |
| 40.0 | 5.8 | -11.8 | -35.2 | -59.5 | -82.4 | -79.7 | -23.9 | -5.0 | 11.5 | 11.4 | 8.9 | 0.8 | |
| 45.0 | 1.1 | -31.0 | -60.9 | -90.0 | -91.1 | -44.5 | -23.2 | -16.5 | -8.3 | -6.5 | -0.7 | -3.3 | |
| β | 0.0 | 2.0 | 4.0 | 6.0 | 8.0 | 10.0 | 12.0 | 14.0 | 16.0 | 20.0 | 25.0 | 30.0 | 40.0 |

(b) RMA/Q: Antisymmetric component of roll moment data.
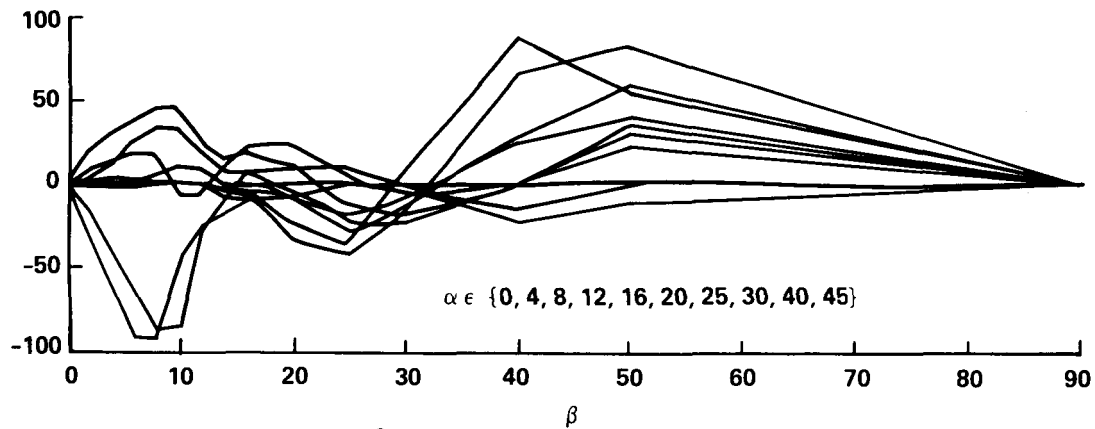


(c) $\widehat{RMU}$: Revised antisymmetric component

Figure B5.- Roll moment decomposition. Notes: $RMS = 0.5(RMU + RMU_1)$;
$RMA = 0.5(RMU - RMU_1)$; $RMU_1(\beta, \alpha) = RMU(\beta_1, \alpha_1)$   $\beta_1(\beta, \alpha)$, $\alpha_1(\beta, \alpha)$ from equation B1.

| $\alpha$ | 0.0 | 2.0 | 4.0 | 6.0 | 8.0 | 10.0 | 12.0 | 14.0 | 16.0 | 20.0 | 25.0 | 30.0 | 40.0 |
|---|---|---|---|---|---|---|---|---|---|---|---|---|---|
| 0.0 | 0.0 | 0.0 | 0.0 | 0.0 | 0.0 | 0.0 | 0.0 | 0.0 | 0.0 | 0.0 | 0.0 | 0.0 | 0.0 |
| 2.0 | -12.7 | -21.5 | -20.4 | -18.2 | -11.6 | -11.1 | -10.3 | -9.3 | -10.4 | -4.5 | 10.5 | -8.7 | 3.5 |
| 4.0 | -26.9 | -30.0 | -39.7 | -28.1 | -22.3 | -18.6 | -12.5 | -16.9 | -18.4 | -6.4 | 7.9 | -9.7 | 17.7 |
| 6.0 | -26.1 | -27.0 | -42.9 | -32.1 | -30.4 | -26.4 | -27.0 | -23.4 | -23.6 | -18.1 | -3.0 | -20.6 | 26.5 |
| 8.0 | -26.4 | -22.4 | -38.1 | -34.9 | -33.2 | -36.1 | -38.9 | -30.4 | -29.1 | -30.0 | -22.4 | -29.1 | 16.9 |
| 10.0 | -24.3 | -22.1 | -35.3 | -34.6 | -44.1 | -50.6 | -61.9 | -56.8 | -48.6 | -47.6 | -38.4 | -42.3 | 14.5 |
| 12.0 | -28.9 | -25.3 | -34.7 | -34.2 | -52.4 | -81.0 | -84.4 | -69.3 | -54.5 | -43.0 | -36.1 | -29.7 | 53.7 |
| 14.0 | -35.9 | -30.3 | -37.8 | -40.9 | -48.1 | -85.8 | -82.3 | -69.7 | -53.3 | -30.7 | -21.5 | 33.7 | 56.5 |
| 16.0 | -36.8 | -33.0 | -40.9 | -47.7 | -51.1 | -64.7 | -57.8 | -48.0 | -48.9 | -34.0 | -39.4 | -12.1 | 50.6 |
| 20.0 | -44.6 | -44.9 | -46.3 | -24.2 | -12.8 | -18.0 | -32.1 | -33.6 | -38.0 | -35.4 | -38.9 | -35.2 | -5.3 |
| 25.0 | -47.6 | -36.7 | -32.9 | -20.6 | -8.3 | -10.0 | 6.7 | -1.9 | -14.6 | -21.8 | -44.8 | -46.0 | -10.8 |
| 30.0 | -51.6 | -36.1 | -28.3 | -20.5 | -10.6 | 7.3 | 4.0 | -6.2 | -10.4 | -1.4 | -22.5 | -35.3 | -4.1 |
| 40.0 | -72.2 | -59.7 | -38.2 | -25.3 | -13.8 | -18.4 | -28.3 | -25.6 | -25.9 | -9.8 | -9.8 | -10.4 | |
| 45.0 | -83.3 | -71.4 | -49.9 | -40.0 | -33.0 | -45.6 | -39.5 | -35.0 | -26.0 | -13.5 | -8.4 | -2.3 | |
| $\beta$ | 0.0 | 2.0 | 4.0 | 6.0 | 8.0 | 10.0 | 12.0 | 14.0 | 16.0 | 20.0 | 25.0 | 30.0 | 40.0 |

(a) $\delta PM/Q$: Difference from pitching moment derived from measurements at equivalent points.
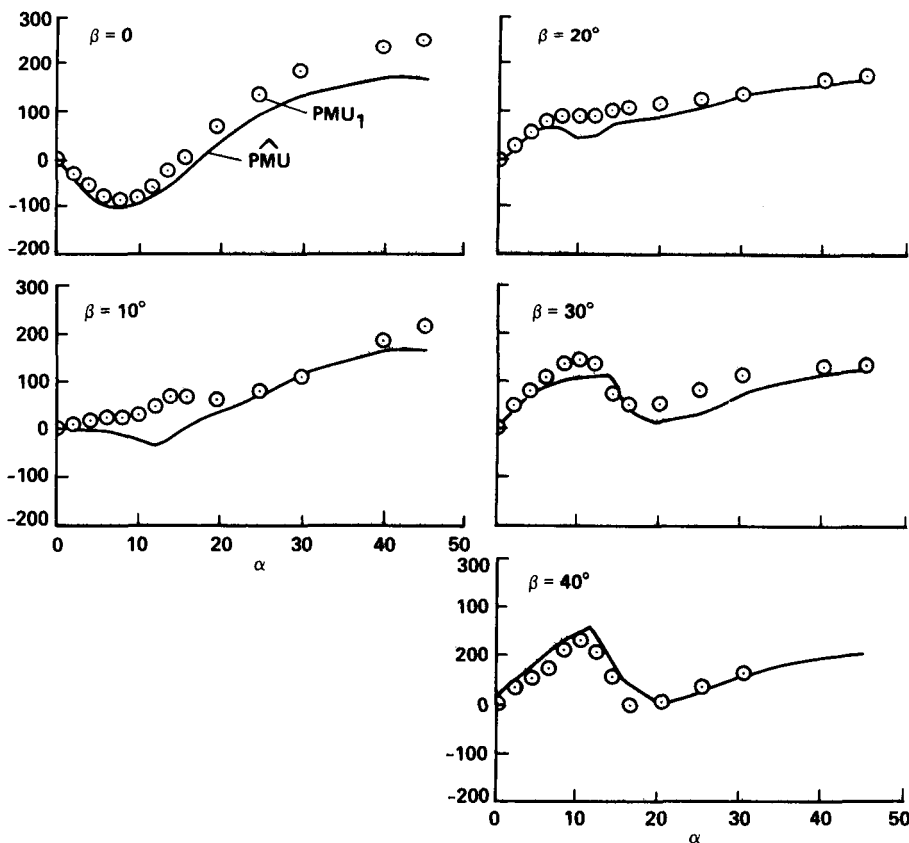


(b) Comparison of pitching moment from measurements at equivalent points.

Figure B6.- Comparison of pitch and yaw moment data at equivalent points. Notes: $\delta PM = \widehat{PMU} - PMU_1$; $PMU_1(\beta, \alpha) = \cos \phi_w \widehat{PMU}(\beta_1, \alpha_1) - \sin \phi_w \widehat{YMU}(\beta_1, \alpha_1)$; and $\phi_w(\beta, \alpha)$, $\beta_1(\beta, \alpha)$, $\alpha_1(\beta, \alpha)$ from equation B1.

72

## $\Delta PM/Q$:

| $\alpha$ | 0.0 | 2.0 | 4.0 | 6.0 | 8.0 | 10.0 | 12.0 | 14.0 | 16.0 | 20.0 | 25.0 | 30.0 | 40.0 | 50.0 | 90.0 |
|---|---|---|---|---|---|---|---|---|---|---|---|---|---|---|---|
| 0.0 | 0.0 | 0.0 | 0.0 | 0.0 | 0.0 | 0.0 | 0.0 | 0.0 | 0.0 | 0.0 | 0.0 | 0.0 | 0.0 | 0.0 | 0.0 |
| 2.0 | -5.5 | 4.4 | 0.1 | -1.6 | -0.6 | -2.9 | -3.7 | -5.4 | -5.1 | -9.3 | -27.1 | -13.8 | -14.0 | -12.5 | 0.0 |
| 4.0 | -21.0 | -2.6 | 5.5 | -4.1 | -3.8 | -8.5 | -9.8 | -7.0 | -8.3 | -20.4 | -34.2 | -22.3 | -26.2 | -17.3 | 0.0 |
| 6.0 | -22.2 | -12.5 | -1.7 | -2.6 | -0.1 | -13.8 | -15.8 | -18.1 | -20.8 | -30.4 | -45.2 | -32.1 | -45.8 | -9.9 | 0.0 |
| 8.0 | -40.6 | -34.5 | -23.4 | -11.1 | -1.1 | -9.7 | -16.8 | -23.9 | -24.4 | -21.0 | -38.0 | -42.1 | -73.7 | -6.4 | 0.0 |
| 10.0 | -38.6 | -32.7 | -25.6 | -7.2 | 7.7 | -1.1 | 4.2 | 0.3 | -0.6 | -3.2 | -30.5 | -43.1 | -95.5 | 18.8 | 0.0 |
| 12.0 | -43.5 | -40.9 | -37.4 | -19.4 | 1.4 | 11.2 | 19.0 | 11.8 | 7.1 | -10.4 | -35.9 | -61.1 | -128.1 | 45.6 | 0.0 |
| 14.0 | -41.3 | -42.4 | -40.7 | -31.1 | -20.2 | 0.2 | 14.2 | 9.6 | 2.8 | -32.3 | -49.2 | -77.2 | -95.4 | 44.7 | 0.0 |
| 16.0 | -45.9 | -46.1 | -49.6 | -45.1 | -42.1 | -25.3 | -10.6 | -7.6 | 1.5 | -38.6 | -39.2 | -21.1 | -51.1 | 39.7 | 0.0 |
| 20.0 | -51.3 | -50.2 | -47.2 | -43.7 | -45.1 | -46.2 | -48.3 | -44.3 | -31.8 | -45.9 | -31.9 | -2.1 | 7.7 | 27.0 | 0.0 |
| 25.0 | -39.7 | -40.1 | -32.8 | -28.3 | -26.0 | -20.2 | -47.7 | -49.8 | -38.7 | -32.8 | 4.4 | 24.5 | 12.1 | 26.4 | 0.0 |
| 30.0 | -25.1 | -24.8 | -15.2 | -7.5 | -7.7 | -18.8 | -24.6 | -23.2 | -20.7 | -26.8 | 5.2 | 32.2 | 16.2 | 32.0 | 0.0 |
| 40.0 | 20.4 | 21.5 | 8.4 | 10.6 | 8.0 | 10.3 | 24.7 | 18.0 | 15.2 | 9.7 | 23.6 | 38.4 | 48.2 | 79.0 | 0.0 |
| 45.0 | 57.6 | 56.6 | 42.5 | 41.1 | 36.1 | 38.8 | 39.8 | 30.2 | 23.7 | 21.4 | 36.5 | 42.2 | 61.2 | 96.9 | 0.0 |

## $\Delta YM/Q$:

| $\alpha$ | 0.0 | 2.0 | 4.0 | 6.0 | 8.0 | 10.0 | 12.0 | 14.0 | 16.0 | 20.0 | 25.0 | 30.0 | 40.0 | 50.0 | 90.0 |
|---|---|---|---|---|---|---|---|---|---|---|---|---|---|---|---|
| 0.0 | 0.0 | 18.2 | 47.9 | 48.3 | 67.0 | 63.0 | 72.4 | 77.2 | 82.8 | 95.9 | 87.3 | 76.7 | 51.7 | 22.5 | 0.0 |
| 2.0 | 0.0 | 19.1 | 36.5 | 44.0 | 62.2 | 58.6 | 69.0 | 74.6 | 79.7 | 95.5 | 78.6 | 64.6 | 40.9 | 15.6 | 0.0 |
| 4.0 | 0.0 | 20.4 | 34.3 | 44.8 | 62.0 | 61.2 | 72.7 | 78.5 | 90.0 | 96.0 | 67.5 | 47.2 | 35.8 | 6.4 | 0.0 |
| 6.0 | 0.0 | 19.2 | 31.0 | 34.9 | 48.1 | 45.9 | 60.7 | 78.3 | 97.3 | 72.8 | 51.7 | 31.4 | 22.8 | -6.2 | 0.0 |
| 8.0 | 0.0 | 12.1 | 26.1 | 30.2 | 34.2 | 35.7 | 49.9 | 66.6 | 94.9 | 56.7 | 38.2 | 23.5 | 14.1 | -10.2 | 0.0 |
| 10.0 | 0.0 | 13.8 | 26.9 | 38.6 | 42.2 | 47.7 | 67.6 | 87.2 | 92.2 | 50.5 | 21.3 | 8.8 | -2.3 | -5.1 | 0.0 |
| 12.0 | 0.0 | 13.9 | 22.1 | 43.7 | 57.0 | 58.6 | 68.8 | 71.4 | 73.7 | 80.6 | 25.2 | 5.3 | -15.2 | 0.5 | 0.0 |
| 14.0 | 0.0 | 14.8 | 23.6 | 41.9 | 54.7 | 57.0 | 58.7 | 61.6 | 54.5 | 81.7 | 35.6 | 8.6 | -3.3 | 5.9 | 0.0 |
| 16.0 | 0.0 | 15.7 | 26.5 | 45.0 | 53.1 | 46.6 | 46.4 | 49.9 | 41.7 | 69.7 | 40.4 | 12.7 | -10.3 | 5.5 | 0.0 |
| 20.0 | 0.0 | 14.1 | 27.3 | 51.1 | 47.5 | 47.0 | 49.0 | 63.9 | 68.2 | 79.9 | 43.6 | 25.3 | 12.8 | 6.5 | 0.0 |
| 25.0 | 0.0 | 17.7 | 26.9 | 54.6 | 60.1 | 71.0 | 65.7 | 79.4 | 90.5 | 66.5 | 31.7 | 18.4 | 3.5 | -7.9 | 0.0 |
| 30.0 | 0.0 | 25.4 | 33.8 | 65.3 | 77.2 | 101.9 | 47.0 | 36.9 | 47.4 | 31.2 | 27.2 | 6.4 | -8.4 | -16.7 | 0.0 |
| 40.0 | 0.0 | 14.3 | 4.1 | 55.1 | 90.6 | 85.7 | 13.6 | 1.3 | 7.3 | 1.4 | -4.6 | -10.6 | -28.5 | -29.3 | 0.0 |
| 45.0 | 0.0 | 16.3 | 26.3 | 62.6 | 63.1 | -41.5 | -17.5 | -8.7 | 1.2 | 4.6 | -11.9 | -23.5 | -37.8 | -36.3 | 0.0 |

| $\beta$ | 0.0 | 2.0 | 4.0 | 6.0 | 8.0 | 10.0 | 12.0 | 14.0 | 16.0 | 20.0 | 25.0 | 30.0 | 40.0 | 50.0 | 90.0 |

(a) Differences from revised Ames data.

Figure B7.- Pitch and yaw moment comparisons with Ames data. Notes: $\Delta PM = \widehat{PM} - \widehat{PMU}$; and $\Delta YM = \widehat{YM} - \widehat{YMU}$.
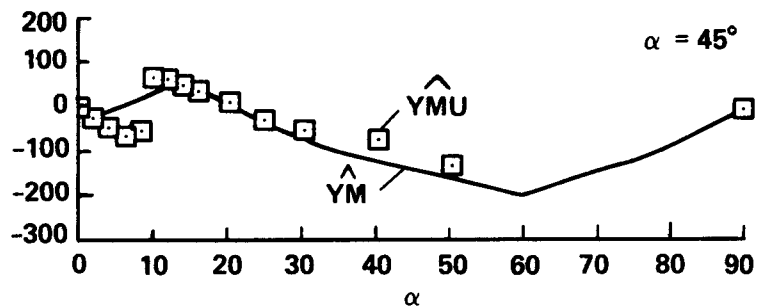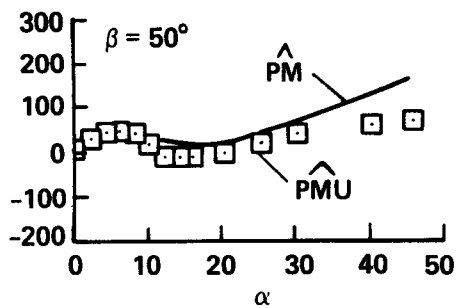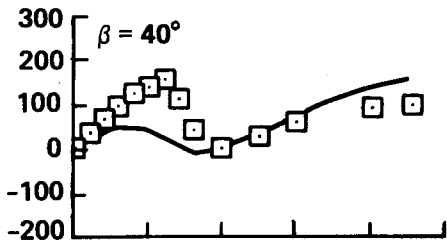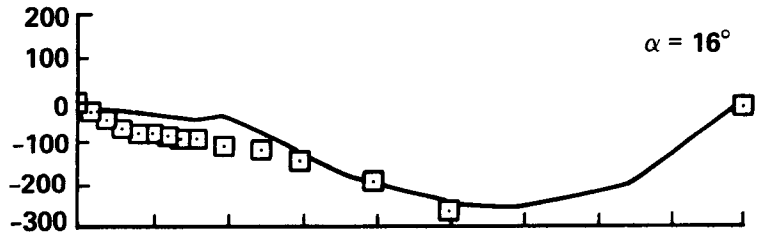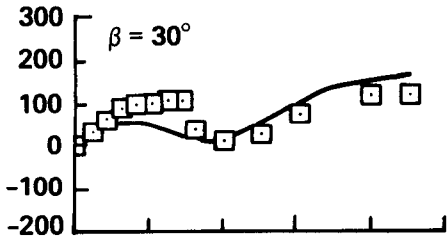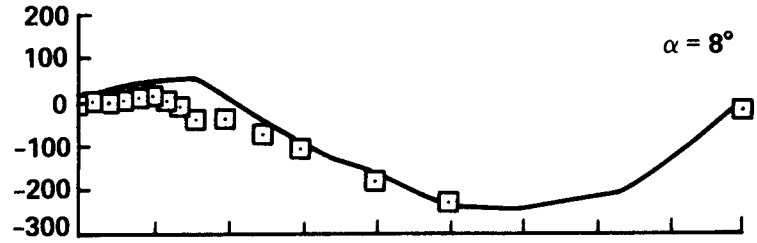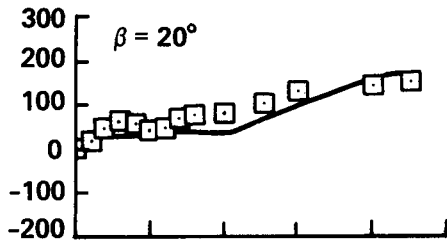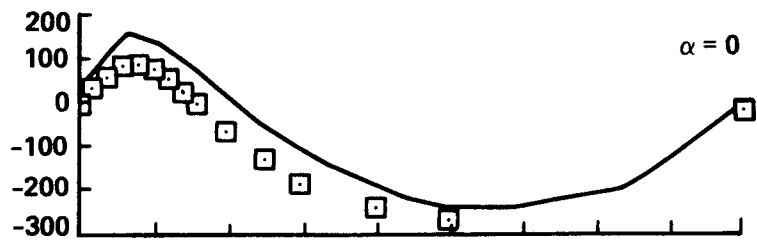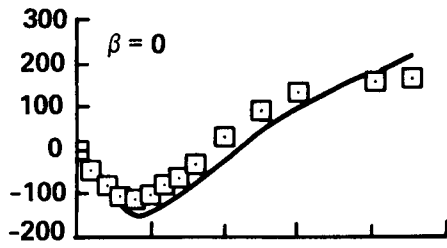
(b) PITCHING MOMENT        (c) YAW MOMENT

Figure B7.- Concluded.

# APPENDIX C.-NORTHROP CORP. WIND TUNNEL DATA

The measurements made at the Northrop Corp. 8- by 10-ft wind tunnel are given graphically in reference 4 for a smooth-surfaced box. Reference 5 contains limited additional data plus extensive data on a truck and tracked vehicle. The original tabulated data are apparently lost. The accuracy of the tables presented here in reproducing those data is limited by; 1) the resolution accuracy of the graphs; and 2) apparent revisions of the measurements in the graphical results to impose null values at some of the expected zero lines.

The available data are the "lateral-directional" components (side force, roll, and yaw moments) in both wind and body axes. Values of drag and pitching moment can be derived from these using the transformation relations between body and wind axes components

$$T_{b,w} = E_2(\alpha)E_3(-\beta)$$

from which we obtain:

$$D = (Y\cos\beta - YB)/\sin\beta \qquad (C1)$$

$$PM = (RM\cos\alpha\cos\beta - RMB - YM\sin\alpha)/\cos\alpha\sin\beta \qquad (C2)$$

where $YB$ and $RMB$ refer to the body-axes side-force and roll-moment components. These equations are singular at $\beta = 0°$ and ill-conditioned at low $\beta$, up to 10°, because of plot resolution limits. However, some of the affected drag values can be supplied from drag data taken at $\beta = 0°$ (ref. 5), while the $PM$ values at $\beta = 0°$ can be filled in from the $YM$ data at $\alpha = 0°$ in accordance with the equivalence of these measurements discussed in the text. Lift data is available only at $\beta = 0°$, and is omitted.

The results are given in figure C1. The coarse $\alpha$-grid permits only limited comparison with the theoretical symmetry properties derived in section 3. A cursory examination shows; 1) good agreement of drag values along the boundaries $\alpha = 0°$ and $\beta = 0°$, 2) close agreement of side force with the expected zero lines at $\beta = 0°$ and 90°, 3) close agreement of roll moment with the zero lines of an antisymmetric function at $\tan\psi = \sin\alpha$, $\alpha = 0°$, $\beta = 0°$, 4) good agreement of pitching moment with its expected zero lines at $\alpha = 0°$ and $\beta = 90°$, and 5) null yaw moment at $\beta = 0°$, but a noticeable offset from the expected zero crossing at $\beta = 90°$.

**D/Q**

| α | 0. | 5. | 10. | 15. | 20. | 25. | 30. | 35. | 40. | 45. | 50. | 55. | 60. | 65. | 70. | 75. | 80. | 85. | 90. |
|---|---|---|---|---|---|---|---|---|---|---|---|---|---|---|---|---|---|---|---|
| 0. | 52. | 58. | 65. | 73. | 82. | 93. | 104. | 119. | 128. | 147. | 163. | 178. | 189. | 199. | 208. | 213. | 219. | 226. | 226. |
| 10. | 64. | 74. | 77. | 86. | 99. | 116. | 124. | 137. | 139. | 152. | 171. | 178. | 188. | 199. | 203. | 213. | 219. | 226. | 226. |
| 28. | 100. | 130. | 125. | 132. | 152. | 150. | 152. | 159. | 169. | 175. | 174. | 183. | 188. | 187. | 197. | 212. | 219. | 226. | 226. |

**Y/Q**

| α | 0. | 5. | 10. | 15. | 20. | 25. | 30. | 35. | 40. | 45. | 50. | 55. | 60. | 65. | 70. | 75. | 80. | 85. | 90. |
|---|---|---|---|---|---|---|---|---|---|---|---|---|---|---|---|---|---|---|---|
| 0. | 0. | -14. | -24. | -34. | -45. | -56. | -67. | -75. | -85. | -88. | -90. | -91. | -88. | -88. | -83. | -70. | -46. | -22. | 3. |
| 10. | 0. | -21. | -32. | -43. | -56. | -64. | -70. | -72. | -75. | -83. | -90. | -91. | -90. | -88. | -83. | -70. | -46. | -22. | 3. |
| 28. | 0. | -42. | -61. | -67. | -67. | -62. | -54. | -61. | -67. | -74. | -77. | -85. | -90. | -91. | -90. | -75. | -46. | -22. | 3. |

**RM/Q**

| α | 0. | 5. | 10. | 15. | 20. | 25. | 30. | 35. | 40. | 45. | 50. | 55. | 60. | 65. | 70. | 75. | 80. | 85. | 90. |
|---|---|---|---|---|---|---|---|---|---|---|---|---|---|---|---|---|---|---|---|
| 0. | 0. | 0. | 0. | 0. | 0. | 0. | 0. | 0. | 0. | 13. | 13. | 0. | 0. | 0. | 0. | 0. | 0. | 0. | 0. |
| 10. | 0. | 0. | 0. | -6. | -26. | -46. | -19. | 23. | 83. | 106. | 13. | 13. | 13. | 6. | 0. | 0. | 0. | 0. | 0. |
| 28. | 0. | 32. | 38. | 32. | 26. | 0. | -13. | -13. | 6. | 19. | 38. | 51. | 51. | 49. | 26. | -6. | 6. | 0. | 0. |

**PM/Q**

| α | 0. | 5. | 10. | 15. | 20. | 25. | 30. | 35. | 40. | 45. | 50. | 55. | 60. | 65. | 70. | 75. | 80. | 85. | 90. |
|---|---|---|---|---|---|---|---|---|---|---|---|---|---|---|---|---|---|---|---|
| 0. | 0. | 0. | 0. | 0. | 0. | 0. | 0. | 0. | -10. | -5. | -6. | -23. | -22. | -14. | -14. | -13. | -10. | -13. | -10. |
| 10. | -102. | -26. | -26. | -15. | 20. | 49. | 111. | 142. | 141. | 68. | -56. | -44. | -26. | -10. | -2. | 1. | 1. | -10. | -21. |
| 28. | 134. | 125. | 102. | 172. | 119. | 96. | 72. | 62. | 59. | 35. | 24. | 8. | 5. | 7. | 7. | 6. | 17. | -12. | -34. |

**YM/Q**

| α | 0. | 5. | 10. | 15. | 20. | 25. | 30. | 35. | 40. | 45. | 50. | 55. | 60. | 65. | 70. | 75. | 80. | 85. | 90. |
|---|---|---|---|---|---|---|---|---|---|---|---|---|---|---|---|---|---|---|---|
| 0. | 0. | 109. | 102. | 45. | -19. | -96. | -154. | -192. | -220. | -224. | -224. | -218. | -205. | -192. | -160. | -115. | -77. | -19. | 64. |
| 10. | 0. | 13. | 26. | -13. | -64. | -96. | -115. | -134. | -154. | -186. | -224. | -218. | -205. | -192. | -160. | -115. | -77. | -19. | 64. |
| 28. | 0. | -83. | -58. | -26. | -45. | -90. | -122. | -141. | -157. | -179. | -198. | -211. | -205. | -192. | -160. | -115. | -70. | -19. | 51. |

ψ  0. 5. 10. 15. 20. 25. 30. 35. 40. 45. 50. 55. 60. 65. 70. 75. 80. 85. 90.

Figure C1.- NORTHROP wind tunnel data (refs. 4 and 5): Smooth-surfaced 8- by 8- by 20-ft container

# REFERENCES

1. Shaughnessy, J. D.; Deaux, T. N.; and Yenni, K. R.: Development and Validation of a Piloted Simulation Model of an Helicopter and External Slung Load. NASA TP 1285, 1979.

2. Weber, J. H.; Liu, T. Y.; and Chung, W.: A Math Simulation Model of a CH-47B Helicopter. Vols 1, 2. NASA TM 84351, 1984.

3. Laub, G. H.; and Kodani H. M.: Wind Tunnel Investigation of Aerodynamic Characteristics of Scale Models of Three Rectangular Shaped Cargo Containers. NASA TM X-62169, 1974.

4. Watkins, T. C.; Sinacori, J. B.; and Kessler D. F.: Stabilization of Externally Slung Helicopter Loads. USAAMRDL TR-74-42, 1974.

5. Kontos, R. G.: Helicopter Slung Load Program. Aerosciences Laboratory Memorandum 3744-72-126, Northrop Corporation, Hawthorne, CA., Mar. 1973.

6. Windsor, R. I.: Wind Tunnel Tests of Two Models of Rectangular Containers. Wind Tunnel Report No 573. University of Maryland, Glenn L Martin Wind Tunnel, College Park, Maryland, Jan. 1970.

7. Simpson, A.;and Flower, J. W.: Unsteady Aerodynamics of Oscillating Containers and Application to the Problem of Dynamic Stability of Helicopter Underslung Loads. AGARD-CP-235, May 1978.

8. Ronen, T.: Dynamics of a Helicopter with a Sling Load. Ph.D. Thesis, Dept. of Aeronautics and Astronautics, Stanford University, Stanford, CA., Aug. 1985.

9. Weber, J. H.; and Greif, R.: A Lagrange-D'Alembert Formulation of the Equations of Motion of a Helicopter Carrying an Externally Suspended Load. NASA TM 85864, 1985.

# NASA

National Aeronautics and
Space Administration

# Report Documentation Page

| 1. Report No.<br><br>NASA TM-89433 | 2. Government Accession No. | 3. Recipient's Catalog No. | |
|---|---|---|---|
| 4. Title and Subtitle<br><br>A Comprehensive Estimate of the Static Aerodynamic Forces and Moments of the 8- by 8- by 20-ft Cargo Container | | 5. Report Date<br><br>May 1987 | |
| | | 6. Performing Organization Code | |
| 7. Author(s)<br><br>Luigi Cicolani and Gerd Kanning | | 8. Performing Organization Report No.<br><br>A-87126 | |
| | | 10. Work Unit No.<br><br>505-66-01 | |
| 9. Performing Organization Name and Address<br><br>Ames Research Center<br>Moffett Field, CA 94035 | | 11. Contract or Grant No. | |
| | | 13. Type of Report and Period Covered<br><br>Technical Memorandum | |
| 12. Sponsoring Agency Name and Address<br><br>National Aeronautics and Space Administration<br>Washington, DC 20546 | | | |
| | | 14. Sponsoring Agency Code | |

15. Supplementary Notes

Point of Contact: L. S. Cicolani, Ames Research Center, M/S 210-3, Moffett Field, CA 94035
(415) 694-5446 or FTS 464-5446

16. Abstract

A comprehensive static aerodynamic simulation model of the 8- by 8- by 20-ft MILVAN cargo container is determined by combining the wind tunnel data from a 1972 NASA Ames Research Center study taken over the restricted attitude domain, $\{0 \leqslant \psi \leqslant 90°; 0 \leqslant \alpha \leqslant 45°\}$ with extrapolation relations derived from the geometric symmetry of rectangular boxes. It is found that the aerodynamics at any attitude can be defined from the aerodynamics at an equivalent attitude in the restricted domain $\{0 \leqslant \psi \leqslant 45°; 0 \leqslant \alpha \leqslant 90°\}$. However, a similar comprehensive equivalence with the domain spanned by the data is not available; in particular, about two-thirds of the domain with $|\alpha| > 45°$ is unrelated to the data. Nevertheless, an estimate can be defined for this region consistent with the measured or theoretical values along its boundaries and the theoretical equivalence of points within the region. Discrepancies between the NASA Ames Research Center's data and theoretical symmetry properties range from small to gross, depending on the component, and are removed to apply the extrapolation relations. These discrepancies are assumed to be due to measurement errors, but their sources could not be identified. Data from independent wind tunnel studies are reviewed; these are less comprehensive than the NASA Ames Research Center's data but show good to fair agreement with both the theory and the estimate given here.

| 17. Key Words (Suggested by Author(s))<br>Aerodynamics<br>Milvan aerodynamics<br>Helicopter slung load | 18. Distribution Statement<br>Unclassified-Unlimited<br><br>Subject Category - 02 | | |
|---|---|---|---|
| 19. Security Classif. (of this report)<br>Unclassified | 20. Security Classif. (of this page)<br>Unclassified | 21. No. of pages<br>84 | 22. Price<br>A05 |

NASA FORM 1626 OCT 86